UNIVERSITÀ
DEGLI STUDI
FIRENZE

DOCTORAL PROGRAMME IN INDUSTRIAL ENGINEERING
DOTTORATO DI RICERCA IN INGEGNERIA INDUSTRIALE

XXIX

On the development of active fixtures for the mitigation of chatter vibrations in milling

ING/IND-16

Doctoral Candidate
Lorenzo Sallese

Supervisors
Dott. Antonio Scippa

Dott. Gianni Campatelli

External Referees
Prof. Nakano Yutaka

Prof. Marco Sortino

Dean of the Doctoral Programme
Prof. Maurizio De Lucia

Years 2013/2016

To all my friends

Summary

In the last decades, unstable vibrations originated in the milling process, often referred to as chatter vibrations, have collected the interest of several researches, mainly driven by the detrimental effect this phenomenon generates on productivity, surface finishing and tool wear. Although several approaches and techniques have been developed nowadays, their industrial application is still limited by the required expertise, time-consuming procedures or relevant interventions on the machine tool structures.

This research is focused on the investigation and design of active fixtures to mitigate chatter vibrations in milling, considering that this kind of devices could represent an appealing industrial alternative, due to the fact that they can be directly retrofitted to different machine tools and applied to different machining operations. The aim of this thesis was to improve the performance of intelligent active fixtures by carefully addressing the specific design challenges, both in terms of mechanical design and control aspects. The main focus was put in extending the device bandwidth in accordance with the requirements of a general chatter mitigation application, where chatter frequencies can easily reach and exceed several kilohertz.

In particular, specific design guidelines and simplified modeling strategies, aimed at supporting the definition of an adequate mechanical design, are presented and discussed along with the selection of suitable actuation devices capable of granting the needed reliability, even when operated at high frequencies in demanding dynamic applications.

Moreover, this work presents the development of a novel control strategy aimed at exploiting low-frequency excitation to disrupt chatter vibrations, without requiring the further extension of the device bandwidth nor the preliminary system identification and modelling, as generally needed for renowned model-based control techniques.

Preface

Parts of the activities reported in this thesis have been conducted within the iNTEFIX European project and are described in the related project reports and deliverables. The work package partners, Paragon S.A., Tecma S.r.l. and Girardini S.r.l., contributed to the development of the prototype and partially to some of the achievements reported in this work.

In addition, parts of this thesis have been published in peer reviewed journals and conference proceedings. The cited publications reported the research work carried out during my Ph.D. under the supervision of Dr. Antonio Scippa and Dr. Gianni Campatelli and with the support of the co-authors. More in detail, parts of this research activity are presented in the following conference proceedings:

- Campatelli G, Sallese L, Scippa A. Design of An Active Workpiece Holder. Procedia CIRP 2015; 34:217–22. I mainly contributed to the formalization of the kinematic architecture requirements and the related contraddictions.
- Sallese L, Scippa A, Grossi N, Campatelli G. Investigating Actuation Strategies in Active Fixtures for Chatter Suppression. Procedia CIRP 2016; 46:311–4. My contribution was mainly related to the formalization of the open-loop control and the preliminary investigation of the feasibility of this control approach. I wrote most of the manuscript.
- Scippa A, Montevecchi F, Grossi N, Sallese L, Campatelli G. Time domain simulation model for active fixturing in milling. Proc. 8th Int. Conf. Lead. Edge Manuf. 21st Century, LEM 2015, Kyoto, Japan: 2015. I mainly contributed to the definition of the simulation requirements and the experimental validation tests, including the data processing.
- Sallese L, Grossi N, Tsahalis J, Scippa A, Campatelli G. Intelligent fixtures for active chatter control in milling. 5th CIRP Glob. Web Conf. Res. Innov. Futur. Prod., 2016. I contributed to all the aspects of the prototype design and the experimental tests. I wrote most of the paper.

Moreover, parts of this thesis have been submitted for publication on international peer reviewed journal as:

- Sallese L, Scippa A, Grossi N, Campatelli G. Numerical investigation of chatter suppression in milling using active fixtures in open-loop control. In press on Journal of Vibration and Control. My contribution was mainly related to the formalization of the open-loop control and the preliminary

investigation of the feasibility of this control approach. I wrote most of the manuscript.

- Sallese L, Innocenti G, Grossi N, Flores R, Basso M, Campatelli G. Active fixture for chatter suppression in milling using a novel control strategy. In press on International Journal of Advanced Manufacturing Technologies. I was in charge of all the aspects related to the prototype design and some aspects related to the control logic development and implementation. In addition, I conducted all the experimental tests, including data processing and wrote most of the manuscript.

Table of contents

List of figures

List of tables

Acronyms List

AMB	Active Magnetic Bearing
ANN	Artificial Neural Network
AVC	Active Vibration Control
AWH	Active Workpiece Holder
CAD	Computer Aided Design
CMM	Coordinate Measuring Machine
CNC	Computer Numerical Control
CSSV	Continuous Spindle Speed Variation
DDE	Delayed Differential Equation
DOF	Degree Of Freedom
EDM	Electric Discharge Machining
fxLMS	filtered-X Least Mean Square
FE	Finite Element
FEA	Finite Element Analysis
FRF	Frequency Response Function
GA	Genetic Algorithm
GMA	Giant Magnestostrictive Actuator
HIL	Hardware In the Loop
HSM	High Speed Milling
LTI	Linear Time Invariant
MAC	Modal Assurance Criterion
MRR	Material Removal Rate
PZT	Lead Zirconate Titanate (Pb[Zr(x)Ti(1-x)]O3) Piezo ceramic
SLD	Stability Lobe Diagram
SLE	Surface Location Error
SMA	Shape Memory Alloy
SPC	Single Point Constraint
SSV	Spindle Speed Variation
TMD	Tuned Mass Damper
TPF	Tooth-Pass Frequency

Introduction

Fostered by a continuous increase in precision and performance, machining represents nowadays one of the most widespread manufacturing technologies. In the last decades, research and industry contributed to the evolution of this technology by developing new materials, integrating sensors and improving the performance of computer numerical controls (CNCs) [1]. Among the various metal cutting technologies, milling holds a leading position mainly due to its flexibility: this manufacturing process could indeed be suitable for parts with different geometries, sizes and for a variety of different materials.

The cutting process in milling is characterized by discontinuous cuts, due to the periodic inward and outward motion of the cutting tool (mill), generally composed of multiple cutting edges (flutes). The periodic nature of this process leads to several vibration issues that could get relevant when productivity is pushed to the limit. Particularly, the onset of unstable vibrations, usually referred to as chatter [2], represents one of the most limiting factors of modern milling operations, given their detrimental effect over surface finishing and tool wear. In order not to trigger these unwanted vibrations, precautionary cutting parameters are usually employed and the achievable Material Removal Rate (MRR) could be drastically compromised, impacting over productivity. This issue is particularly pronounced in the manufacturing of parts for the aerospace, energy and mold&die sectors, where parts of complex geometries are manufactured from blank material by removing up to 95% of its initial weight. In those cases, an increase of productivity goes through an unavoidable maximization of the MRR. A tangible perception of the impact of chatter vibrations on productivity was provided by Le Lan et al. [3] back in 2006: according to their work, the cost due to chatter in manufacturing a Renault cylinder block is estimated in 0.35€ per piece. Given that those cylinder blocks are produced by Renault S.A.S. in lots of around 3 million pieces per year, the economic impact of this detrimental effect is self-evident.

For decades the scientific research has been focusing on the study of this phenomenon to pursue the development of dedicated techniques to avoid these unwanted vibrations and their detrimental side effects. Prediction approaches, such as the computation and use of Stability Lobe Diagrams (SLDs) [4], are nowadays available to exploit the most suitable combination of cutting parameters and tool engagements granting the maximum material removal rate within the stability boundaries [5], hence avoiding the onset of chatter vibrations. Nevertheless, the widespread industrial application of these approaches is still limited by the required expertise and time-consuming tests. Moreover, the predicted optimal conditions are representative of only the specific tool/material combination, hence the procedures must be repeated several times to optimize a full machining cycle. While alternative in-process strategies have been long since developed to overcome some of these

limitations, for example by automating the selection of optimal cutting parameters [6], in those cases the achievable MRR is still imposed by the stability limits of the process.

On the other hand, dedicated active techniques could grant an increase of the MRR by either improving the machine tool dynamics, as in the active structural control techniques [7], or interacting with the process with dedicated counteracting actions, such as in the Spindle Speed Variation (SSV) techniques [8], or with mechatronics devices integrated either in the spindle [9] or the fixture [10].

Most of these techniques are still relegated to the research field and an industrial application is very limited to this days: indeed, the required expertise, time-consuming set-up procedures and the relevant interventions on the machines still represent barriers for a widespread adoption. In this regard, intelligent retrofittable active fixture could be seen as a more industrially oriented alternative, but the maturity of this solution is not adequate enough to deal with general milling operations. Specific design challenges need to be tackled to cope with the requirement of an actual industrial application. To date, the few literature works dealing with this technique show mostly model-based control strategies and narrow device bandwidths that actually limit the potential application to the mitigation of chatter vibrations originated by structural mode of the machine tool structure only.

In this research the whole development of an intelligent active fixture is presented and discussed. The goal was to address most of the present limitations by providing guidelines for both the mechanical design and the development of a model-less control logic that could be effective in mitigating chatter vibrations in general applications.

1. Thesis structure and goals

The goal of this thesis, as aforementioned, is to investigate the development and use of active fixtures for chatter mitigation in milling, focusing on those features that could ease the industrial implementation of this kind of chatter mitigation approaches. The research covers most of the topics involved in the development of this mechatronic device, from the peculiar mechanical design solutions adopted to increase the achievable bandwidth and to improve long-term reliability, to the novel model-less control strategy that could be used to mitigate chatter vibrations, even when their frequencies could drastically exceed the device bandwidth.

As discussed in Chapter 2, chatter vibrations represent a major issue in modern machining operations, given the continuous effort in improving performance and productivity. Even though this phenomenon is being the aim of several studies since the late 1950s [11], an effective industrial solution to prevent or mitigate/suppress the phenomenon is still lacking. As anticipated, to date the various techniques and approaches still require dedicated expertise and skills or complex integration of sub-systems in the machine tool itself (e.g., sensors and control interfaces), complicating their widespread industrial adoption. In this scenario intelligent active fixtures could represent an effective alternative, given that they could generally be configured as retrofittable devices, hence enabling a straightforward integration in a variety of different machine tools. Nonetheless, active fixtures have collected only a marginal interest in the research field, presumably because of the challenges imposed by the need of displacing a workpiece, potentially with substantial mass, at a frequency in the range of chatter vibrations, easily exceeding several kHz. These are the aspects that provided the motivation for the presented research.

The thesis is organized as follows:

- **Chapter 2** summarizes a state of the art analysis to introduce the relevance of chatter vibrations in milling and to provide an overview of the different strategies proposed in literature to predict, prevent or mitigate this phenomenon.
- **Chapter 3 and Chapter 4** cover the fixture design. More in detail, Chapter 3 describes the definition of suitable fixture architectures and focuses on the study of the monolithic flexure hinges that are used to decouple axes motion and ensure the required flexibility. An analysis of different hinge geometries is provided along with the derivation of empirical design equation to ease the dimensioning and positioning of these mechanical component within the fixture frame by exploiting dedicated reduced numerical model. Chapter 4, instead, presents the fixture detailed design and the numerical analysis of its behavior. Moreover, in Chapter 4 the selection of suitable actuation devices is discussed, highlighting the main aspects

that should drive this selection in order to achieve the desired behavior without affecting the long-term reliability. Chapter 4 also covers the prototype assembly and preliminary testing.

- **Chapter 5** deals with the development of the novel control strategy that is aimed at interfering with the cutting process by means of dedicated counter-excitations, constrained within the device bandwidth, to disrupt the chatter vibration potentially occurring at higher frequencies. All the steps of the control development are discussed: section 5.1 presents the dedicated time-domain simulation model developed to study the active fixture behavior and its interaction with the cutting process. This simulative environment was used to investigate the feasibility of low-frequency excitations interfering with the unstable vibrations, as discussed in section 5.3, and provides an empirical definition of suitable actuation parameters for the purpose. Moreover, Chapter 5 provides the theoretical explanation of the proposed control strategy, presented in section 5.2, and the adaptation of the proposed control strategy into a closed-loop formulation in order to improve its performance.
- **Chapter 6** describes the practical implementation of the proposed control strategy and the experimental validation of the achievable chatter mitigation in real milling operations.

The thesis organization is summarized in Table 1.1, along with the specific topics addressed in each chapter and the related goals.

Table 1.1: Thesis organization and topics addressed in the different chapters.

Thesis Chapter	Main topic	Addressed topics	Goal
Chapter 2	State of the art analysis	• Literature survey	**Formalization of goals and requirements**
Chapter 3	Active fixture mechanical design	• Fixture architecture • Flexure hinges design	**Definition of suitable design guidelines to improve active fixture performance**
Chapter 4		• Detailed design • Actuators selection • Preliminary testing	
Chapter 5	Control logic design and implementation	• Time domain model • Numerical investigation • Theoretical aspects • Closed-loop formulation	**Description of the novel model-less low-frequency control strategy**
Chapter 6	Active fixture experimental testing	• Assessment of chatter mitigation performance	**Demonstration of the feasibility of the proposed solution**

2. Chatter vibrations in milling: state of the art analysis

‘‘Machine tool development in recent decades has created an increasing number of vibration problems. Machine tool designers in early development phases are worried about vibration characteristics; production engineers know that vibrations diminish tool life, generate unacceptable surface finishes on the parts and reduce productivity’’ [11]. With this statement, back in 1961 Prof. Tobias summarized the reasons why vibrations in machine tools have been collecting the interest of a large quantity of research works since the beginning of the 20th century [12]. The continuous efforts in improving process performance and precision have kept the interest in this topic up to date [13], as clearly stated by Quintana [2]: “nowadays, authors still refer to vibrations as a limiting factor, one of the most important machining challenges and, of course, an aspect to be improved”.

As general machinery, machine tools structures are composed of elastic components, so that they behave like flexible bodies that respond to external or internal forces with finite deformations (i.e., vibrations). Three different types of vibrations can be originated in metal cutting:

- **Free vibrations**: by definition these vibrations occur when a mechanical system is displaced from its equilibrium and is allowed to vibrate freely. In this case the structure will vibrate near to this equilibrium point at one of its natural frequencies. In practice, these vibrations may be originated by shocks transmitted through the foundation from other machines in the workshop (e.g., presses) or generated within the machine tool itself, for example due to unbalanced reciprocating masses (e.g., table motion reversal in grinding and milling machines) [14].
- **Forced vibrations**: are generated by external periodic forces applied on the machine tool structure. Forced vibrations could be induced by several sources like unbalanced rotating masses or faulty gears, or it could again be transmitted by other machinery through the workshop floor. In milling the main source of periodic forces are represented by the cutting forces themselves, which are periodically varying due to the interrupted nature of the cutting process (i.e., rotating multi-fluted cutting tool, periodically engaging the cutting area). When the frequency of the external force is close to structure natural frequency, a resonance condition is induced and the machine tool could undergo wide oscillations. Forced vibrations in milling are particularly regarded in investigating the milled surface generation and the related errors, such as the Surface Location Error (SLE) [15].

- **Self-excited vibrations**: these vibrations are originated by the closed-loop interaction between the cutting process and the dynamics the machine tool structure, as formalized by Merritt [16]. This interaction can become unstable due to the fact that the oscillating movements of the structure themselves are sustaining the periodic excitation forces leading to an exponential increase of vibration amplitudes. This phenomenon is generally called "chatter" and is regarded as the most detrimental effect for the cut. Literature generally classifies these self-excited vibrations into "primary" and "secondary" chatter, the former being originated by the cutting process itself, for example by effect of friction between the tool and the workpiece, by thermo-mechanical effects on the chip formation or by mode coupling. The "secondary" chatter, often referred to as regenerative chatter, is caused by the regeneration of a wavy surface on the workpiece and the associated periodic variations of the chip thickness, hence cutting forces, that self-excite the unstable vibrations, as exemplified in Figure 2.1.

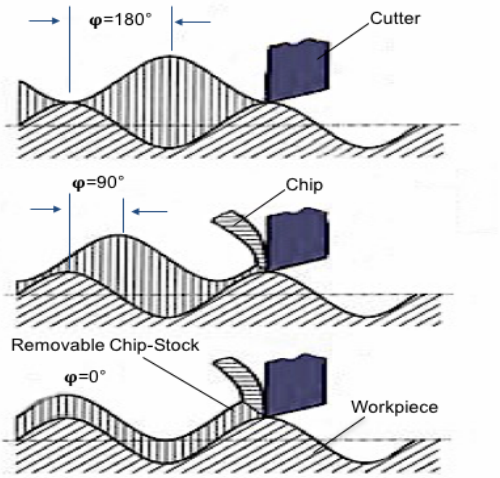

Figure 2.1. Schematization of the regenerative effect and the phase different leading to the self-excitement of chatter vibrations.

This regenerative effect is the most important cause of chatter vibrations; hence it has become a shared convention to refer to it as "chatter" in general. In accordance, henceforth the term "chatter" will be used in this thesis to imply the secondary chatter vibrations originated by the regenerative effect, which represent the aim of this work and are generally regarded as the most destructive among all the other types of vibrations.

It is worth highlighting that in literature chatter vibrations are usually classified as unstable. Nonetheless, in general practice, with fixed tool engagements and cutting parameters, the level of self-excited and forced vibration generally grows until causing the tool to disengage for a part of its vibratory period. As a consequence, in that time period the cutting forces decrease, damping the uncontrolled growth of chatter vibrations as in a general unstable phenomenon. This non-linear behavior poses an upper limit to the growth of the vibrations level in chatter affected milling process, as discussed by Tlusty et al. [17]. It should hence be pointed out that, for reasonable combination of cutting parameters and tool

engagements, the level of self-excited vibrations is unlikely to grow uncontrollably, as for an unstable phenomenon, leading to potential damages and tool breakage. Hereafter the text will refer to chatter vibrations as "unstable" implying what just mentioned, as common terminology in the dedicated literature.

The occurrence of these self-excited vibrations produces several detrimental effects on the manufactured product and on the process itself. According to Quintana and Ciurana [2], the chatter occurrence leads to:

- Poor surface quality.
- Unacceptable inaccuracy.
- Excessive noise.
- Disproportionate tool wear.
- Machine tool damage.
- Reduced material removal rate (MRR).
- Increased costs in terms of production time.
- Waste of materials.
- Waste of energy.
- Environmental impact in terms of materials and energy.
- Costs of recycling, reprocessing or dumping non-valid final parts to recycling points.

These issues motivated the continuous interest of scientific and industrial research into the study of this vibrational phenomenon. Nowadays, several different approaches have been proposed to prevent its occurrence or to mitigate its detrimental effects, as recently presented by Munoa et al. [18].

According to Quintana et al. [2] two main methods can be pursued to achieve stable cutting conditions: the first approach could be aimed at selecting suitable combinations of cutting parameters, based on different chatter prediction strategies. The alternative method relies on improving the dynamic response of the system by means of dedicated passive or active strategies.

In the following subsections a brief description of these alternative techniques is presented and discussed for the purpose of highlighting the peculiar features of active fixtures and motivate the choice of the specific research topic. An extensive discussion of each chatter avoidance technique is not in line with the scope of this sections; a more detailed description of specific aspects is demanded to the related literature references.

2.1. Chatter prediction and spindle-speed selection

Since the earliest works dealing with chatter vibrations in machining processes, several models have been presented with the purpose of studying the phenomenon and predict its occurrence [19]. In the last decades a variety of modeling approaches were used for this purpose: analytical formulations [11,20], time-domain and frequency-domain models have been proposed to describe the arising of chatter vibrations in different cutting conditions.

Disregarding the modeling procedure used, the main outcome of this chatter prediction approach is the definition of a sort of "stability map", called Stability Lobe Diagrams (SLDs) [19], that could assist the machinist in selecting suitable combinations

cutting parameters in order to avoid the onset of chatter vibrations. An example of a generic SLD is reported in Figure 2.2.

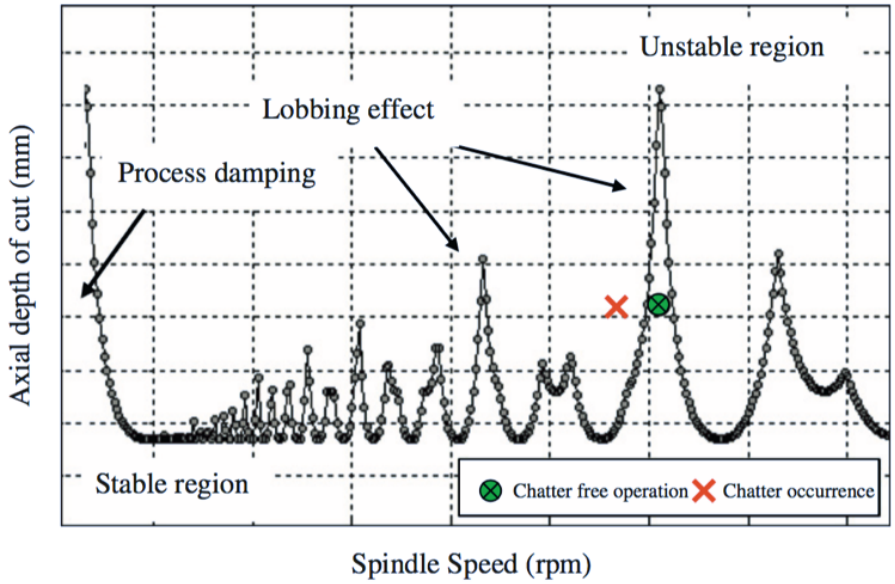

Figure 2.2: Example of a stability lobe diagram [2]**.**

The SLD identification is traditionally conducted exploiting one of the aforementioned modeling procedures, combined with experimentally defined inputs, such as tool-tip Frequency Response Functions (FRFs) and specific cutting force coefficients [1]. Even though in recent years the development of dedicated software solutions [21] allowed simplifying the SLD computation, the limitations in terms of required expertise and time consuming experimental tests endure. Moreover, the accuracy of prediction approaches based on SLD is affected by several effects, such as the spindle-speed dependency of both cutting force coefficients [22,23] and FRFs [24], or the uncertainties of the experimental identification procedures [25]. More recently, alternative experimental procedures contributed to easing the exploitation of chatter prediction approaches by simplifying the SLD identification [26,27]. As an alternative, chatter avoidance by means of optimal spindle speed selection could be performed by means of automated procedures [6,28], nowadays integrated also in a few commercial NCs [29]. The basic idea of these automated spindle speed selection approaches is to adapt the spindle-speed so that the Tooth-Pass Frequency (TPF) matches the natural frequency of the dominant mode, moving the process into a resonance condition where forced vibrations are dominant. It is worth here highlighting that such a resonance condition could be assumed as suitable from the point of view of chatter vibrations, given that it represents the theoretically maximum achievable MRR. In resonance conditions, though, the forced vibrations could grow drastically, leading to potential detrimental side effects, as previously cited.

Even though the spindle-speed selection approach could be helpful in preventing the onset of chatter vibrations, especially in High Speed Milling (HSM) where the stability pockets are broader, it shows two main limitations. Machinability issues could indeed constraint the allowable spindle-speeds in a narrow range, defined on a tool wear basis, hence drastically limiting the degree of freedom in potentially changing the spindle-speed.

As clearly stated by Altintas et al. [30] "such a solution is acceptable in practice when cutting materials like aluminum at high speeds without accelerating the tool wear".

In addition, the spindle-speed selection approaches could only guide the selection of suitable parameters within the stability boundaries, defined by the system dynamics. As a matter of fact, this approach cannot grant an actual increase of the maximum achievable material removal rate, but it only represents a useful tool in exploiting the maximum productivity allowed by the given cutting conditions (i.e., machine tool, tooling, workpiece, etc.).

2.2. Passive chatter suppression/mitigation techniques

When the machinability constraints do not allow an adequate change in the employable spindle speed, an alternative strategy could be pursued: by enhancing damping of the critical mode in the system dynamics, an increase in the absolute stability limit is indeed produced. This additional damping is usually introduced by means of dedicated passive auxiliary systems (e.g., viscoelastic dampers, friction dampers, Tuned Mass Dampers (TMDs) etc.) integrated in specific locations within the machine tool structure (i.e., where the critical mode has large modal displacements). Figure 2.3 summarizes the different types of dampers used for this purpose.

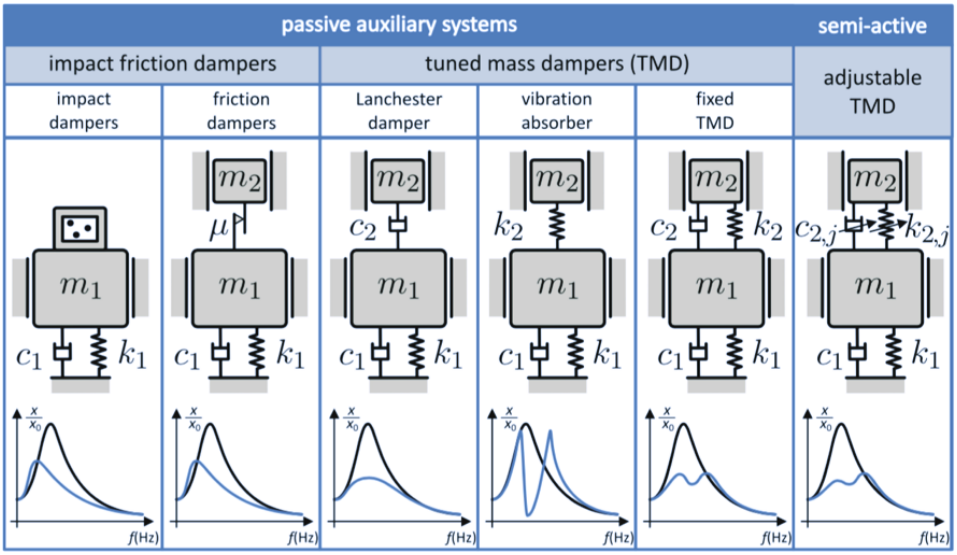

Figure 2.3: Auxiliary systems to change dynamic response at the critical vibrational mode [18]**.**

While this approach could produce drastic improvements in terms of stability limits in all the zones of the SLD, as exemplified in Figure 2.4, the tuning procedures and integration of this auxiliary sub-systems, could be challenging. Moreover, the application of this passive strategy is limited when the dynamic response varies, for example depending on cutting direction or tool position within the working area, as common for most machine tools [31,32].

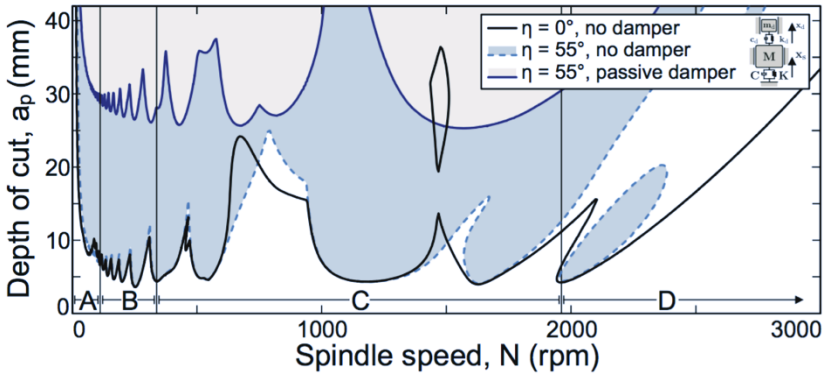

Figure 2.4: Example of the achievable effect in terms of stability improvements by means of TMDs (η flutes helix angle) [18]**.**

Semi-active adjustable mass dampers have been the focus of several research studies in recent years [33,34], given that they could improve some of the aforementioned limitations. The application of such devices seems still relegated to the research field even though the proved effectiveness and a future reduction in the device costs could foster the industrial development. It should be highlighted that the introduction of TMDs shall be limited to newly built machine tools. Retrofitting such devices in existing machine tools appears to be very challenging and the advantages could probably not balance the cost and time of the required interventions.

Among the passive chatter avoidance strategies is worth mentioning that dedicated designs of cutting tools could produce appreciable improvements in terms of stability limits mainly by either increasing process damping or disrupting the regenerative effect [35]. Serrated tools for high-productivity roughing, variable pitch cutters and monobloc tools (i.e., integrated tool-holder) are some of the commercial solutions nowadays available to increase productivity by improving the cutting process stability, especially in rough milling.

2.3. Active techniques for chatter suppression/mitigation

The growing availability and performance of actuation, sensing and control devices fostered the development of several active techniques for the control of vibrations in machining in general [36,37]. A summary of the different approaches to mitigate or suppress chatter vibrations in milling through active means is provided in the following sub-sections.

2.3.1. Active structural control and active spindle systems

Active structural control can be seen as an alternative approach to the aforementioned passive techniques in improving the machine tool structural dynamics that could lead to the onset of structural chatter vibrations, characterized by low-frequency vibrations, generally in the 20-200 Hz range, of large mechanical components within the machine tool structure. Unlike the passive approaches, active structural control could more easily cope with those applications where the machine dynamics can sensibly change with respect to position or direction or when multiple vibrational modes need to be damped.

As in general Active Vibration Control (AVC) applications, inertial actuators, often referred to as proof mass dampers, can be used to produce a reaction force on the machinetool structure in order to reduce the vibration at a given point. The application of this AVC technique to chatter mitigation has been extensively investigated, particularly focusing on the control algorithms potentially employable [38–40]. As an example, Figure 2.5 reports two different integrations of inertial actuators into the machine tool structures.

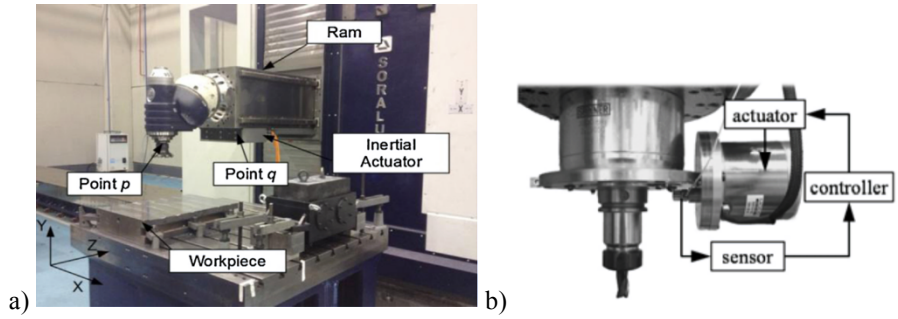

Figure 2.5: Examples of the integration of inertial actuators: a) biaxial inertial actuators on the machine tool ram [41]**, b) inertial actuator at the spindle base** [40]**.**

As an alternative solution to avoid the need of integrating big-size actuators within the machine tool structure, Munoa et al. investigated the feasibility of using the machine tool feed drives to exert the reaction forces needed [42], as shown in Figure 2.6.

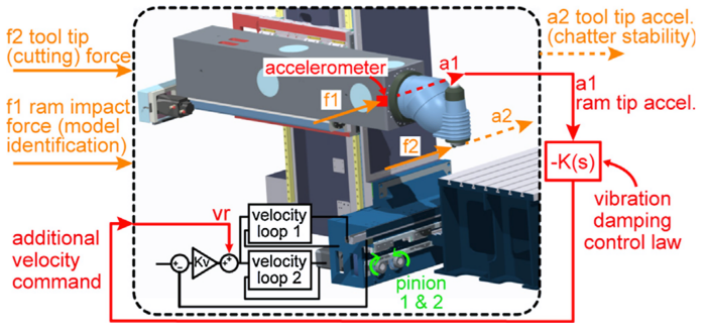

Figure 2.6: Schematization of the setup for active chatter suppression using machine feed drives [42]**.**

Even though the bandwidth of the feed drives would not allow a general application, the authors proved that this AVC strategy can increase the productivity between 85% and 600% by mitigating structural chatter vibrations.

All these active chatter suppression techniques seem to be among the most mature solutions developed, as demonstrated by the several commercially available devices [43,44], but their applicability is limited to the control of structural chatter that is not representative of general milling operations. While structural chatter can be triggered by heavy-duty machining operations, such as face-milling, usually the tool itself represents the most flexible component in the system. More in detail, in general milling operations the tooling (i.e., the system composed by the tool, tool-holder and spindle shaft) is likely to be the responsible for

chatter vibrations: in that cases the chatter vibrations would be originated at a frequency close to the tooling natural frequency, which could easily exceed several kHz.

Traditional AVC strategies, based on inertial actuators, show drastic limitations in that scenario, but alternative solutions have been investigated for the purpose. These techniques are usually referred to as active spindle systems and are based on the integration of dedicated subsystems in proximity of the spindle shaft. A clear exemplification of these approaches is represented by the integration of Active Magnetic Bearings (AMBs) to support the spindle shaft, as proposed by van Dijk [45] and exemplified in Figure 2.7.

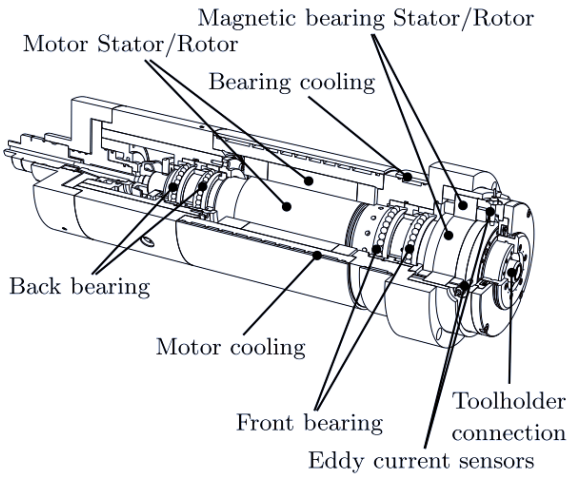

Figure 2.7: Active spindle system integrating an active magnetic bearing [45]**.**

Similarly, several authors proposed the integration of piezo actuators in the spindle supports, as exemplified in Figure 2.8 and Figure 2.9.

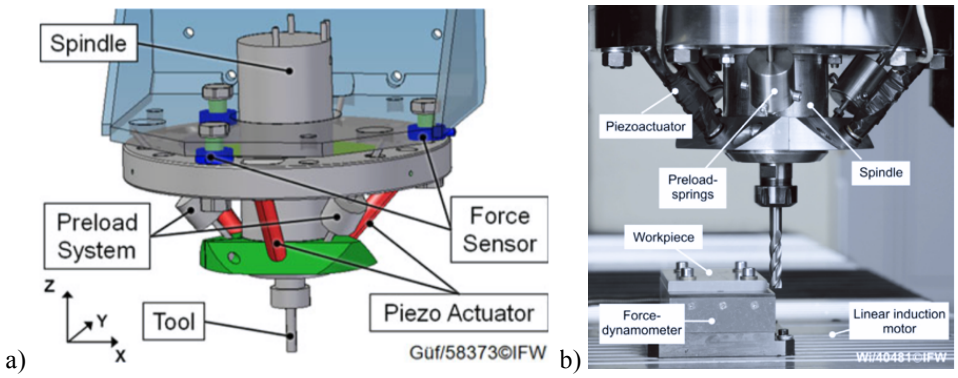

Figure 2.8: Adaptronic spindle integrating piezo actuators: a) assembly description [46]**, b) physical prototype** [47]**.**

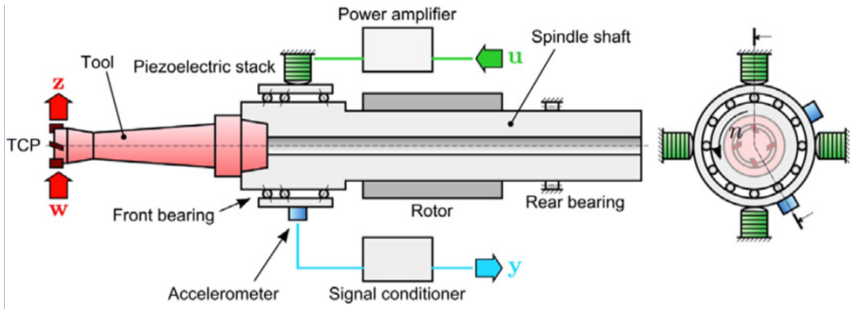

Figure 2.9: Active spindle system with integrated piezo actuators to excite the front bearing support [48]**.**

Monnin et al [48] investigated the use of such an active spindle system with two different control logics: on the one hand, a disturbance rejection control law optimizes the tool tip FRF. On the other hand, by defining the specific cutting conditions in advance, the controller can optimize the stable depth of cut. Denkena et al. [46] investigated the effect of over-imposed low-frequency vibrations in disrupting the regenerative effect and stabilizing the process, presumably using an open-loop control. The results achieved in both numerical and experimental tests showed that their proposed strategy could stabilize chatter frequencies above 1.3kHz using counter-excitations at 47Hz, as shown in Figure 2.10a, leading to an increase in the limit axial depth of cut, reported in Figure 2.10b.

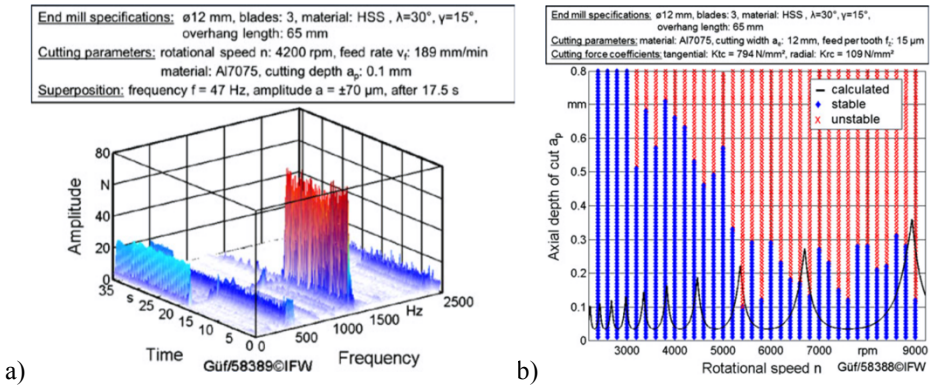

Figure 2.10: a) Vibration reduction achieved by means of the adaptronic spindle using low-frequency counter-excitations. b) simulated effects in increasing the stability limits [46]**.**

The same adaptronic spindle was also tested by Denkena et al. in dynamic compensation of tool-deflections in previous activities [47]. A similar solution was proposed also by Aggogeri et al. [49], which proposed a potential cross-platform device, called smart platform, to be mounted either on the spindle or the machine tool table, as shown in Figure 2.11.

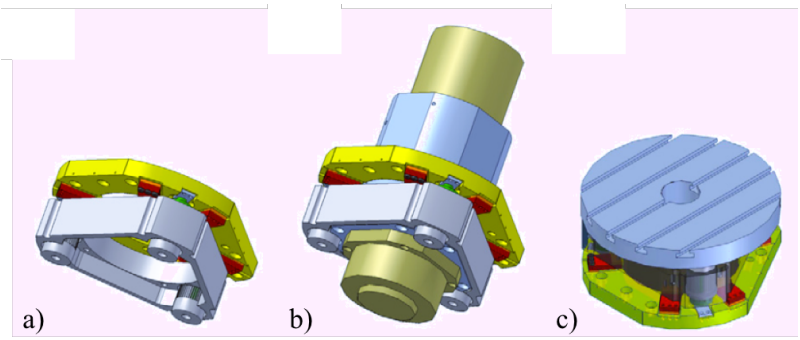

Figure 2.11: a) Smart platform for AVC, b) integration on the spindle, c) integration on the machine tool table [49]**.**

As previously pointed out for active and passive damping techniques, the main limitation of these techniques is related to the need of relevant intervention on the machine tool structures in potential retrofitting applications, that would lead to an increase of the associated cost.

2.3.2. Spindle-speed variation

Among active chatter suppression approach is worth mentioning the Continuous Spindle Speed Variation (CSSV) techniques that exploit continuous variations of the spindle speed around the nominal value with the purpose of disrupting the regenerative effect and stabilizing the process. This technique somehow follows the principle of variable-pitch cutters, but the capability of adapting the Spindle Speed Variation (SSV) allows higher flexibility. The effects of the application of CSSV are exemplified in Figure 2.12.

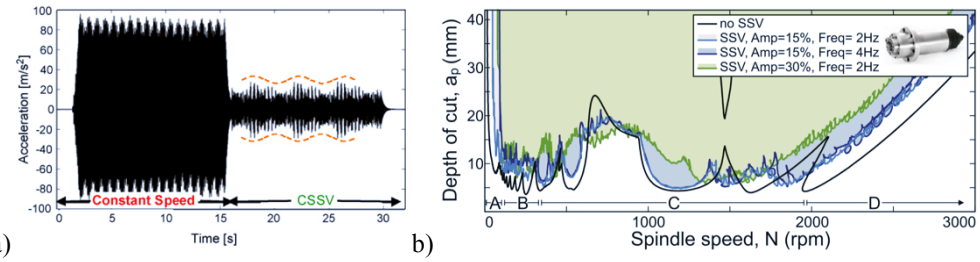

Figure 2.12: Effects of the application of CSSV: a) reduction of vibration level [50]**, b) effect in increasing the stability limits** [18]**.**

The main focus of the research in this field is on the definition of the most suitable modulation and the related parameters that should be defined considering also the spindle dynamics and should not sensibly impact on the spindle life and reliability. This seems to still represent an open issue: the suitable modulation is nowadays computed by means of complex process simulations that would not make an industrial application feasible [18], only Al Regib et al. [51] proposed a simple formulation to derive the suitable parameters for sinusoidal spindle speed variation on the basis of the nominal spindle speed and chatter frequency. Nonetheless, the a-priori identification of the chatter frequency leads to the chatter prediction procedures defined in Section 2.1, with all the related disadvantages.

Even though some machine tool builders, such as Haas, have already integrated SSV on their latest products, especially in turning, the definition of SSV parameters is demanded to the machine tool operator, that is not yet assisted with adequate guidelines.

2.3.3. **Active fixtures**

The use of active fixtures, often referred to as Active Workpiece Holders (AWHs), has been investigated in literature by few researchers. Those mechatronic devices, integrating sensors and actuators in the physical fixture, are generally used to suppress chatter by influencing the relative vibration between tool and workpiece [52] or to improve other aspects of the milling process. As an example, back in 1995 Tansel et al. [53] studied the effect of such active fixtures in micro-milling, by exploiting suitable workpiece motion patterns with the purpose of improving the evacuation of chips from the cutting zone, preventing tool damage and increasing the tool life.

For what concerns chatter mitigation applications, the use of AWHs was preliminary investigated by Lockwood et al. [54] and Haase et al. [55], respectively discussing the aspects related to the control logic, based on adaptive filters, and some preliminary feasibility studies. Those activities led to the development of a prototype, shown in Figure 2.13, that was effectively tested in mitigating the effects of structural chatter vibrations [56], reducing the vibration levels at the spindle head and improving the surface finish.

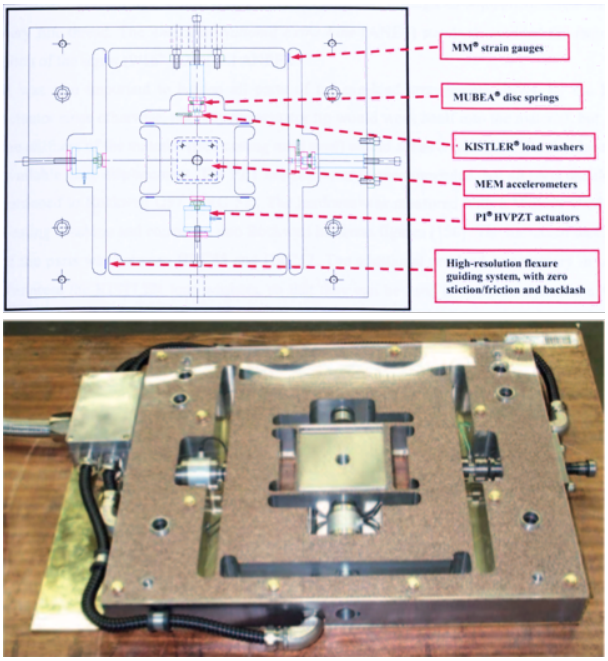

Figure 2.13: Active workpiece holder prototype [56]**.**

Analogous solutions were developed by several authors to suppress structural chatter vibrations [57], workpiece-related chatter vibrations [58], forced vibrations [59] or to improve the fixture dynamic response [60]. Those works present minor differences for what

concerns the global device design and exploit different model-based control logic for the vibration control application, as will be discussed more in detail in Chapter 5.

Even though some additional works, somehow dealing with active fixture, can be cited, such as the integration of piezo patches to improve machinability of flexible workpieces [61], the literature related to this specific topic appears still quite limited. This is probably due to the fact that the development of such AWHs poses some intrinsic challenges that complicates the related research, as also formalized by Munoa et al. [18]. As an example, on the one hand it is still difficult to size the actuators accurately for a given condition, on the other hand inertial forces originated by the workpiece actuations could preclude an adequate extension of the device bandwidth, as needed to cope with chatter mitigation in general applications. Moreover, specific issues related to the actuation devices need to be tackled to ensure reliable operability in demanding dynamic applications, as will be highlighted in Chapter 4.

On the other hand, compared to all the previously mentioned approaches, active fixtures have some peculiar advantages: according to Brecher et al. [57], indeed, “the main difference to other supplementary structure integrated active systems is the feature that AWHs can be universally applied to arbitrary vertical machine tools without any design changes”. This feature could sensibly foster an industrial application, assuming that some open issues are tackled. In particular, as already mentioned, an industrially suitable device should be capable of coping with high frequency chatter vibrations, such as the ones originated by the long and slender tools often used in milling processes. Moreover, a model-less control strategy is advised to reduce the efforts and expertise required for the exploitation of renowned model-based approaches.

These open issues provided the motivation for this PhD research work that has pursued the development of active fixture featuring an increased bandwidth and a novel model-less control strategy, as will be discussed in detail in the next chapters.

3. Active fixture: main design aspects

As discussed in the previous chapter, the few literature contributions dealing with active fixtures do not provide adequate guidelines for the development of a suitable design. Only Abele et al. [10] and Haase [62] discussed some of the main design aspects involved in the development of such a mechatronic device. Nevertheless, those works present conflicting design solutions, such as the kinematic scheme adopted or the solutions to decouple axes motion. These two specific topics were addressed in the first part of this research work in order to highlight the differences between the alternative configurations and to provide a better understanding of the design of this kind of devices in its early stages. Moreover, this chapter presents the main aspects of the simplified modeling strategy developed with the purpose of reducing the efforts needed to numerically investigate alternative designs in the preliminary design phase.

3.1. Active fixture architecture

As anticipated, among the AWH related literature the definition of a univocal design solution is still lacking. As an exemplification, referring to the global design aspects, two kinematic architectures have been proposed in literature for a two Degrees of Freedom (DOFs) device capable of controlling tool vibrations along the plane normal to the tool axis (i.e., the plane where tool flexibility is concentrated). Following a traditional kinematic architecture used in micro and nano-positioning applications, Abele et al. [10] and Rashid et al. [60] developed a 2 DOFs device based on parallel kinematics, as shown in Figure 3.1.

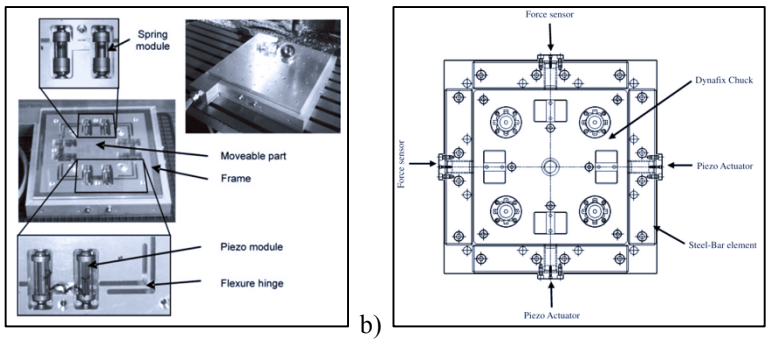

Figure 3.1: Examples of AWH based on parallel kinematics, as presented by: a) Abele et al. [10]**, b) Rashid et al.** [60]**.**

This kinematic architecture has some intrinsic advantages derived by the single moving part (i.e., the inner stage) upon which all the actuators are acting, as exemplified in the scheme reported in Figure 3.2. The main advantages are related to the symmetric axes dynamics and the reduced overall mass and dimensions.

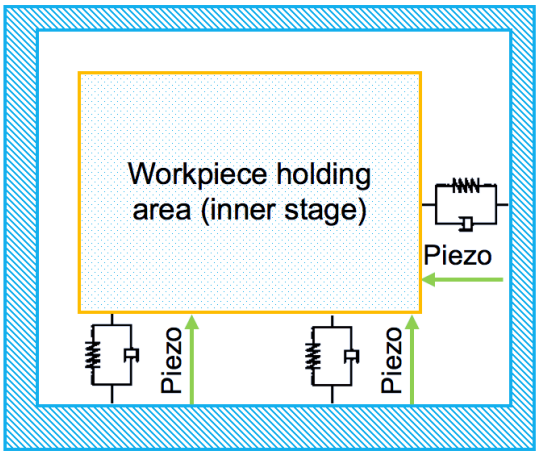

Figure 3.2: Schematization of an XY parallel kinematic architecture, as used for the AWHs in [10,60]**.**

While on the one hand this favorable features would simplify the bandwidth increase, on the other hand the parallel kinematic architecture shows potentially relevant cross-talk issues, often referred to as axis cross-coupling [63]. It is worth here highlighting that the positioning resolution required for the specific AVC application would be definitely lower, if compared to the requirements of a micro or nano-positioner. Nevertheless, the influence of cross-talk effect in affecting the active fixture performance was clearly highlighted also in AVC applications by Abele et al. [10]. The cross-coupling in this kind of devices is well covered by the micro and nano-positioning dedicated literature that proposed the use of either dedicated closed-loop controllers [64] or complex mechanical designs [65] to compensate for this unwanted effect. The first solution would obviously complicate the device control in AVC applications and, in its simplest implementation, would require at least an additional actuator and dedicated sensors. By adopting complex mechanically decoupled design, on the other hand, the consequent increase of flexibility of the guiding systems could drastically impact on the device bandwidth.

In order to mitigate some of these drawbacks, an alternative parallel kinematic architecture, such as the one proposed by Acer et al. [66], was evaluated at first. This solution, schematized in Figure 3.3a, would allow adopting simpler open-loop controllers, once an experimental kinematic identification of the stage is performed. Nonetheless, an additional actuator and dedicated guides would still be required (e.g., a flexure guiding system based on two revolute and one prismatic joints, as proposed by Acer et al. and shown in Figure 3.3b).

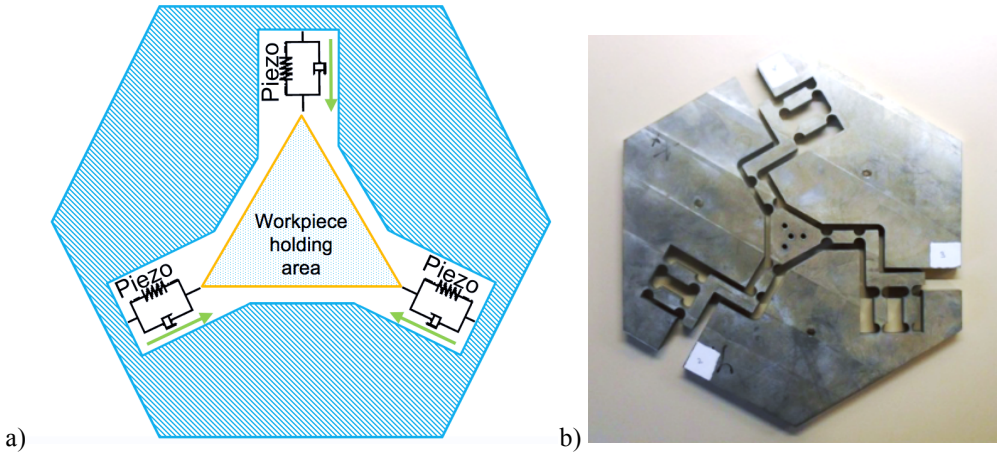

Figure 3.3: Alternative parallel kinematic architecture. a) Schematization, b) example of a manufactured device [66]**.**

As an alternative, a serial kinematic architecture could be selected with the purpose of overcoming most of the aforementioned issues. This kinematic configuration, in practice, could be achieved by stacking or nesting two stages (for a 2 DOFs device), each responsible for controlling the motion along a given direction [63]. This architecture, schematized in Figure 3.4 for a nested stages configuration, was exploited by Ford et al. [56], Brecher et al. [57] and Long et al. [59] in AWH applications, as previously shown in Figure 2.13.

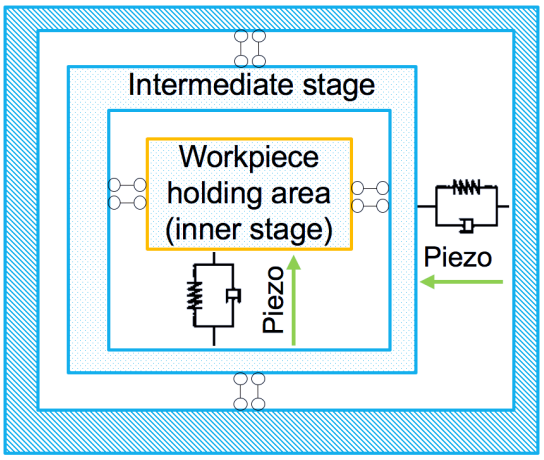

Figure 3.4: Schematization of a planar XY serial kinematic architecture, as used in [56,57,59]**.**

Unlike the case of parallel kinematics, this architecture cannot ensure symmetric dynamic responses along the actuated directions, given that the two axes feature different masses. From this point of view, this architecture imposes some compromises in terms of achievable bandwidth. Crucial attention should be paid on this aspect in the design since its early stage, particularly focusing on increasing as much as possible the natural frequency of the outer stage (i.e., the one composed of the intermediate and inner stages), which would be the one featuring higher mass. Moreover, the design of adequately rigid guiding systems is

an absolute requirement for this kinematic architecture, in order to prevent the onset of low-frequency out-of-plane or off-axis vibrational modes that could drastically affect both bandwidth and reliability, as highlighted by Kenton and Leang [67].

On the other hand, such a serial kinematic architecture could grant better decoupling the axis motion, hence preventing relevant cross-talk effects. It should be pointed out that this assumption is not valid in general. In high-resolution positioning applications several factors, such as manufacturing errors or hysteresis and creep of the piezo actuators, could indeed influence the axis motion and induce cross-coupling. Nevertheless, for the specific application cross-talk appears to be negligible with this kind of kinematic architecture, hence avoiding the need for dedicated compensation solutions. This would simplify both the mechanical and control design and, in addition, the absence of additional sensors and actuators would make this solution more cost effective. The actuators, and particularly the related drivers, represent indeed the main cost item of such kind of active fixtures.

Taking all these factors into account the serial kinematic architecture was selected as the basis for the development of the AWH prototype, discussed more in detail in Chapter 4.

3.2. Flexure hinges design

As shown in the references previously discussed, the proposed AWH devices feature flexure based guiding systems to grant flexibility along the actuation directions. This kind of monolithic guides is usually preferred to more traditional guiding systems, such as sliding bearings, due to the higher resolution deriving from the absence of friction, stiction and backlash [56,68]. The accurate design of these mechanical components, integrated in the fixture, is one of the crucial steps in assessing the active fixture performances and dynamic response. The main design challenge derives by the fact that the hinge stiffness should be tuned in order to grant the maximum rigidity along all the cross-actuation directions, while maximizing the flexibility in the actuation direction in order not to sensibly reduce the maximum displacements producible by the piezo actuators, as will be discussed in Section 4.1.

The following subsections cover the work conducted to identify a suitable hinge geometry and to develop supporting tools for the study of the hinge stiffness with the purpose of adequately guiding the sizing and positioning of these mechanical components within the fixture frame.

3.2.1. Flexure hinges configurations

Precision positioning dedicated literature provides an extensive discussion of all the alternative hinge geometries that could be exploited to achieve the desired motion of the guiding systems [63,69]. Flexure hinges of single-axis, such as the one needed for the specific application, can be divided into two main categories: leaf and notch type hinges. Because of relative low rotation precision and stress concentration, leaf type hinge is seldom adopted [70,71]. Figure 3.5 shows some of the different geometries commonly used in notch type flexure hinges.

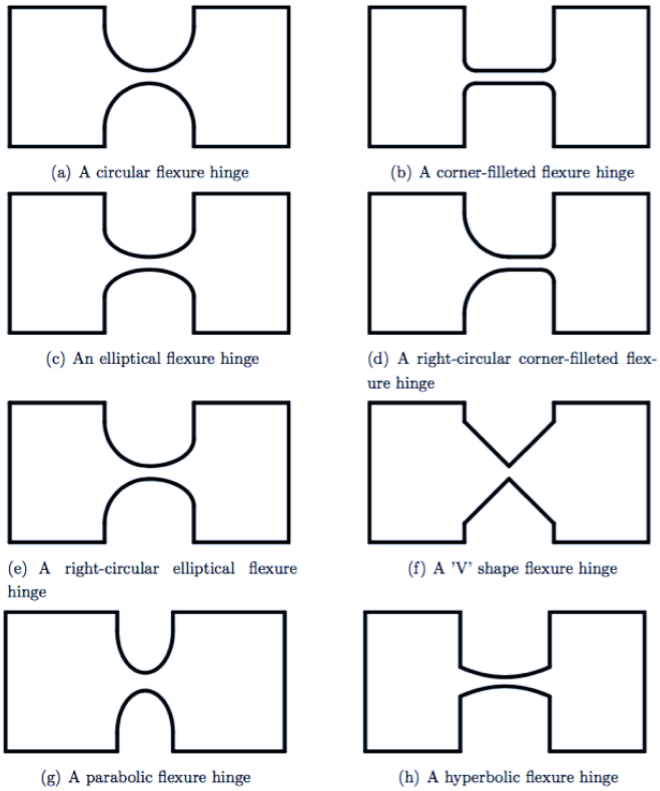

Figure 3.5: Notch type flexure hinges with different geometries [71]**.**

All these flexure hinges are usually employed to provide the relative rotation between adjacent rigid members, as common rotational joints. Nevertheless, more complex motion features can be achieved as a function of the hinge geometry, that should also consider the force needed to produce the desired compliance (i.e., hinge stiffness) and the stress distribution along the hinge itself. Moreover, the flexure hinges can be arranged in serial configurations in order to achieve a pure translational motion and reduce stress-stiffening effects [67], as shown in Figure 3.6. A similar configuration was used in an AWH application by Long et al. [59].

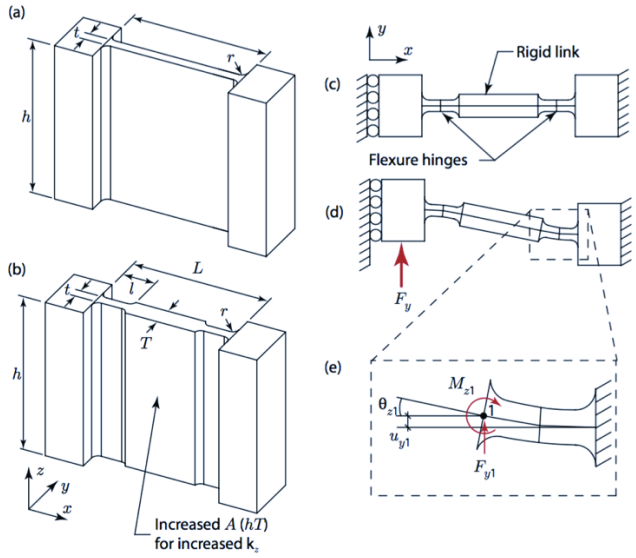

Figure 3.6: Examples of corner-filleted flexure hinge configurations: (a) trimetric view of constant cross section corner-filleted flexure beam, (b) trimetric view of corner-filleted serial-compliant flexure, (c) top view, (d) top view with applied load, and (e) expanded view of corner-filleted [63]**.**

The dedicated literature provides also some comparative study that could support the geometry selection for the given application [69,72,73]. According to those literature contributions, corner-filleted flexure hinges seem to represent the best compromise in terms of achievable compliance, stress distribution and stiffness. As an example, the work of Schotborgh et al. [72] showed that, compared to a circular flexure hinge of equivalent geometry, a corner-filleted flexure hinge is approximately equally stiff in rotation, while providing two times higher stiffness along *X*-direction (i.e., hinge axis, as also shown in Figure 3.6) and a 10% higher stiffness along *Z*-direction for the majority of geometries. In general, based on the stress and stiffness analysis presented in the mentioned work, corner filleted flexure hinges should be preferred over circular ones. Contextualizing such features in our specific applications, a corner-filleted flexure hinge would allow the same flexibility along the actuation directions, while increasing the stiffness along all the other directions. The fillets at the hinge extremities would also grant an adequate stress-distribution that would be proficient from a fatigue life point of view.

Taking those considerations into account, and neglecting the potential loss in terms of motion accuracy that are not the main design requirement of the AVC application, corner-filleted flexure hinges were preferred to other geometries. This was also motivated by the fact that those flexures should serve mainly as prismatic joints within the selected serial kinematic architecture. Nevertheless, a serial arrangement of corner-filleted flexure hinges was discarded mainly due to the fact that their integration within the AWH frame would have required additional space and the increased flexibility would have made the fixture more prone to the bending modes for witch the inner stage bends out of the fixture plane, as highlighted by Kenton and Leang [67].

3.2.2. Derivation of empirical stiffness equations

The design of flexure hinges is usually aided by dimension-less graphs and empirical equations that give support for the selection of suitable geometrical parameters capable of ensuring the desired compliance and stiffness [73–75]. Nevertheless, most of the literature works are targeted to precision positioning applications, hence investigating mainly the stiffness along the compliant plane (i.e., translation along *X* and *Y* directions and rotation about *Z*, as shown in Figure 3.7). Moreover, the range of geometries investigated is usually too narrow and consistent only with precision positioning applications: in this specific AVC applications, indeed, the active fixture may need to withstand relevant cutting forces, hence the out-of-plane bending plays a relevant role. In that sense, the effect of the hinge height (i.e., *H* in Figure 3.7) needs to be investigated more accurately.

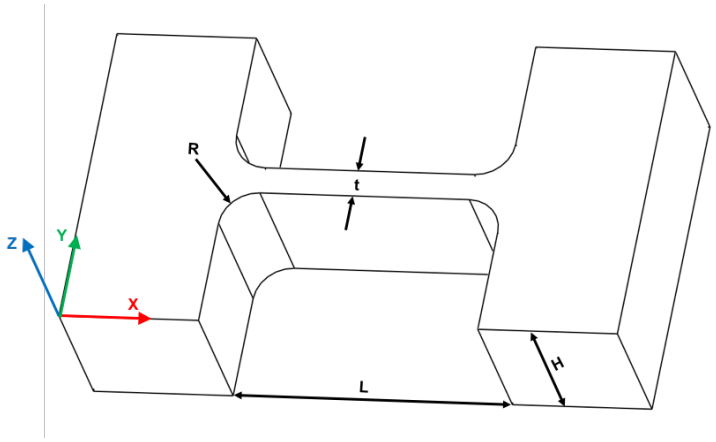

Figure 3.7: Geometrical parameters of a corner-filleted hinge geometry.

Considering the poor applicability of literature solutions in supporting the AWH design, dedicated empirical equations where derived in order to have a complete definition of the hinge stiffness along the 3 DOFs as a function of hinge geometrical parameters. Alternative approaches can be pursued to derive an empirical formulation of the hinge compliance/stiffness, for example by integrating the linear differential equations of a beam [68], or by following the Castigliano's first and second theorems [74,76] or using the inverse conformal mapping technique [77]. Each of these methods has shown to provide good results only in limited dimensional ranges, while methods based on regression analysis and Finite Element Analysis (FEA) have provided higher accuracy and flexibility, according the application reported for both circular [78] and corner-filleted [75] flexure hinges.

Accordingly, the derivation of dedicated empirical stiffness equations for the corner-filleted flexure hinges was conducted exploiting regression analysis on FEA data, investigating a range of geometrical parameters consistent with the AWH application, as previously mentioned. A set of dimensionless geometrical parameters was defined, as common practice, in order to reduce the number of independent variables, hence simplifying the regression analysis. Moreover, the dimensionless analysis would allow extending the general applicability of the derived relations, disregarding the specific geometry investigated. Using the hinge length as a basis (i.e., *L* in Figure 3.7), the defined dimensionless parameters are: *R/L*, *t/L*, *H/L,* respectively representing the dimensionless hinge fillet radius, the

dimensionless hinge thickness and the dimensionless hinge height. The investigated ranges of dimensionless parameters are:

0.2<R/L<0.5,

0.1<t/L<0.35,

0.5<H/L<1.

This ranges of dimensionless geometrical parameters allowed the simultaneous investigation of both corner-filleted and circular flexure hinges (i.e., *R/L* = 0.5), while the *H/L* range was defined considering that the hinge height should be consistent with the required stiffness along the *Z* axis, as previously mentioned. The *t/L* range was defined taking into account the specific application, that demands for the lowest possible stiffness along the Y axis in order not to compromise the actuator performance, as mentioned. Ten equally spaces values for each dimensionless parameter were investigated within the proposed ranges.

In order to preliminary assess the dependency on the hinge geometry of the stiffness along the 3 DOFs, an equivalent cantilevered beam, shown in Figure 3.8, was analyzed.

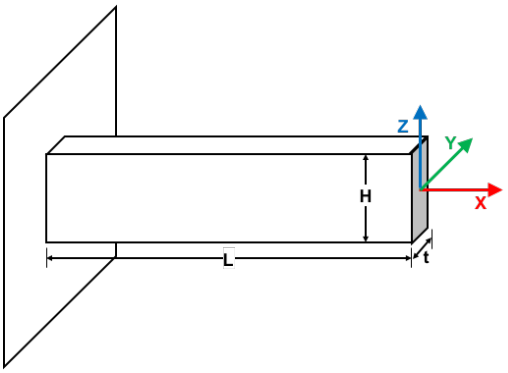

Figure 3.8: Equivalent beam for the preliminary assessment of hinge stiffness.

According to elementary beam theory [79], the six stiffnesses along the 3 DOFs for the equivalent beam shown in Figure 3.8 can be expressed as follows:

$$
\begin{aligned}
K_x &= \frac{EtH}{L} \\
K_y &= \frac{Et^3H}{L^3} \\
K_z &= \frac{EtH^3}{L^3} \\
K_{\varphi x} &= \frac{GtH(t^2+H^2)}{12L} \\
K_{\varphi y} &= \frac{EtH^3}{3L} \\
K_{\varphi z} &= \frac{Et^3H}{3L}
\end{aligned}
\qquad \textbf{(3.1)}
$$

where K_x, K_y and K_z represent the translational stiffness along the X, Y and Z axes respectively, while $K_{\varphi x}$, $K_{\varphi y}$ and $K_{\varphi z}$ represent the rotational stiffness along the coordinated axes.

By rearranging equations (3.1) as a function of the dimensionless geometrical parameters, we derive the following dimensionless stiffness formulations:

$$\begin{aligned}
&\frac{K_x}{EH} = \frac{t}{L} \\
&\frac{K_y}{EH} = \left(\frac{t}{L}\right)^3 \\
&\frac{K_z}{Et} = \left(\frac{H}{L}\right)^3 \\
&\frac{K_{\varphi x}}{GL^3} = \frac{1tH}{12L}\left(\frac{t}{L}\right)\left(\frac{H}{L}\right)\left[\left(\frac{t}{L}\right)^2 + \left(\frac{H}{L}\right)^2\right] \\
&\frac{K_{\varphi y}}{EH^3} = \frac{1}{3}\left(\frac{t}{L}\right) \\
&\frac{K_{\varphi z}}{Et^3} = \frac{1}{3}\left(\frac{H}{L}\right)
\end{aligned} \tag{3.2}$$

The derived dimensionless stiffness formulations, reported in equation (3.2), could assist the definition of suitable regressors orders in the regression analysis, which would be needed in order to investigate also the influence of the *R/L* parameter, which cannot be included in such a simplified formulation.

As anticipated, the regression analysis was carried out on FEA data. A convergence analysis was preliminarily conducted in order to assess the minimum mesh size requirements needed to ensure accurate results. In order to maintain the desired mesh refinement for each hinge geometry tested, the mesh size was parametrically defined in dependency of the hinge thickness (i.e., *t*), which represents the smallest geometrical feature of the model. The mesh size was hence defined as *t/4* in order to ensure that the hinge thickness is always meshed with an adequate number of elements (i.e., four elements, according to the preliminary convergence analysis carried out).

Analogously, the definition of correct boundary conditions is mandatory to achieve adequate accuracy: particularly, the border effects need to be mitigated by applying loads and constraints on additional overhangs at the hinge extremities, as discussed by Meng et al. [75] and Yong et al. [78]. Again, after a preliminary convergence analysis, a parametric model was used to size the additional overhangs, hence the distance between the load/constraints and the hinge itself, as a function of the specific hinge geometry, as shown in Figure 3.9.

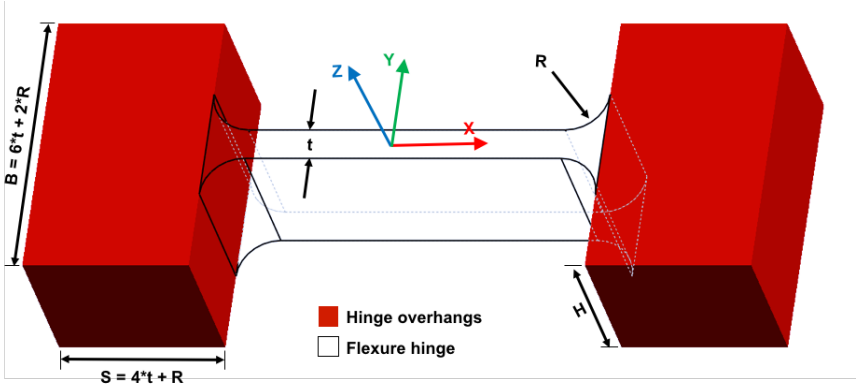

Figure 3.9: Parametric definition of hinge overhangs to reduce border effects in the FEA.

MSC Nastran was used as Finite Element (FE) solver. Figure 3.10 shows the actual model layout used of the FEA: a unit load was applied at the end of the overhang extremity (i.e., node 4 in Figure 3.10), while the opposite part was constrained along all the 6 DOFs (i.e., node 1). Interpolation constraint elements (i.e., RBE3 [80]) were used to distribute loads and constraints as a weighted average to all the elements on the external faces of the hinge overhangs, as shown in Figure 3.10 and Figure 3.11.

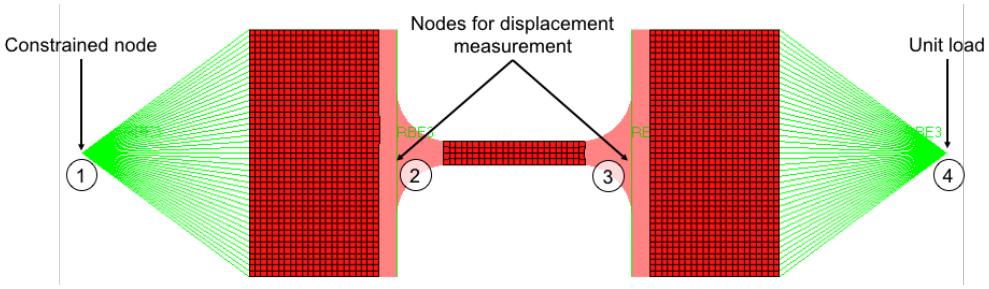

Figure 3.10: Hinge modelling layout (hinge extremity shaded for sake of clarity, the shaded part is meshed in the actual FE model used).

Analogously, the measurement of the generated hinge displacement was averaged with RBE3 elements on the basis of the displacements of the elements on the inner faces of the hinge, as shown more in detail in Figure 3.11. In order to cleanse the actual displacement generated by the hinge from the contributions of the overhangs parts, the displacement measurements were made at the hinge extremities on both the loaded and constrained sides (i.e., respectively node 3 and 2 in Figure 3.10). The actual value of the generated hinge displacement is computed by subtracting the displacement measured on the constrained side (i.e., node 2) from the one measured on the loaded side (i.e., node 2), as proposed by Yong et al. [78].

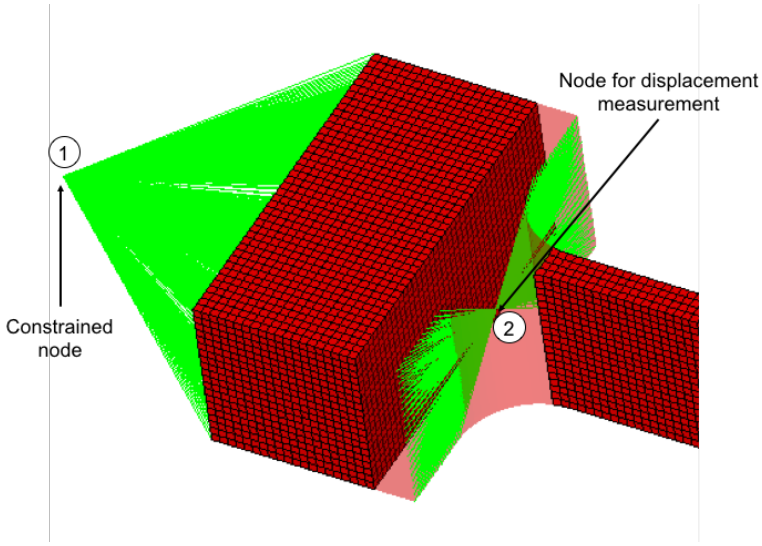

Figure 3.11: Detail of the rigid interpolating elements used to distribute loads/constraints and to average the measured displacements (hinge extremity shaded for sake of clarity, the shaded part is meshed in the actual FE model used).

As anticipated, a set of one thousand different hinge geometries was investigated and a regression analysis was used to estimate polynomial empirical equations describing hinge stiffness as a function of the dimensionless geometrical parameters. Minitab software was used for the purpose since it makes available dedicated tool boxes to simplify the definition of suitable regressors. In addition, dedicated Matlab routines, based on the Matlab curve fitting toolbox, were used to analyze the errors induced by the fitted stiffness equations with respect to the results of the numerical analysis, as shown in the following.

Third order polynomials ensured adequate accuracy for most of the dimensionless stiffness investigated, only $\frac{K_y}{EH}$ and $\frac{K_{\varphi z}}{Et^3}$ imposed the use of higher order polynomials (i.e., fourth and fifth order respectively) to improve the fitting accuracy. Anyway this is in line with the previous literature results, where even higher order polynomials are used [75,78].

Figure 3.12 reports the residual plots for the regression analysis of the dimensionless stiffness along the hinge translational axis (i.e., K_y). Similar results were obtained for the other stiffnesses and are here not reported for sake of synthesis.

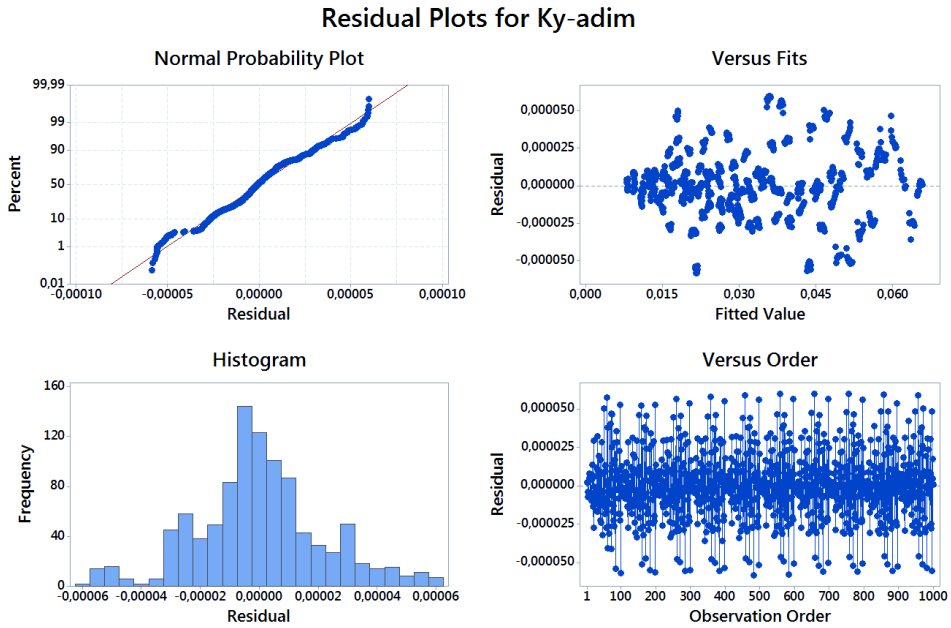

Figure 3.12: Residual plot for the regression analysis of dimensionless K_Y hinge stiffness.

As shown in Figure 3.13, the resulting errors for all the fitted stiffnesses are below 0.3%, which is lower than the ones proposed by Meng et al. in their work [75] and absolutely acceptable for the given application.

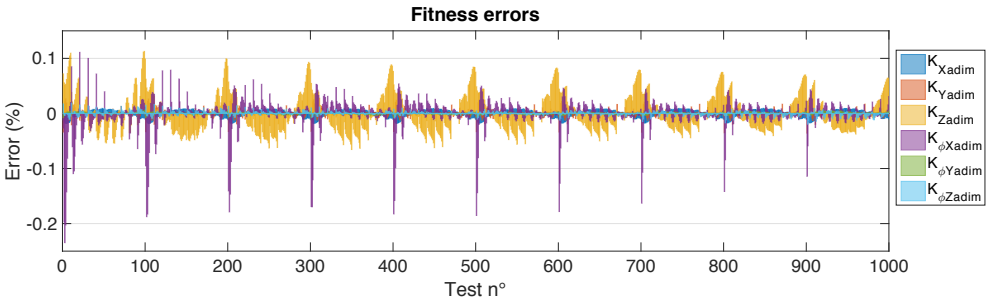

Figure 3.13: Fitness errors of each dimensionless stiffness (see Eq. (3.2)) for the tested hinge geometries.

As an example of the achieved results, Figure 3.14 shows the response surfaces of the dimensionless stiffness along the flexure hinge translational axis (i.e., K_y) based on data computed both with FEA and the identified empirical equations. As shown, the two surfaces are in good agreement disregarding the dependency over the given dimensionless geometrical parameters.

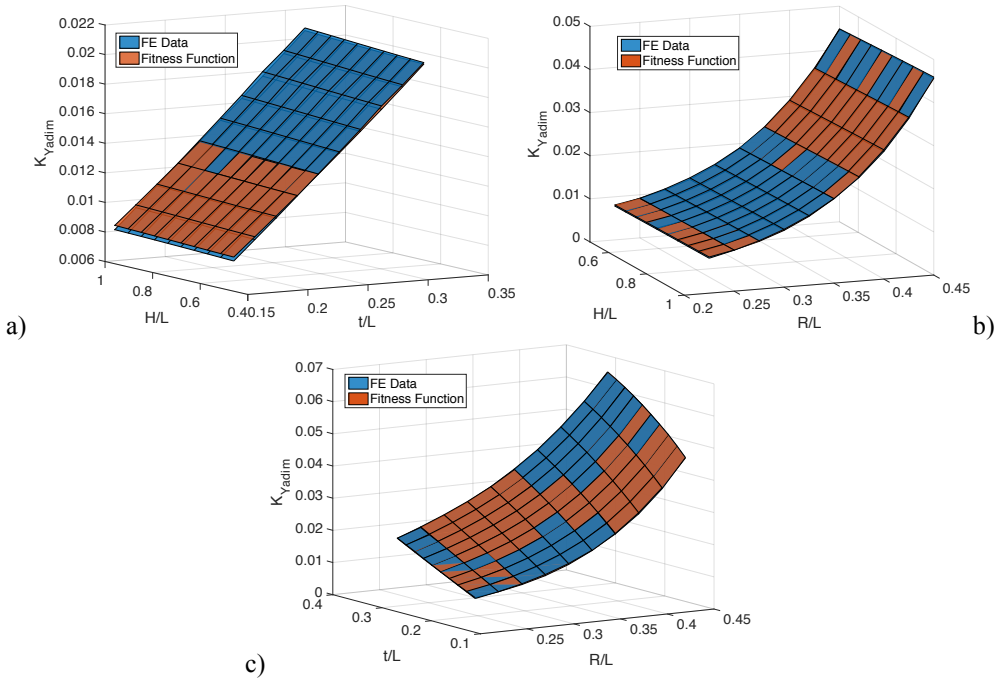

Figure 3.14: Surface responses of both FE data and estimated data for the dimensionless K_Y stiffness (along the hinge translational axis) for: a) constant *R/L*, b) constant *t/L*, c) constant *H/L*.

The derived empirical equations for the six dimensionless stiffnesses are:

$$\frac{K_x}{EH} \approx 0.0909\frac{R}{L} + 0.3264\frac{t}{L} - 0.0893\left(\frac{R}{L}\right)^2 + 0.0747\left(\frac{R}{L}\right)^3 + 0.0021\frac{t}{L}\frac{R}{L} - 0.0197\left(\frac{R}{L}\right)^2\frac{t}{L} \tag{3.3}$$

$$\frac{K_y}{EH} \approx 0.0211 - 0.0123\frac{R}{L} - 0.182\left(\frac{R}{L}\right)^2 + 0.2013\left(\frac{R}{L}\right)^3 - 0.0011\frac{H}{L} - 0.2331\frac{t}{L} + 0.30305\left(\frac{t}{L}\right)^2 + 0.0457\left(\frac{t}{L}\right)^3 - 0.0023\frac{t}{L}\frac{H}{L} + 0.0023\frac{R}{L}\frac{H}{L} + 0.0026\left(\frac{H}{L}\right)^2\frac{t}{L} + 0.0023\left(\frac{H}{L}\right)^2\frac{R}{L} - 0.0014\left(\frac{H}{L}\right)^3\frac{R}{L} + 0.785\frac{t}{L}\frac{R}{L} - 0.2585\left(\frac{R}{L}\right)^2\frac{t}{L} - 0.6713\left(\frac{t}{L}\right)^2\frac{R}{L} \tag{3.4}$$

$$\frac{K_z}{Et} \approx -0.0022\frac{t}{L} - 0.054\frac{H}{L} + 0.0194\frac{R}{L} + 0.0776\left(\frac{H}{L}\right)^2 - 0.0686\left(\frac{R}{L}\right)^2 + 0.0171\left(\frac{H}{L}\right)^3 + 0.0249\left(\frac{R}{L}\right)^3 + 0.0137\frac{t}{L}\frac{R}{L} + 7\frac{t}{L}\frac{H}{L} + 0.0945\frac{R}{L}\frac{H}{L} - 0.1712\left(\frac{H}{L}\right)^2\frac{t}{L} + 0.0644\left(\frac{R}{L}\right)^2\frac{t}{L} - 0.2644\frac{R}{L}\frac{H}{L}\frac{t}{L} \tag{3.5}$$

$$\frac{K_{\varphi x}}{GL^3} \approx -0.0716\frac{t}{L} - 0.0063\frac{R}{L} + 0.0282\frac{H}{L} - 0.0075\left(\frac{H}{L}\right)^2 + 0.0139\left(\frac{R}{L}\right)^2 + 0.0452\left(\frac{t}{L}\right)^2 - 0.0007\left(\frac{H}{L}\right)^3 - 0.0063\left(\frac{R}{L}\right)^3 - 0.1223\left(\frac{t}{L}\right)^3 - 0.1031\frac{t}{L}\frac{R}{L} - 0.1124\frac{t}{L}\frac{H}{L} - 0.055\frac{R}{L}\frac{H}{L} + 0.027\left(\frac{H}{L}\right)^2\frac{t}{L} + 0.0277\left(\frac{R}{L}\right)^2\frac{t}{L} + 0.0238\left(\frac{R}{L}\right)^2\frac{H}{L} + 0.01\left(\frac{H}{L}\right)^2\frac{R}{L} + 0.1595\left(\frac{t}{L}\right)^2\frac{H}{L} - 0.0278\left(\frac{t}{L}\right)^2\frac{R}{L} + 0.0932\frac{R}{L}\frac{H}{L}\frac{t}{L} \quad (3.6)$$

$$\frac{K_{\varphi y}}{EH^3} \approx 0.0107 + 0.0636\frac{t}{L} - 0.0082\frac{H}{L} + 0.0073\frac{R}{L} - 0.0617\left(\frac{t}{L}\right)^2 + 0.0053\left(\frac{R}{L}\right)^2 - 0.0201\frac{t}{L}\frac{R}{L} + 0.0103\frac{t}{L}\frac{H}{L} - 0.0002\frac{R}{L}\frac{H}{L} \quad (3.7)$$

$$\frac{K_{\varphi z}}{Et^3} \approx -0.8833 + 5.7848\frac{t}{L} + 4.8694\frac{H}{L} + 0.0067\frac{R}{L} - 8.9492\left(\frac{R}{L}\right)^2 - 9.2749\left(\frac{t}{L}\right)^2 + 5.7249\left(\frac{R}{L}\right)^3 - 30.3018\frac{t}{L}\frac{R}{L} + 55.4781\left(\frac{R}{L}\right)^2\frac{t}{L} - 33.4766\left(\frac{R}{L}\right)^3\frac{t}{L} + 48.8849\left(\frac{t}{L}\right)^2\frac{R}{L} - 88.2899\left(\frac{R}{L}\right)^2\left(\frac{t}{L}\right)^2 + 51.7811\left(\frac{R}{L}\right)^3\left(\frac{t}{L}\right)^2 \quad (3.8)$$

3.2.3. **Simplified modelling strategy of flexure hinges**

The purpose of identifying the empirical stiffness equations for the flexure hinges was twofold: on the one hand it was needed to assess the effect of the hinge geometry in defining its stiffness and to support the selection of suitable geometrical parameters, as previously discussed. On the other hand, the derived stiffness values could be used in simplified numerical models of the flexure hinges that can be exploited in the preliminary design phase, for example with the purpose of efficiently optimizing the hinge number and positioning within the fixture frame in order to achieve the desired dynamic response. The mesh refinement of detailed FE models of the active fixture would indeed be somehow imposed by the small geometrical features of the flexure hinges. Full detailed FE models would hence be characterized by a higher number of elements that would return a high computational cost, directly impacting on the time needed for the iterations generally involved in the preliminary design phases. Moreover, investigating alternative hinge positioning within the fixture frame would imply iterative remeshing that would make the preliminary design both time consuming and hardly automable (e.g., hardly implementable in optimization procedures).

The simplified modeling strategy should hence address these two issues: by simply using spring elements, indeed, the hinge stiffness can be included in the model with a simplified formulation without requiring the hinge to be fully meshed. Nevertheless, such approach would make the stiffness of the spring element intrinsically depend on the spring element length (i.e., hinge length). In practice, this aspect translates in the fact that investigating the effect of hinges with different lengths would impose to change the actual spring element length, hence the geometry of the surrounding frames, resulting in the need of remeshing it.

This issue could be worked around by employing the Direct Matrix Input technique (DMIG in MSC Nastran solver [80]) that allows defining a stiffness matrix relating two nodes of the FE model. The stiffness matrix to be defined for the DMIG elements used for

the reduced hinge models can be defined as the 12x12 matrix reported in equation (3.9) (i.e., 6 DOFs for each of the two nodes):

$$\begin{bmatrix}
K_x & 0 & 0 & 0 & 0 & 0 & -K_x & 0 & 0 & 0 & 0 & 0 \\
0 & K_y & 0 & 0 & 0 & lK_y & 0 & -K_y & 0 & 0 & 0 & lK_y \\
0 & 0 & K_z & 0 & -lK_z & 0 & 0 & 0 & -K_z & 0 & -lK_z & 0 \\
0 & 0 & 0 & K_{\varphi x} & 0 & 0 & 0 & 0 & 0 & -K_{\varphi x} & 0 & 0 \\
0 & 0 & -lK_z & 0 & K_{\varphi y} + l^2K_z & 0 & 0 & 0 & lK_z & 0 & l^2K_z - K_{\varphi y} & 0 \\
0 & lK_y & 0 & 0 & 0 & K_{\varphi z} + l^2K_y & 0 & -lK_y & 0 & 0 & 0 & l^2K_y - K_{\varphi z} \\
-K_x & 0 & 0 & 0 & 0 & 0 & K_x & 0 & 0 & 0 & 0 & 0 \\
0 & -K_y & 0 & 0 & 0 & -lK_y & 0 & K_y & 0 & 0 & 0 & -lK_y \\
0 & 0 & -K_z & 0 & lK_z & 0 & 0 & 0 & K_z & 0 & lK_z & 0 \\
0 & 0 & 0 & -K_{\varphi x} & 0 & 0 & 0 & 0 & 0 & K_{\varphi x} & 0 & 0 \\
0 & 0 & -lK_z & 0 & l^2K_z - K_{\varphi y} & 0 & 0 & 0 & lK_z & 0 & K_{\varphi y} + l^2K_z & 0 \\
0 & lK_y & 0 & 0 & 0 & 0 & 0 & -lK_y & 0 & 0 & 0 & K_{\varphi z} + l^2K_y
\end{bmatrix} \quad (3.9)$$

As shown, the reduced stiffness matrix includes the hinge stiffness, which can be estimated with the previously described empirical equations, and the hinge length. In contrast with the simple spring element previously mentioned, this formulation intrinsically includes the hinge length which can be modelled without the need of matching it with the actual FE model geometry. To clarify, referring to Figure 3.15 the distance between node 2 and node 3 can be kept unaltered while different hinge geometries, including different hinge lengths, can be virtually changed by recomputing the reduced stiffness matrix accordingly. By doing so, the geometry of the frame surrounding the flexure hinges would not be changed, avoiding the need of remeshing it. Moreover, as in the case of simple spring elements, the use of simplified models would allow reducing the FE model size given that the small geometrical features of the hinge itself would not need to be accurately meshed, as exemplified in Figure 3.15. This would obviously return a drastic reduction in terms of computational time.

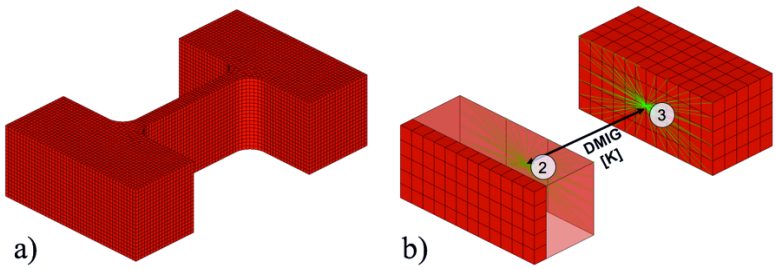

Figure 3.15: Exemplification of the reduced hinge FE model. a) Fully meshed flexure hinge with mesh size defined by hinge thickness (model size: 40400 elements), b) reduced hinge model with DMIG matrix relating node 2 and 3 (model size: 600 elements. Partly shaded for sake of clarity).

Static and dynamic analyses were carried out on a test hinge geometry (i.e., R/L=0.45, H/L=1, t/L=0.1) to assess the equivalence between the proposed reduced model and the full FE model. The results of the static and dynamic analysis are reported in Table 3.1 and Table 3.2 respectively.

Table 3.1: Static equivalence results.

	Static Stiffness [N/mm]		
	Full Model	**Reduced Model**	**Error**
K_x	299523	299523	0.0%
K_y	7174	7153	0.3%
K_z	31175	29524	5.3%
$K_{\varphi x}$	575406	575406	0.0%
$K_{\varphi y}$	12340827	12582683	2.0%
$K_{\varphi z}$	1923304	1908684	0.8%

Table 3.2: Dynamic equivalence results.

	Eigen − Frequency [Hz]		
	Full Model	**Reduced Model**	**Error**
Mode 1	1340	1409	5.1%
Mode2	2011	2020	0.4%
Mode 3	5340	5696	6.7%
Mode 4	8063	8698	7.9%
Mode 5	14720	14470	1.7%
Mode 6	18140	16590	8.5%

As shown, the errors induced by the model reduction is actually negligible for a static analysis, while it gets higher in the dynamic analysis, mainly due to the fact that the hinge mass is not accurately modeled in the reduced model. Nevertheless, the proposed reduction strategy could represent a useful tool in the early design phase, since it would allow time efficient testing of alternative geometries. The following detailed design phase could indeed exploit full FE model to more accurately assess the fixture performance, for example in terms of dynamic response, overcoming the errors induced by the simplification strategy.

Accordingly, the simplified numerical models were used to define a suitable fixture geometry and the related hinge dimensioning/positioning in the early design stage. Detailed FE model were then used to accurately assess the dynamic response of the AWH prototype and estimate the achievable bandwidth, as will be discussed in the following chapter.

4. Active fixture detailed design, modeling and assembly

This chapter covers the main design aspects of the developed AWH prototype, from the selection of suitable actuation devices to the detailed design of the fixture frame, aided by dedicated FE models with the purpose of extending the device bandwidth and investigating the dynamic response.

4.1. Actuators selection

The choice of suitable actuators was a crucial task of the whole design process as it had relevant influence on the further mechanical design. Many different actuation technologies are nowadays available, offering different features: the most important characteristics for this application are efficiency, bandwidth, ‘‘passive’’ mechanical stiffness and compactness (power density). Smart materials in that sense offer peculiar advantages [81,82], even though each specific technology show specific limitations. Shape Memory Alloys (SMA), for example, are capable of very high energy densities and can deliver large forces over long distance, but their energy efficiency is poor, returning high current needs and higher temperature issues [83]. Similarly, actuators based on magnetostrictive materials, usually referred to as Giant Magnestostrictive Actuators (GMAs), have high force and strain capabilities and they can operate at low voltages, but the power requirements are greater than piezoelectric materials and they are more expensive compared to the alternatives based on other smart materials. In comparison, piezoelectric materials have faster response, higher stiffness and larger force output, as clearly highlighted by Yao et al. [83]. The energy density is higher than SMAs and the electric current requirement is very low in static or quasi static status, which helps to alleviate heating problems. Furthermore, the energy conversion efficiency is higher since electrical energy is directly transformed into mechanical energy. One of the primary concerns when using piezoelectric actuators is their very small displacement output. For a piezoelectric ceramic block, the maximum strain capability is about 0.1%. Nonetheless, the displacement output can be generally increased through the use of lever transmission mechanisms that would in return lower the actuator stiffness. A comparison between the mentioned smart materials is summarized in Table 4.1 [49].

Considering the discussed features, piezoelectric actuators seem to represent the most suitable technology for the specific application. It should also be considered that nowadays piezo technology is supported by an adequate commercial offer from several vendors, confirming the maturity of this actuation technology.

Table 4.1: Comparison of different smart actuators.

	Efficiency	Speed	Power density	Stiffness
Electro-magnetic	High	Fast	Medium	Low
Electrostatic	High	Fast	Low	Low
Piezoelectric	High	Very fast	High	High
Shape memory	Low	Slow	Very high	Medium
Magnetostrictive	Medium	Medium/fast	Medium/high	High

Even though piezo actuators show major advantages, some specific aspects need to be carefully considered in selecting a suitable piezo actuator for demanding dynamic applications, such as the one of interest in this work.

As an example, self-heating phenomenon is a renowned issue for dynamic applications and should be carefully regarded since it can induce deformations in the piezoelectrical microcomponents that can reach the order of magnitude of the deformations coming from the electrical actuation itself [84]. Moreover, the electromechanical and electrical properties of a piezoelectric actuator can sensibly vary with temperature [63], as exemplified in Figure 4.1, compromising the achievable performance and reliability.

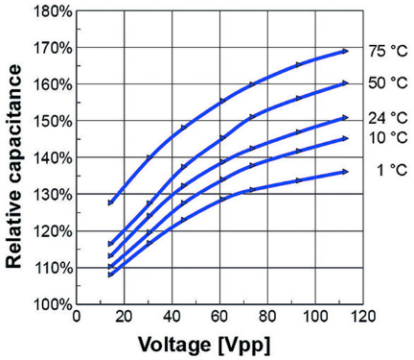

Figure 4.1: Relative capacitance values for different actuator temperatures (source: www.piceramic.com).

The usual approach to prevent or mitigate this issue is based on dedicated heat management, such as creative heat sink designs, that should not hinder the motion of the actuator though, or by means of specialized actuator configurations, such as the "ThermoStable" technique commercially offered by American Piezo [85]. This aspect gets particularly relevant for high-frequency applications, such as ultrasonic piezo motors. The average thermal power generated in dynamic applications can indeed be approximated as:

$$P_{therm} = \frac{\pi}{4} \cdot tan\delta \cdot f \cdot C \cdot V_{pp}^2 \tag{4.1}$$

where f is the frequency the actuator is operated at, C is the actuator capacitance, V_{PP} is the peak-top-peak voltage provided to the actuator and $tan\delta$ is the dielectric dissipation factor of the employed piezo ceramic.

For the frequency range of interest in the AWH application, an alternative solution is represented by actuators based on hard doped PZTs (i.e., lead zirconate titanate

(Pb[Zr(x)Ti(1-x)]O3) ceramics) that show lower dielectric dissipation factors and lower capacitance values, which can be expressed for a stacked piezo actuator as:

$$C = n \cdot \varepsilon_{33}^{T} \cdot \frac{A}{d_s} \tag{4.2}$$

where n is the number of stacks, d_s is the layer (i.e., stack) height, A is the actuator cross-sectional area, and ε_{33}^{T} is the PZT permittivity.

A comparison between different types of piezo ceramic is reported in Table 4.2 [86].

Table 4.2: Comparison of different piezo ceramics (data extracted from standard catalogue material data). Pz21 and Pz29 are very soft PZTs, Pz27 is a medium-soft PZT, Pz24 and Pz26 are hard doped PZTs.

PZT ceramic	Pz21	Pz24	Pz26	Pz27	Pz29
ε_{33}^{T}	3800	400	1300	1800	2900
$tan\delta$ (%)	1.8	0.2	0.3	1.7	1.9

It should also be considered that the lower capacitance values of hard doped PZTs would foster the matching of the piezo actuators with adequate piezo amplifiers/drivers, given that the current demand in dynamic application will be consequently lower. The maximum current required in pure sinusoidal applications can indeed be expressed as:

$$I_{max} = \pi \cdot f \cdot C \cdot V_{pp} \tag{4.3}$$

Considering the mentioned advantages and the commercial availability, stacked piezo actuators made of NCE46 hard doped PZT have been selected (i.e., Noliac SCMAP-NCE46-10-10-2-200-H36-C01) for this specific application. The main specification of the selected actuators are reported in Table 4.3.

Table 4.3: Main specifications of the selected piezo actuators (referred to a single actuator).

Blocking force	Dimensions (WxHxL)	Maximum displacement	Maximum voltage	Stiffness	Capacitance
3200 N	10x10x36mm	32 μm	200 V	100 N/μm	5400 nF

The blocking force value, which represents the maximum force theoretically producible by the actuators when no strain is allowed, would suggest that a single actuator should be capable of counteracting cutting forces in most applications, excluding demanding high feed rough-milling for example. In dynamic applications, though, inertial forces could represent a major force contribution to be counteracted, hence the blocking force of a single piezo actuator could be not sufficient. Given that the purpose of this work was to increase the device bandwidth as much as possible, four actuators were chosen for the integration in each AWH axis, in order to reach a theoretical maximum force of approximately 13 kN that was considered to be adequate for the purpose. Alternatively, a single piezo actuator with equivalent cross section could have been selected, given that the blocking force is approximately related to the cross section only. From this point of view, the choice is mainly driven by the commercial offer of the piezo actuator vendors.

Obviously, by increasing the number of piezo actuators, the total capacitance to be driven by the piezo amplifier increases accordingly. The matching with the piezo driver appears hence to be even more crucial in order to exploit the maximum performance over the widest possible frequency range. A pair of Noliac NDR6880 piezo amplifiers has been selected to drive each AWH axis respectively. The driver specifications are reported in Table 4.4.

Table 4.4: Main specifications of the Noliac NDR6880 piezo drivers.

Output voltage (V_{out})	Load current	Frequency limit	Maximal capacitance	V_{out} Linearity
0-300 V	7 A (10 A peak)	0 – 6 kHz (-2dB)	200 μF	5 %

The integration of piezo actuators in the AWH poses specific requirements, especially in dynamic applications: the common PZTs are rather fragile material with respect to bending and shear stresses, hence adequate countermeasures must be adopted to prevent premature failures [87]. This aspect is even more relevant for stacked piezo actuators, often referred to as piezo stacks, where several discs of PZT are glued together and the shear resistance is practically demanded to the glue itself only. Analogously, piezo stacks cannot withstand relevant tensile stresses: manufacturers often suggest that the tensile load should be within 5%–10% of the compressive load limit in order to avoid damaging the stack. Neglecting these aspects could cause cracking of the ceramic material as well as separation of the layers.

Best practice suggests the use of guiding systems (e.g., flexures) to guide the motion generated by the piezo actuators while ensuring adequate prevention from bucking, bending and shear loads. In the present case, the flexure hinges integrated in the serial kinematic architecture, previously described, would also serve as guiding system for the actuators themselves. In addition, spherical hinges are often created at the actuator extremities to provide further decoupling with respect to shear and torsional stresses. All these aspects are summarized in the graphical mounting guidelines reported in Figure 4.2.

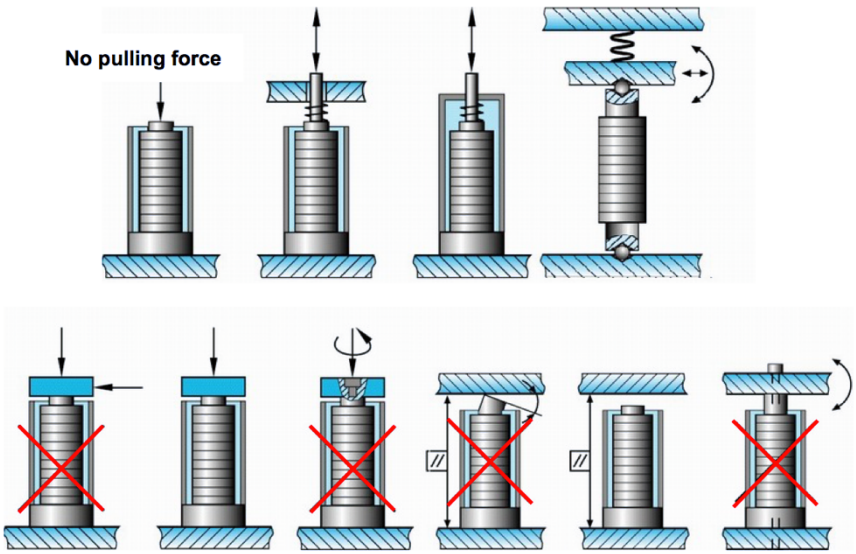

Figure 4.2: Mounting guidelines for stacked piezo actuators.

As shown in Figure 4.2, preloading of the piezo actuator is usually needed in order to keep the actuators under compression also when relevant inertial forces are generated (i.e., dynamic applications), hence preventing the onset of detrimental tensile stresses. As discussed by Yong et al. [63], the application of the required preload force is usually

achieved by either using dedicated mechanical solutions (e.g., set screws, as shown in Figure 4.3a) or by exploiting the pre-deformation of the flexure guiding systems [63,88]. In the latter case the preload on the piezo-stack actuator is achieved when it is first installed into the flexure-guided structure by pressing the piezo-stack against the flexures using fasteners (Figure 4.3b).

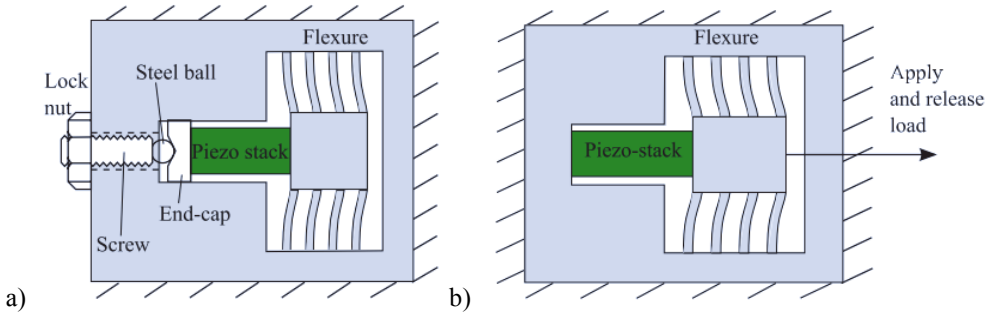

Figure 4.3: Alternative strategies for the application of the needed preload force. a) Preload applied by means of a dedicated set-screw, b) preload applied with the deformation of the flexures [63]**.**

In general precision positioning applications, the needed preload force can be estimated using Newton's second law [88]. For a pure sinusoidal actuation, the minimum preload force (i.e., the tensile peak force that the actuator would withstand without preload applied) can be computed according to:

$$F_{preload} \geq 4\pi^2 \cdot m_{eff} \cdot \frac{\Delta L}{2} \cdot f^2 \tag{4.4}$$

where, m_{eff} is the effective mass displaced by the piezo actuator, ΔL is the generated displacement and f is the actuation frequency.

On the one hand the minimum preload force can be computed exploiting Newton's second law, at least in traditional positioning applications. On the other hand, though, an upper limit for the maximum applicable preload force exists: the piezo ceramic could indeed withstand relevant compressive stresses (i.e., approximately 250 MPa in general [87]), but de-poling effect could arise already at 10-20% of the maximum allowable compressive load. Even though reduced de-poling effects are generally reversible when a large electrical load is applied to the PZT, long-term performance degradation is expected for excessive preload forces.

In the AWH application, the computation of the correct preload force is made even more complex by the fact that the actuators would be exposed also to cutting forces, with multiple frequencies (e.g., tooth pass frequency with the related harmonics and eventually chatter frequencies). Numerical simulations can be exploited for the purpose, as will be discussed in section 4.4.1. Considering the uncertainties related the preload force estimation at that stage, the use of commercially available encapsulated and preloaded actuators was discarded due to the fact that the pre-applied preload force would not be easily modifiable in that case. Moreover, the external dimensions would significantly increase, making their integration in the AWH more complex.

The means of applying the preload forces should be carefully regarded since the preload stiffness could affect the performance of the piezo actuators themselves. In

particular, the stiffness of the guiding systems (i.e., flexure hinges) and eventual preload springs could reduce the maximum generable displacement ΔL, according to:

$$\Delta L \approx \Delta L_0 \cdot \left(\frac{K_a}{K_a + K_s}\right) \tag{4.5}$$

where ΔL_0 is the nominal maximum actuator displacement, K_a is the actuator stiffness and K_s is the stiffness of the preload system (e.g., flexures and preload springs).

Generalizing, the effect of the additional stiffness in the systems affects the working point of the piezo actuator. This aspect is usually formalized in stroke/force diagrams, exemplified in Figure 4.4, that map the ideal performance of a given piezo actuator, according to the simplest formulation of the piezo actuator force, expressed as:

$$F_{piezo} = K_\varphi V - \left(\frac{K_a}{K_a + K_s}\right)\Delta L \tag{4.6}$$

where F_{piezo} represents the force generated by the piezo actuator, K_φ is the force generation coefficient and V is the voltage applied to the piezo actuator. As shown, in case of null displacement (i.e., $K_s = \infty$, equivalent to blocked conditions) the theoretical maximum force is generated (blocking force), while if $F_{piezo} = 0$ the voltage provided to the piezo actuators produces the maximum elongation.

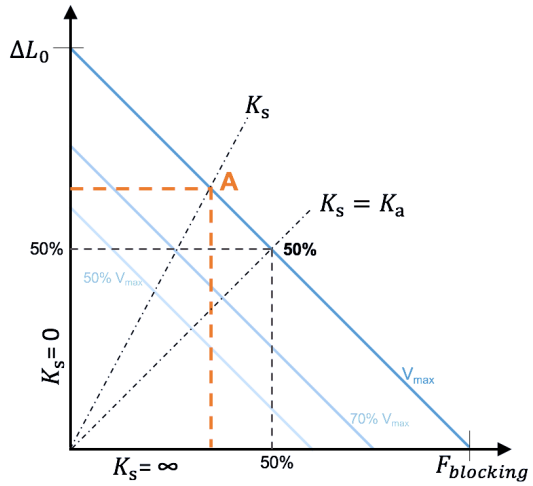

Figure 4.4: Stroke/force diagram for a piezo actuator, showing the variations of the working point (A) as a function of the preload stiffness (K_s) and for different driving voltages.

This proves once more the importance of accurately dimensioning the flexure hinges integrated in the AWH prototype, or in an analogous mechatronic device in general. As stated in the previous chapter, the flexure hinges should be as rigid as possible to avoid unwanted dynamic behavior of the AWH, such as low frequency out-of-plane bending modes. On the other hand, it appears now clear that the flexure hinge should show the lowest stiffness possible in order not to sensibly affect the maximum producible displacement of the piezo actuators. Suitable tools, such as the empirical equations and simplified numerical models discussed in the previous chapter, would hence sensibly aid the definition of adequate designs.

4.2. Detailed design

The detailed AWH prototype design was in the first phase driven by the specific requirements of the piezo actuators integrated in the fixture. As an example, the fixture frame should not only provide enough space for housing the four piezo actuators integrated in each of the actuated axis, but it should also integrate dedicated solutions to prevent shear and bending stresses on the actuators and to provide the required preload, as discussed in the previous section.

In order to accomplish adequate decoupling of the piezo actuators with respect to shear and bending stresses spherical joints were designed at the actuator ends: stainless steel hemi-spherical end-tips were glued at the actuators extremities (commercially available as a standard option on the selected piezo stack), as shown in Figure 4.5.

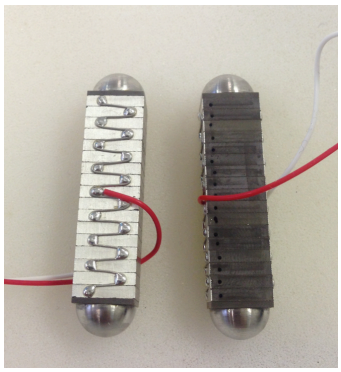

Figure 4.5: Detail of the selected piezo actuators including the optional hemi-spherical end-tips.

In addition, dedicated hemi-spherical supports were considered for both the fixture frame and the set screws designed to secure the actuators in place. A detailed view of the designed piezo actuators mounting is shown in Figure 4.6.

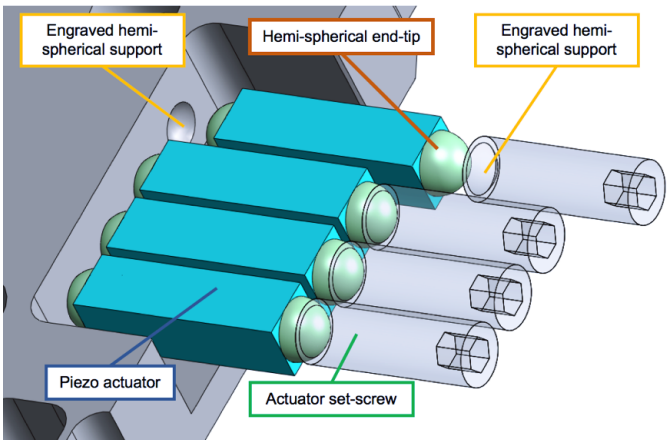

Figure 4.6: Designed spherical hinges at the actuators extremities to prevent shear and bending stresses.

Given that the actuators set screws would also serve to eventually adjust positioning of the piezo actuators, external fine threading (M8x1) was selected for the purpose.

For what concerns the application of adequate preload forces on the piezo actuators, specific subsystems were considered, instead of relying only on the integrated flexure deformations, previously discussed. This choice was mainly motivated by the fact that additional preload springs would allow to more easily manage the application of the required preload force over a wider force range (e.g., by simply changing the spring themselves). Moreover, is should be noted that, at this design stage, the number and geometry of the flexure hinges was not defined yet given that the geometry of the fixture frame itself was still to be defined in accordance with the size of the other components (e.g., preload arrangements). Thus, relying on the flexure deformation for the application of the preload force would have somehow constrained their design, that should instead be driven by other factors, such as the improvement of the fixture dynamic response or the reduction of the stiffness in the actuation directions, already discussed in the previous sections.

That said, following the work of Haase [62], the preload arrangement was designed to exert the force on the actuated stage (i.e., inner or intermediated stage in the serial kinematic architecture selected) opposite to the driving actuators. Belleville springs were selected to apply the preload, given that this type of springs offers several advantages, such as capability of generating large loads within a small installation space, proficient in reducing the overall device dimensions and masses, and the freedom in adjusting the stiffness by using creative stacking configurations or combination of springs with different geometries.

Instead of using a single disc spring stack, as proposed by Haase [62], the preload arrangement was designed as three independent disc spring stacks acting over the same surface, similarly to the AWH proposed by Abele et al. [10]. The motivation of this choice was twofold: on the one hand it allows a more uniform distribution of the preload force, reducing potential rotational motion contributions of the actuated stages. On the other hand, using three stacks in such a parallel configuration would allow reaching higher preload forces without needing to stack several disc springs in parallel on the single stacks. Parallel stacking of disc springs should, indeed, be generally reduced as much as possible in order to prevent the onset of relevant hysteresis due to friction between the springs surfaces (i.e., unequal relationship between the loading and unloading characteristics) [89]. The proposed solution for the preload arrangement is shown in Figure 4.7.

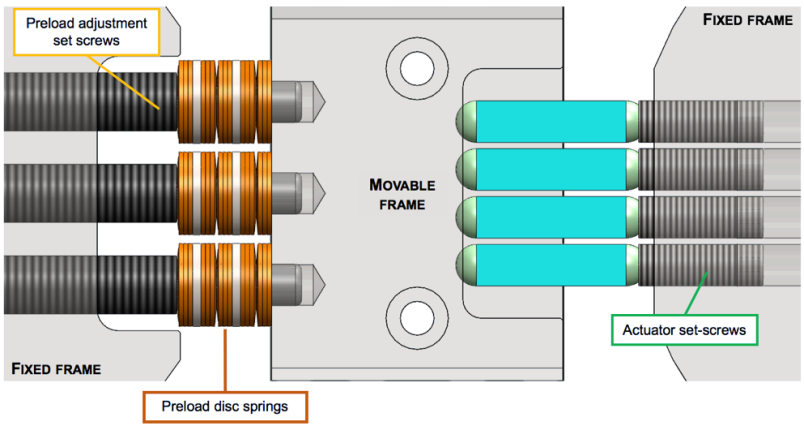

Figure 4.7: Detail of the Preload arrangement for the preloading of piezo actuators

An example of the manufactured preload springs set screws is shown and described in Figure 4.8. Again fine threading was considered in order to ease the adjustment of the preload forces. The designed set screws would not only allow the tuning of the preload force, but they should also serve as internal guides for the springs in order to increase the stack stability, as suggested by the spring manufacturer [90].

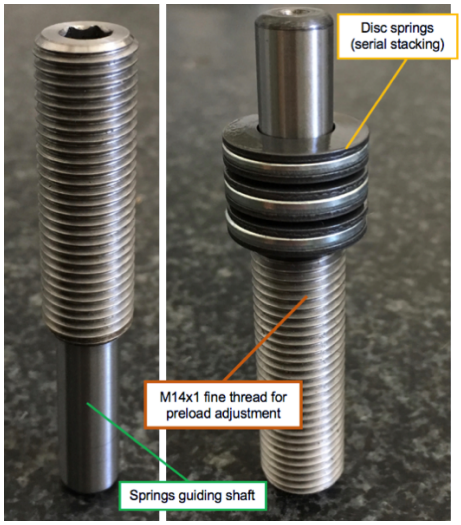

Figure 4.8: Detail of the manufacture preload set screws (spring guiding shaft grinded to R_a=0.4 μm and hardened to 55 HRC, as suggested by the spring manufacturer [90]**).**

The same design solutions with respect to actuators housing and preload arrangement were considered for both the inner and outer stages of the active fixture.

The geometries of the fixture frames and the integration of flexure hinges were defined with the main practical purpose of providing adequate housing to the actuators, the preload arrangements and the required flexure hinges. In addition, the geometries of the fixture frame were defined focusing on the reduction of the fixture dimensions and particularly the consequent stages masses, with the purpose of increasing the bandwidth of the actuated axes. The detailed design was aided by the hinge reduced models, described in section 3.2.3, the details of the iterative procedure for the definition of suitable hinge geometry, conceptually described in section 3.2.3, is not here reported for sake of synthesis.

The final fixture design is shown in Figure 4.9 and Figure 4.10

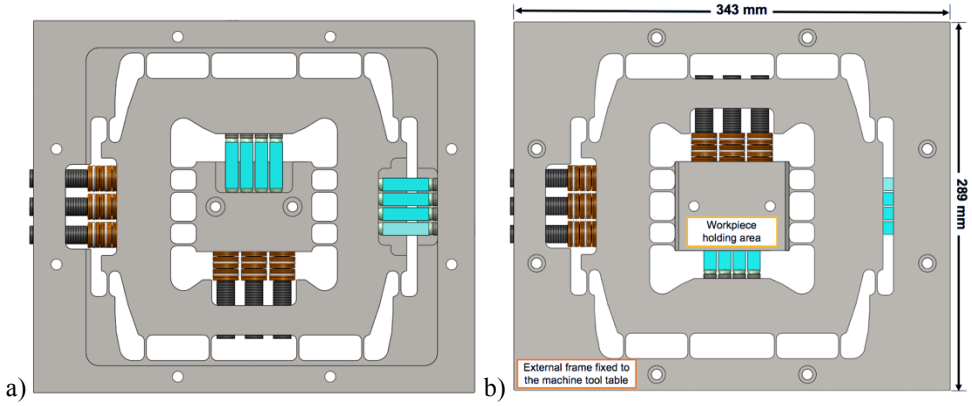

Figure 4.9: Assembled designed AWH prototype. a) bottom view, b) top view with external dimensions (total thickness 25 mm).

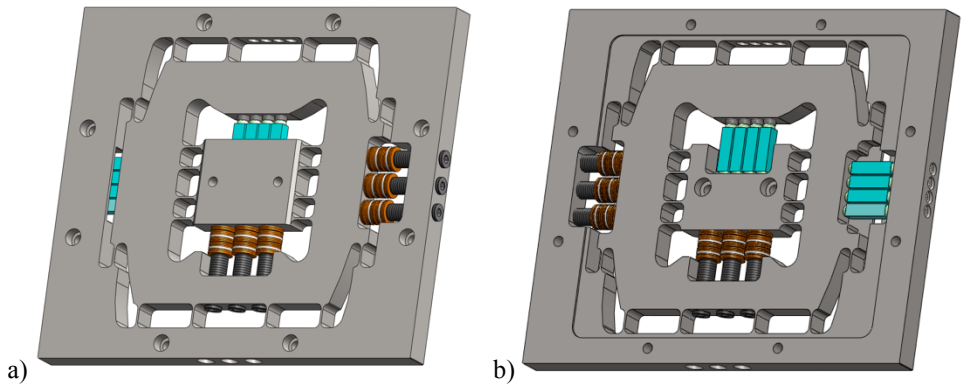

Figure 4.10: Additional views of the designed AWH.

As shown in Figure 4.9a, and more in detail in Figure 4.10b, a 2 mm deep pocket is machined at the bottom of the fixture to prevent the moving part from sliding on the machine tool table when actuated. Analogously, the workpiece holding area (i.e., inner stage) is designed to be 3 mm higher than the surrounding frame. This would also prevent any interference with the workpiece motion even if a cover is placed on the fixture top to prevent chips and fluids getting in contact with the piezo actuators.

For what concerns the flexure guiding systems, four corner filleted flexure hinges where integrated on each side of the inner stage, while the outer stage features six flexure hinges on each side. This choice was mainly driven by the need of preventing low-frequency pitching and out-of-plane modes. The outer stage, due to its higher masses and dimensions, imposed the use of a higher number of flexure hinges for this purpose. The selected flexure hinges geometry is shown in Figure 4.11.

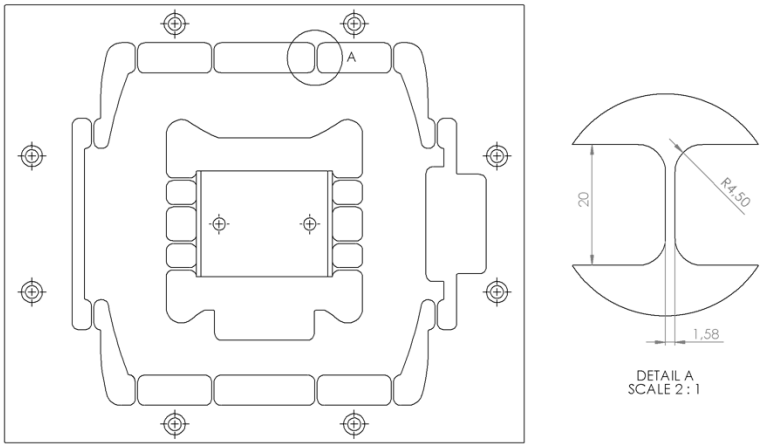

Figure 4.11: Detail of the flexure hinges geometry (hinge thickness, H, 20 mm).

In addition to the aforementioned criteria for the selection of a suitable hinge geometry, the corner fillet radii at the hinge extremities were selected considering machinability issues. The selected geometry would indeed allow the prototype to be manufactured by means of conventional machining operations, without requiring the use of Electric Discharge Machining (EDM) or alternative manufacturing technologies.

The stiffness along the actuation direction for a single flexure hinge of the selected geometry is approximately estimable in 2.7 N/μm which would not drastically impact on the achievable displacement produced by the piezo actuators: the total stiffness of the flexure hinges for the outer stage would be approximately 32 N/μm, that would represent less than 10% the actuators stiffness (i.e., the total nominal stiffness is 400 N/μm for the four actuators integrated in each axis). The material used for the fixture frame, and flexure hinges as a consequence, is 1.2738 steel (40CrMnNiMo8), selected for its mechanical characteristics (typically: 900 MPa < UTS < 1100 MPa).

For what concerns the preload springs, Mubea 170063 disc springs were selected and considered in a serial configuration in order to reduce the overall stiffness of the preload arrangement while ensuring an adequate force range that could be consistent with the potentially required preload forces. According to the spring manufacturer, the stiffness of the preload arrangements in that configuration (i.e., 3 stacks in parallel, each composed of 7 springs in serial stacking) should be approximately 2 N/μm, hence negligible in affecting the piezo displacement. It should be highlighted that the actual stiffness value of a disc springs changes with the spring deflection, but the expected variations are not so relevant to actually affect the piezo displacements.

In addition, an aluminum adapter plate was designed as an interface between the active fixture and the machine tool table in order to make it more easily adaptable to different table specifications. The adapter plate, shown in Figure 4.12, also presents some dedicated slots for securely route out of the fixture the actuators and sensors cables, preventing any interference during the AWH operations.

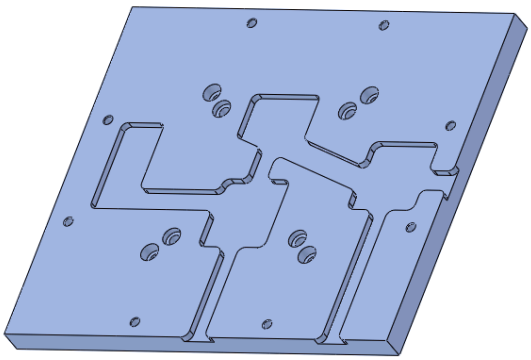

Figure 4.12: CAD view of the designed adapter plate.

4.3. Fixture modeling and assembly

As anticipated, FE models have been extensively used in all the phases of the preliminary design, with the simplified modeling strategy developed, and obviously in the final steps of the detailed design. As said, the main purpose of the FE analysis conducted in the detailed design phase was to investigate the dynamic response of the AWH prototype in order to assess its feasibility with the active vibration canceling application. Numerical modal analysis was conducted on the full-FE model of the selected AWH design in order to evaluate the dynamic response of both the actuated axes. Again MSC Nastran solver was used for the FEA, employing a mapped mesh for the fixture frame and the actuators (hexahedric CHEXA solid elements used [80]) and springs elements (PBUSH) for the preload springs. The choice of modeling the piezo actuators with solid elements instead of simple springs was mainly driven by the need of investigating stress distributions along the actuators in simulated operative conditions for the preload force estimation, as will be discussed in the following sections. In order to avoid the need of using conformal meshing for the whole AWH prototype modes, that would have drastically complicated the meshing of some components (e.g., set screws, flexure hinges, etc.), a double sided contact algorithm (i.e., glued contact feature in MSC Nastran [80]) was used to join components with non-conformal interfaces (i.e., different meshes).

The results of the mode shapes and natural frequencies of the inner and outer axes, as identified by the FE modal analysis in a free-free configuration, are shown in Figure 4.13.

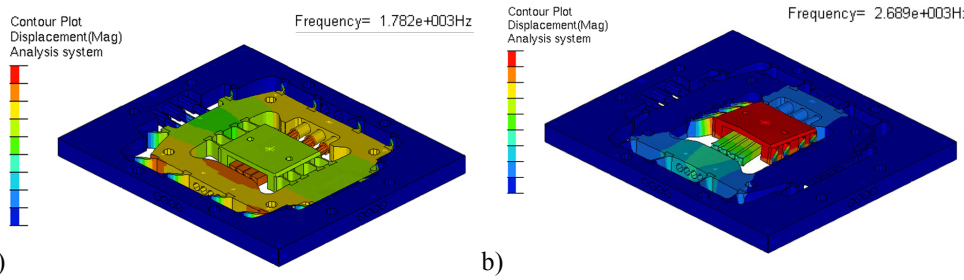

a) b)

Figure 4.13: Mode shapes and natural frequencies for the actuated axes: a) Outer stage, b) Inner stage.

The results of the FEA show that the proposed design allowed sensibly increasing the natural frequencies of both the actuated stages, contributing to the increase of the achievable device bandwidth. If compared to previous literature works on similar AWHs, the increase in the natural frequencies values for both the stages gets even more tangible: the AWH prototype developed by Haase [62], for example, showed natural frequencies lower than 500 Hz and 1 kHz for the inner and outer stage respectively. Likewise, the AWH prototype proposed by Long et al. [59] showed even lower natural frequencies for the actuated axes (i.e., 232 Hz and 432 Hz for the outer and inner stage respectively). It is worth mentioning that the estimated natural frequency values for the proposed design appear to be at least comparable with the ones reported by Abele et al. [10] for their AWH prototype based on parallel kinematics (i.e., slightly higher than 1 kHz), in that case aided by the related advantage of lower overall masses, as already discussed in the previous sections.

The FE models allowed also the investigation of stress distributions along the designed flexure hinges with the purpose of approximately assessing the feasibility of the proposed design in terms of fatigue life. A linear static analysis was conducted on the AWH full FE model, imposing to the dynamic axes the maximum producible displacements of the piezo actuators (i.e., SPCD in MSC Nastran [80], with enforced motion of 32 μm). The results, exemplified in Figure 4.14, showed that the maximum stress achievable in such a limit case would be safely allowable for the selected material (40CrMnNiMo8), even from a fatigue life point of view.

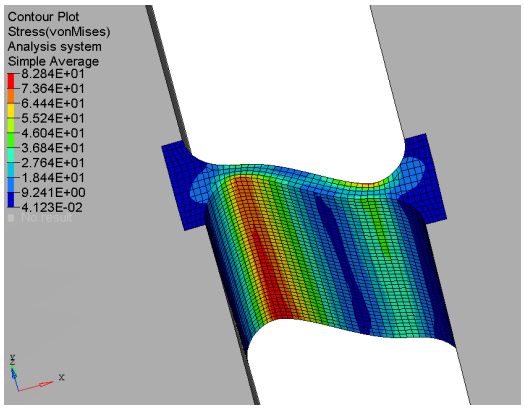

Figure 4.14: Simulated stress distribution on the flexure hinges under operative conditions (estimated maximum stress ≈ 83 MPa).

It is worth highlighting that Long et al. reported a peak stress value of 61.5 MPa for the double notched hinges integrated in their AWH prototype, in a serial configuration [59]. As discussed in the previous sections, the serial arrangement of flexure hinges was here discarded to avoid the resulting excessive flexibility, even though it would have allowed reducing the stress values along the flexure hinges in translational motion. Nonetheless, the designed flexure hinges show similar stress values, suggesting that a suitable compromise could be achieved by accurately tuning the flexure hinge geometry. It should also be highlighted that the theoretical maximum displacement generated by the piezo actuators would be lowered by the additional stiffness in the system, as will be discussed in section 4.4.2. The resulting stresses within the flexure hinges will result reduced accordingly.

4.3.1. FE models validation

Once the prototype was manufactured, the AWH FE models were validated by means of experimental modal analysis and model updating procedures. The purpose of this was manifold: on the one hand the FE model validation would have allowed the identification of some features of the AWH components, such as the actuator stiffness and actuator force generation coefficient, which can sensibly differ from the nominal values reported in the manufacturer datasheets. Those updated data would be useful to develop effective process simulation tools, such as the milling process time-domain simulator that will be presented in section 5.1. In addition, a validated FE model would represent a useful and effective simulation tool to investigate the active fixture dynamics and to conduct specific simulated tests, such as the ones needed to assess the required preload force, as described in section 4.4.1.

The experimental modal analysis and the model updating procedures were performed at several assembly steps to identify material proprieties, components behavior (e.g., actuators and preload springs stiffness values), and boundary conditions. Experimental modal analysis was used to acquire the reference data upon which optimizing the FE model in order to achieve the good agreement between the FE model and the physical prototype. Unconstrained (i.e., free-free) conditions were preferred for the experimental modal analysis, at least in the first assembly steps, in order to reduce the potential inaccuracies in defining the boundary conditions. Six different assembly configurations were tested in the assembly procedure:

1) Prototype frame only;
2) Prototype frame equipped with actuators (secured in place with the set screws);
3) Prototype frame, actuators and preload springs installed;
4) Adapter plate only;
5) Assembled prototype secured to the adapter plate;
6) The final fixture installed on the machine (not in free-free configuration).

Experimental modal analysis was performed via impact testing on the prototype: in order to reduce the number of experiments and sensors needed, the roving hammer technique was preferred [91]. A Bruel&Kjær type 8202 instrumented impact hammer (sensitivity: 0.98 pC/N) was used for the excitations, while vibration responses were acquired using two tri-axial accelerometer PCB 356B21(sensitivity: 10 mV/g, mass: 4 grams). Signal acquisition and conditioning were performed using a LMS SCM202V acquisition system. LMS TestLab software was used for the computation of both the Frequency Response Function (FRF) computation and mode shapes extraction using the Polymax algorithm [92]. The correlation between the FE data and the experimental results was estimated both in terms of natural frequencies and mode shapes agreement, formalized by means of the Modal Assurance Criterion (MAC) [93]. This method is commonly adopted to correlate two sets of mode shapes, generally the predicted and the measured one. Basically when a modal analysis is performed, the goal is to have the corresponding mode shapes of the two sets proportional to each other. At the same time uncorrelated mode shapes should be orthogonal vectors, in order to be able to discern them. The MAC index can be mathematically formulated as:

$$MAC = \frac{\left|\{\psi_{ex}^{i}\}^{T}\{\psi_{FE}^{j}\}\right|^{2}}{\{\psi_{ex}^{i}\}^{T}\{\psi_{ex}^{i}\}\{\psi_{FE}^{j}\}^{T}\{\psi_{FE}^{j}\}} \tag{4.7}$$

where ψ_{ex}^{i} is the ith experimental mode shape and ψ_{FE}^{j} is the jth FE model mode shape.

For the sake of brevity and clarity, the results of the model validation in each step are reported focusing on the behavior within approximately 2 kHz, since the aim was the derivation of a validated model reliable within the actuated axis bandwidth. However, the model resulted to be accurate even beyond that limit.

As anticipated, the first component investigated was the fixture frame only. The model updating procedures were in that case aimed at identifying the actual material properties (i.e., Young modulus, Poisson ratio and density) in order to validate the fixture frame FE model. Material density was derived by weighting the frame and extracting the exact volume from 3D CAD files. For the 40CrMnNiMo8 steel composing the fixture frame a density value of 7,770 kg/m^3 is identified, which is in line with the nominal material properties, as expectable.

As said, the experimental modal analysis was conducted via impact testing in a free-free configuration (i.e., component suspended by means of low-stiffness springs and bungee ropes), as shown in Figure 4.15a. The experimental tests were performed over 20 different points on the structure in order to accurately identify the first mode shapes. The identification points are highlighted in yellow in Figure 4.15b, showing also the full FE model of the fixture frame (CHEXA solid elements used in a mapped mesh, as discussed previously).

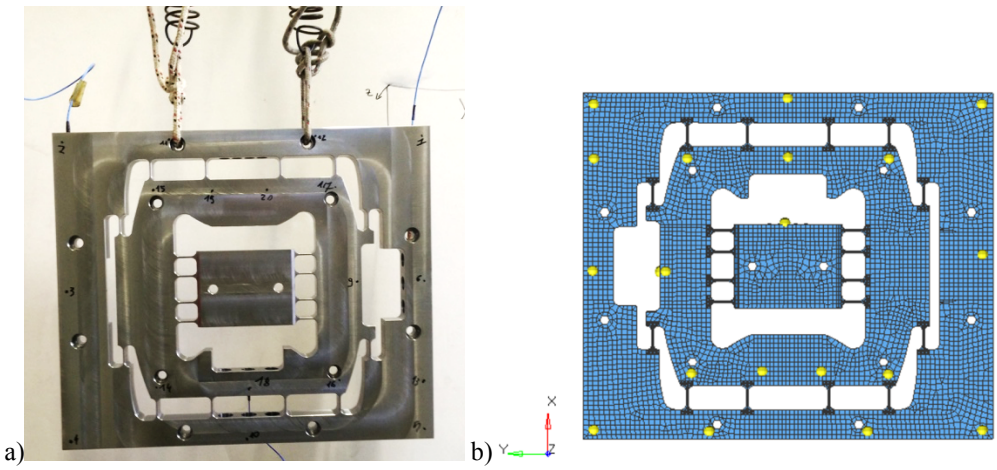

Figure 4.15: Validation tests on the fixture frame FE model. a) Experimental setup, b) FE model and measuring point highlighted.

It should be highlighted that the manufactured fixture frame shows four counterbore holes in the intermediate stage that were not accounted for in the prototype design. The need of introducing those additional holes is justified by manufacturing requirements and particularly by the need of additional fixing points in machining the prototype frame preventing excessive deformations. The additional counterbore holes were obviously included in the detailed FE model, as shown in Figure 4.15b.

After updating the FE model the correlation results reported in Table 4.5, in terms of natural frequencies, and in Figure 4.16, in terms of MAC values, were achieved.

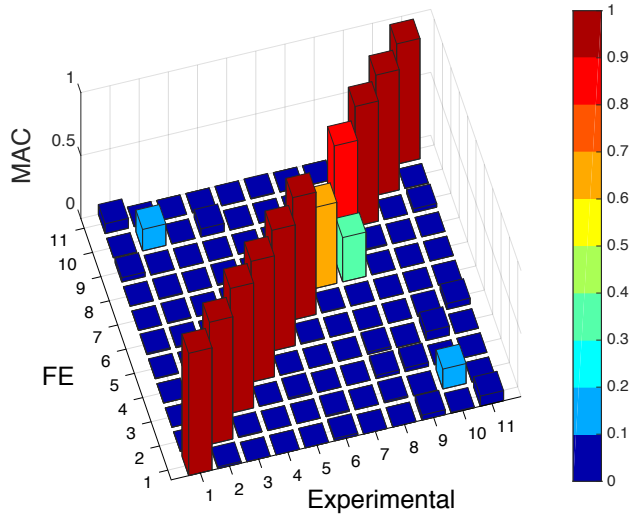

Figure 4.16: MAC results for the correlation tests on the prototype frame.

Table 4.5: Correlation results after FE model validation on the prototype frame.

Mode n°	Natural Frequency Experimental	Natural Frequency FE	Error	Notes
1	393.3 Hz	406.0 Hz	3.2%	
2	619.4 Hz	624.7 Hz	0.9%	
3	791.3 Hz	790.2 Hz	-0.1%	Outer stage Y-translation
4	922.4 Hz	926.0 Hz	0.4%	
5	923.8 Hz	927.3 Hz	0.4%	
6	1049.6 Hz	1068.9 Hz	1.8%	
7	1159.4 Hz	1148.8 Hz	-0.9%	Inner stage X-translation
8	1160.5 Hz	1175.5 Hz	1.3%	
9	1437.7 Hz	1464.0 Hz	1.8%	
10	1772.9 Hz	1785.8 Hz	0.7%	
11	1950.4 Hz	1996.3 Hz	2.4%	

Figure 4.17 and Figure 4.18 exemplify a comparison between the mode shapes identified with the experimental modal analysis (i.e., wireframe of experimental data on the measuring points) and the ones derived by FEA.

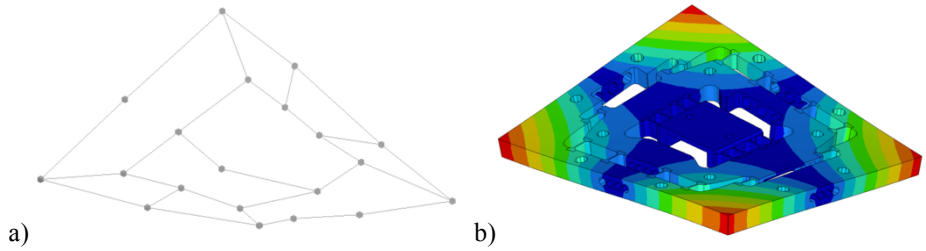

a) b)

Figure 4.17: 1st mode shape comparison. a) wireframe of experimental measuring points, b) FEA results.

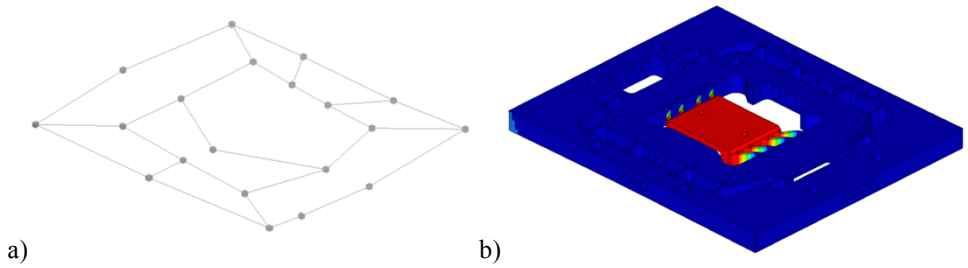

a) b)

Figure 4.18: 7th mode shape comparison (i.e., translational mode of the inner stage). a) wireframe of experimental measuring points, b) FEA results.

As shown, the model updating provided a good agreement between the FE model and the experimental results: the errors in terms of natural frequencies estimation is constrained below 4% and MAC extra diagonal values are below 0.4, while MAC diagonal values are higher than 0.8, exception made for 7th that shows a MAC value higher than 0.6 in any case. The higher natural frequency error on the first mode is probably due to the discretization errors induced in meshing the counterbore holes on the frame. Indeed, the stiffness of these holes is significantly affecting the first mode, as shown in mode shapes (Figure 4.17). For what concerns the lower MAC diagonal value associated to the 7th mode, that represents the inner stage translational mode, shown in Figure 4.18, it should be highlighted that only one measuring point is acquired on the inner stage due to the actual difficulties in exciting the inner stage along X-direction in different points through impact testing, as a consequence of the compact geometry of the fixture frame in that area. This explains the lower MAC value, given that a single measuring point acquires the motion of the inner stage, while the remaining 19 measuring points are almost not sensing any movement, even though they participate in the MAC definition, affecting its value with noisy results.

After the model updating procedures, the following material properties were identified: Young Modulus equal to 208,000 MPa and Poisson Ratio of 0.29 which are in line with the nominal material data of the 1.2738 steel, as provided by the manufacturer (i.e., typical Young Modulus value of 205,000 MPa and Poisson Ratio of 0.291).

After validating the single frame FE model, the piezo actuators were included along with the related set screws. In that phase no actual preload was applied, just a limited torque was applied to the set screws to ensure that actuators were held in place properly during the impact testing procedures. In that phase the main variable under investigation was the actuator stiffness, hence the actuators material properties. As anticipated, indeed, the actuators were not modeled as springs but with solid elements (CHEXA) so that stresses can be investigated in successive FE analysis. Analogously, the actuator set screws were

modeled through solid elements as well. An equivalent material is preliminarily defined for the piezo actuators, with tentative values of Young modulus and Poisson's ratio, while density was again identified by weighting the actuators and comparing with the actuators volume, leading to an equivalent density of 7,830 kg/m^3. It is worth highlighting that the actuators properties identified are referred to the actuators including the stainless steel spherical end-tips, since the components were provided pre-assembled and a dedicated investigation of the properties of the sole PZT was out of the aim of the FE model validation.

The same measuring point were again used for the experimental modal analysis. The experimental setup and the FE model used are shown in Figure 4.19a and Figure 4.19b respectively.

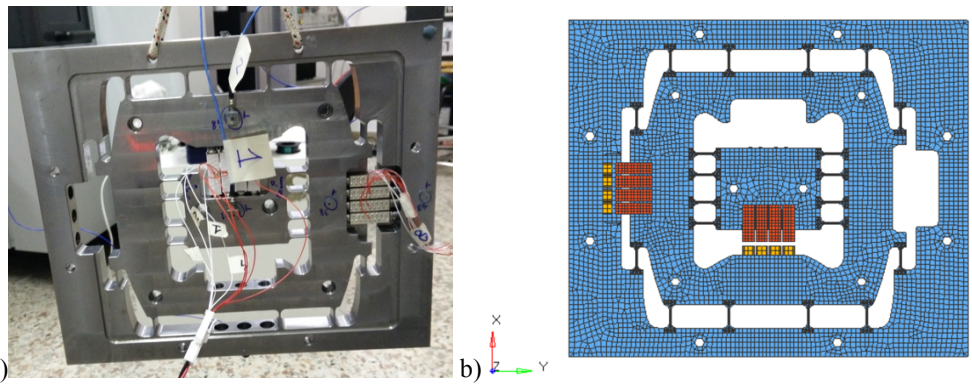

Figure 4.19: Validation tests on the fixture frame with integrated actuators. a) Experimental setup, b) FE model.

The correlation results of the model updating are reported in Table 4.6 and Figure 4.20, again in terms of natural frequencies and MAC values respectively.

Table 4.6: Correlation results after FE model validation on the prototype frame with actuators.

Mode n°	Natural Frequency Experimental	Natural Frequency FE	Error	Notes
1	395.5 Hz	410.3 Hz	+3.7 %	
2	613.4 Hz	616.9 Hz	+0.6 %	
3	908.3 Hz	911.3 Hz	+0.3 %	
4	938.6 Hz	938.0 Hz	-0.1 %	
5	1049.7 Hz	1076.9 Hz	+2.6 %	
6	1145.0 Hz	1156.6 Hz	+1.0 %	
7	1286.7 Hz	1255.1 Hz	-2.5 %	Outer stage translation
8	1433.7 Hz	1450.0 Hz	+1.1 %	
9	1732.6 Hz	1737.4 Hz	+0.3 %	
10	1958.8 Hz	2018.6 Hz	+3.1 %	

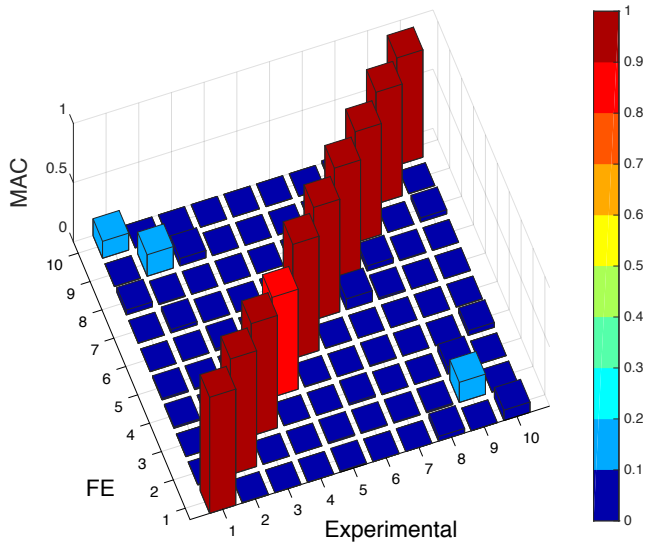

Figure 4.20: MAC results for the correlation tests on the prototype frame with actuators.

Again the correlation results show good agreement between the updated FE models and the experimental data: the MAC diagonal values are all above 0.8 and the errors in terms of natural frequencies is always constrained below 4 %. The computed optimal values for the equivalent material properties are: equivalent Young modulus 26,000 MPa and equivalent Poisson ratio 0.34. The updated material properties would lead to an equivalent actuator stiffness of approximately 72 N/μm (i.e., for a single actuator), lower to the nominal value of 100 N/μm reported in the manufacturer datasheet, as shown in Table 4.3. The reason for that is twofold: on the one hand the spherical end tips could affect the equivalent stiffness of the PZT estimated in the model updating procedures. On the other hand, it should be noted that the actuators stiffness values reported in the manufacturer datasheets are usually not physically identified. Usually, the equivalent stiffness is computed by dividing the blocking force value by the rated maximum displacements [87]. Relevant discrepancies should hence be expected in terms of actual PZT stiffness.

Once the FE model of the AWH frame including actuators was validated, the preload arrangements were assembled to the fixture in order to derive an equivalent stiffness for the preload springs stacks. As anticipated, seven Mubea 170063 belleville springs were stacked in a serial configuration for each preload stack (i.e., 3 preload stacks acting in parallel on each actuated axis). Neglecting stiffness variations induced by the spring deformations, a tentative preload was applied to the preload arrangements. Given that the preload springs stiffness is expected to be sensibly lower than the other components (e.g., piezo actuators), such an approximation is not expected to seriously affect the validation of the FE models.

The FE model was realized by meshing the preload set screws with solid elements (CHEXA), as for the actuators set screws, while the preload springs were modeled as 1-D spring element (CBUSH in MSC Nastran [80]), including lumped masses identified by weighting the springs. The FE model and the experimental setup are shown in Figure 4.21b and Figure 4.21a respectively.

a) 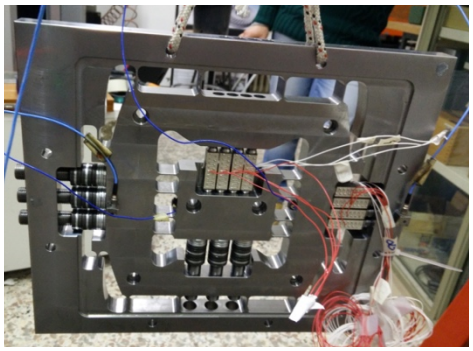 b) 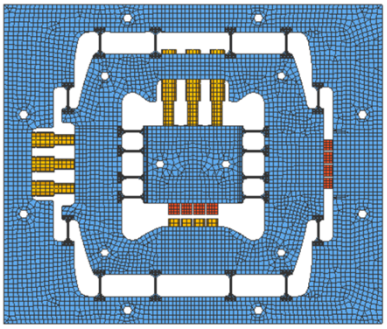

Figure 4.21: Validation tests on the fixture frame with integrated actuators and preload arrangements. a) Experimental setup, b) FE model.

The correlation results after model updating (i.e., stiffness identification) are shown in Table 4.7 .

Table 4.7: Correlation results after FE model validation on the prototype frame with actuators and preload arrangements.

Mode n°	Natural Frequency Experimental	Natural Frequency FE	Error	Notes
1	403.1 Hz	428.9 Hz	+6.4 %	
2	599.1 Hz	606.0 Hz	+1.1 %	
3	891.9 Hz	909.0 Hz	+1.9 %	
4	938.0 Hz	947.6 Hz	+1.0 %	
5	1048.2 Hz	1103.0 Hz	+5.2 %	
6	1126.1 Hz	1157.1 Hz	+2.8 %	
7	1289.6 Hz	1289.9 Hz	+0.0 %	Outer stage translation (Y)
8	1438.9 Hz	1423.2 Hz	-1.1 %	
9	1681.9 Hz	1683.7 Hz	+0.1 %	

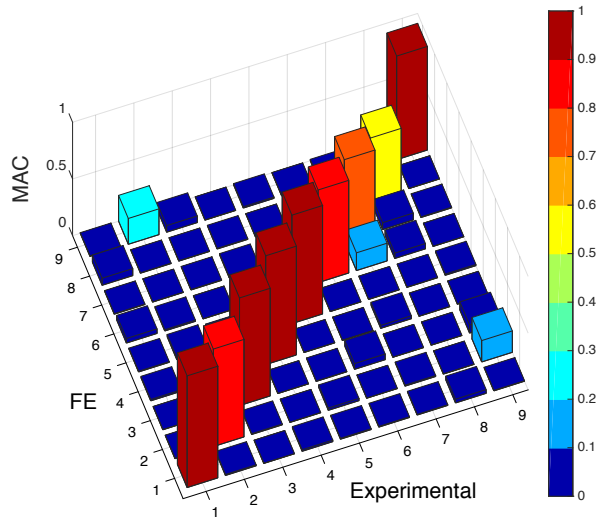

Figure 4.22: MAC results for the correlation tests on the prototype frame with actuators and preload arrangements.

Again the correlation shows good results in terms of both errors on natural frequencies and MAC values. It should be noted though, that the natural frequency of the first mode is associated to an error slightly higher than 5%. This is again probably due to the discretization of the counterbore holes in the fixture frame, as already discussed for the validation tests on the single prototype frame. MAC diagonal values, on the other hand, are all higher than 0.7, exception made for the 8th mode (mode shape presented in Figure 4.23).

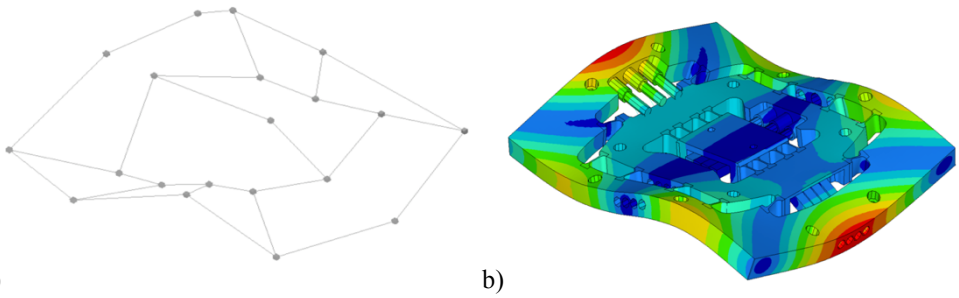

a) b)

Figure 4.23: 8th mode shape comparison. a) wireframe of experimental measuring points, b) FEA results.

This reduced correlation is probably due to the approximation on the spring modelling: indeed, springs are modeled as 1-D element characterized by a lumped stiffness only on the spring axis direction. This approximation is intended to be accurate for the model dynamics representation, but it fails for the 8th mode that is significantly influenced by the spring stiffness on Z-direction, not accounted for in the FE model. However, the error is still considered admissible, especially taking into account that once the fixture will be installed on the machine this type of mode will obviously appear only at high frequency, due to the boundary conditions.

As outcome of this validation step, the updated stiffness value of the preload springs stacks was identified in 4,500 N/mm, sensibly higher than the stiffness rated by the manufacturer. This is presumably due to friction and stick-slip effects that could affect the identification of such components in impact testing procedures. It is worth highlighting that, if the interest is put in achieving an accurate FE based simulation of the dynamic behavior of the AWH prototype, a detailed stiffness identification could be avoided if the FE models are dynamically validated.

Subsequently, the aluminum adapter plate was investigated. Again, being the adapter plate a monolithic component as the fixture frame, the model updating was focused on deriving the actual material properties. The material density was identified in 2,690 kg/m^3 by weighting the component. The experimental impact tests were performed on 10 points, highlighted in yellow on the FE model reported in Figure 4.24b, sufficient to identify the first modes and carry out the FE model updating. In order to consider all the geometrical details of the adapter plate, a solid modeling strategy (i.e., hexahedric elements, CHEXA) was preferred to a shell one. Both the experimental setup and the FE model are reported in Figure 4.24a and Figure 4.24b respectively.

a) 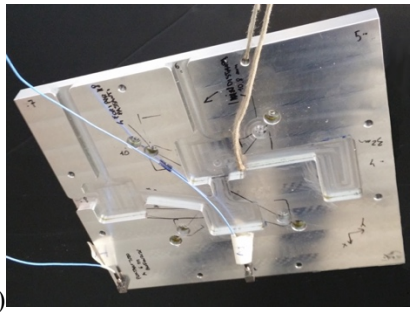 b) 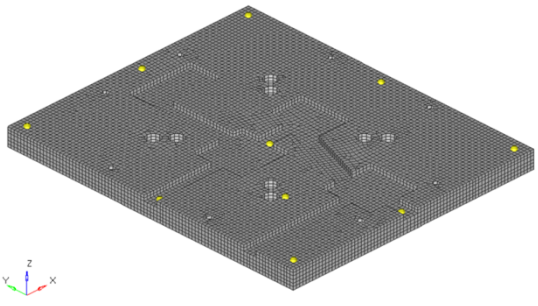

Figure 4.24: Validation tests on the adapter plate. a) Experimental setup, b) FE model, measuring point highlighted in yellow.

The correlation results following the material properties optimization are reported in Table 4.8 and Figure 4.25, again as MAC and natural frequencies values.

Table 4.8: Correlation results after FE model validation on the adapter plate.

Mode n°	Natural Frequency Experimental	Natural Frequency FE	Error
1	550.6 Hz	556.5 Hz	+1.1 %
2	769.1 Hz	757.7 Hz	-1.5 %
3	1075.1 Hz	1071.7 Hz	-0.3 %
4	1377.9 Hz	1382.3 Hz	+0.3 %
5	1575.0 Hz	1571.9 Hz	-0.2 %
6	2286.8 Hz	2271.2 Hz	-0.7 %

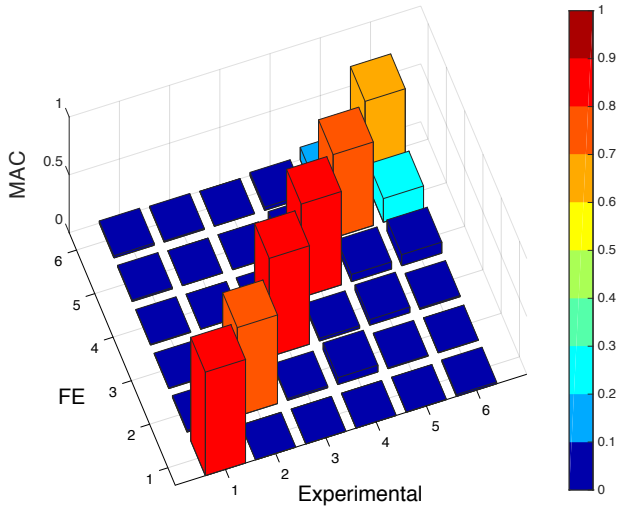

Figure 4.25: MAC results for the correlation tests on the adapter plate.

As shown a good correlation is achieved in terms of both natural frequencies and MAC values. The derived updated material properties resulted in a Young modulus of 69,500 MPa and a Poisson ratio equal to 0.35.

Once all the components were singularly identified, the preliminarily assembled AWH was fixed to the adapter plate to validate the related FE model, particularly to study the best connection strategy between the two subassemblies. The same measuring point were used for both the AWH prototype (20 points) and the adapter plate (10 points), leading to a total of 30 measuring points. Both the experimental setup and the FE model are reported in Figure 4.26a and Figure 4.26b respectively.

a) 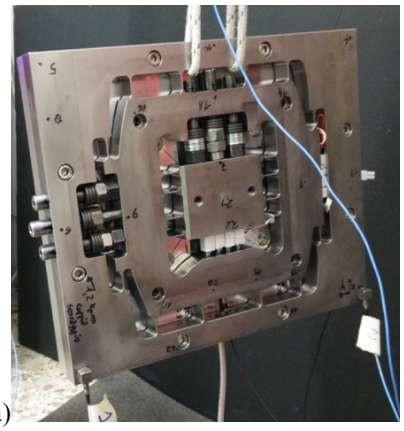 b) 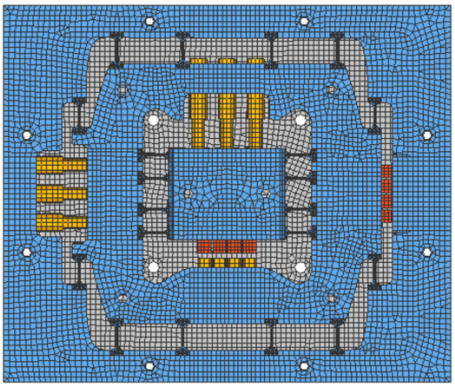

Figure 4.26: Validation tests on the AWH prototype fixed to adapter plate. a) Experimental setup, b) FE model.

A simplified connection between the two components was proposed. The two models were joined on the zones around the eight holes in which connection screws are present. The

joining of the two component with non-conformal interfaces (i.e., different meshes) was again achieved by means of a double sided contact algorithm (i.e., glued contact in MSC Nastran [80]), as already discussed in previous sections. This connection strategy resulted in a good correlation, as presented in Table 4.9 and Figure 4.27.

Table 4.9: Correlation results after FE model validation on the prototype frame fixed to the adapter plate.

Mode n°	Natural Frequency Experimental	Natural Frequency FE	Error	Notes
1	529.8 Hz	551.5 Hz	+4.1 %	
2	841.3 Hz	852.9 Hz	+1.4 %	
3	1068.4 Hz	1063.2 Hz	-0.5 %	
4	1320.4 Hz	1288.9 Hz	-2.4 %	Outer stage translation (Y)
5	1364.5 Hz	1410.4 Hz	+3.4 %	
6	1504.6 Hz	1493.2 Hz	-0.8 %	
7	1844.6 Hz	1900.0 Hz	+3.0 %	

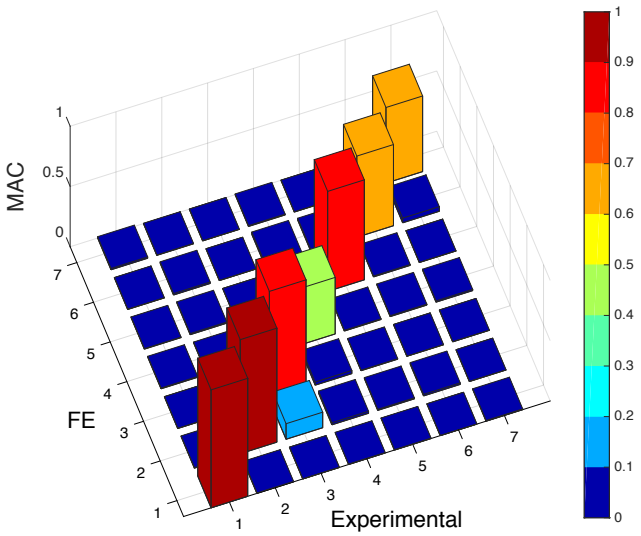

Figure 4.27: MAC results for the correlation tests on the prototype frame fixed to the adapter plate.

As shown, the proposed connection strategy resulted in a good correlation between FE model and experimental data: the errors in terms of natural frequencies are below 5% and MAC diagonal values are over 0.65 for all the modes, except for the 4th (i.e., outer stage translation), shown in Figure 4.28. The reason for this lower accuracy is similar to the frame 7th mode: in the acquired experimental data there is indeed a large number of points returning

small measured displacements, including the measuring points on the adapter plate, leading to noise affected data for the given mode shape.

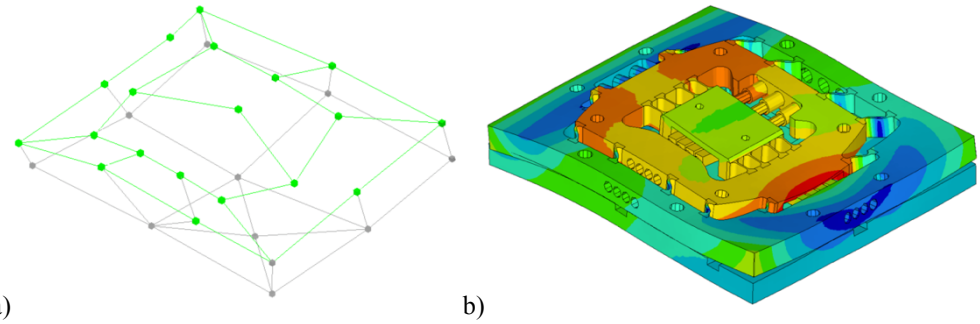

a) b)

Figure 4.28: 4th mode shape comparison. a) wireframe of experimental measuring points (green points represent the prototype and grey points the adapter plate), b) FEA results.

Finally, the impact testing and model updating procedures were conducted on the AWH prototype assembled and fixed to the machine tool table by means of the aluminum adapter plate, as shown in Figure 4.29. More in detail, the AWH is fixed to the adapter plate by means of eight M8 screws on the external frame, while the adapter plate itself is secured to the machine tool table by means of four M8 screws and dedicated T-blocks.

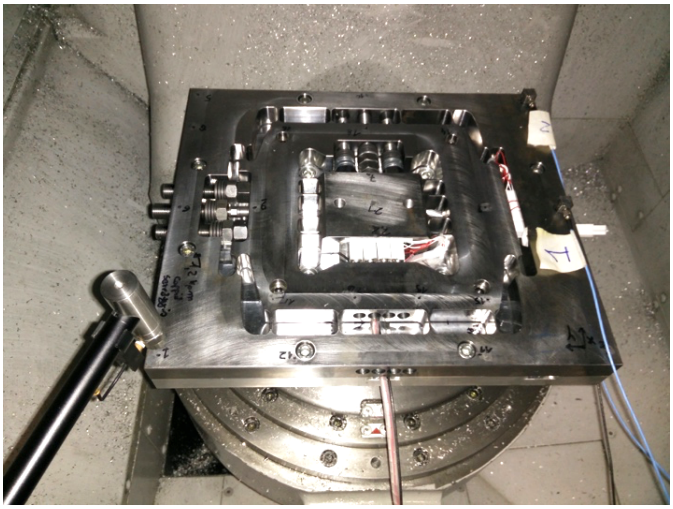

Figure 4.29: Impact testing on the assembled prototype installed on the machine tool table (i.e., Mori Seiki NMV-1500dcg).

Here again the aim of the model updating was to identify suitable boundary conditions of the prototype, to this point investigated only in a free-free configuration. The boundary conditions at the interface between the adapter plate and the machine tool table were defined using single point constraints (i.e., SPC in MSC Nastran [80]) with imposed blocked conditions (i.e., null enforced motion) along all the 6 DOFs. The main uncertainty

motivating the need of model updating was the identification of the actual area on the adapter plate that should be constrained with SPCs.

After the model updating, a suitable distribution of the SPCs on the adapter plate was defined as shown in Figure 4.30.

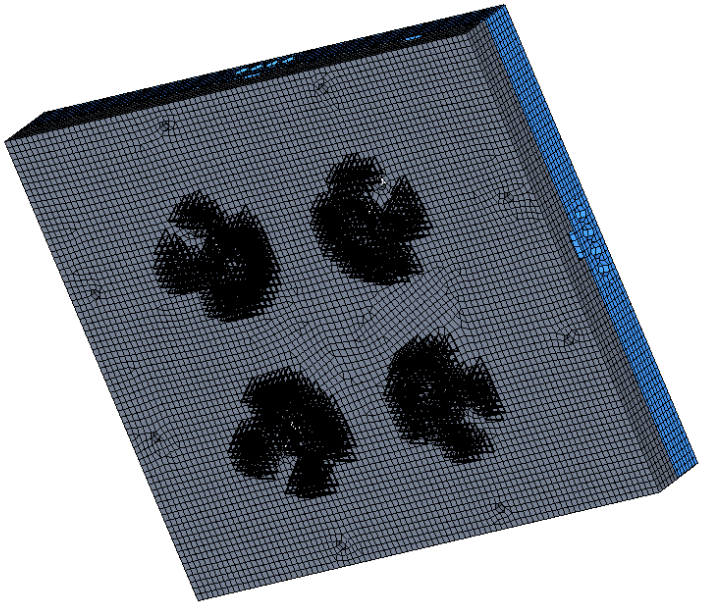

Figure 4.30: Detail of the SPCs (black triangles) applied to the adapter plate at the interface with the machine tool table.

The achieved correlation results are shown in Table 4.10 and Figure 4.31, in terms of natural frequencies and MAC values respectively.

Table 4.10: Correlation results after FE model validation on the prototype frame installed on the machine tool table.

Mode n°	Natural Frequency Experimental	Natural Frequency FE	Error	Notes
1	947.7 Hz	941.4 Hz	-0.7 %	
2	967.1 Hz	967.5 Hz	+0.0 %	
3	1138.2 Hz	1176.4 Hz	+3.4 %	Outer stage translation (Y)
4	1540.8 Hz	1485.7 Hz	-3.6 %	
5	1634.5 Hz	1625.0 Hz	-0.6 %	
6	1882.1 Hz	1819.6 Hz	-3.3 %	
7	2011.2 Hz	1916.3 Hz	-4.7 %	Inner stage translation (X)

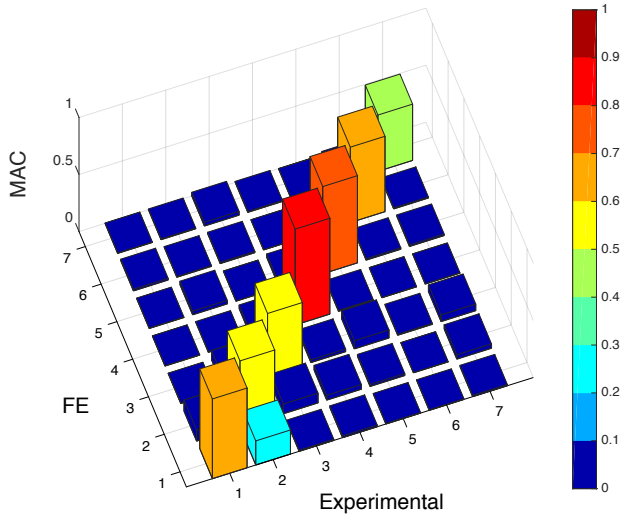

Figure 4.31: MAC results for the correlation tests on the prototype frame installed on the machine tool table.

As shown the errors in terms of natural frequencies are below 5% and the MAC values and distribution are satisfactory, even if lower than the ones achieved in free-free conditions, as should be expected though.

4.3.2. Identification of actuators properties

The validated FE models derived with the procedures presented allowed to investigate the actual properties of the actuators in terms of force generation capabilities. As anticipated in section 4.1, the force generated by the piezo actuators could be expressed, in the simplest formulation, as a function of the provided voltage by means of a force generation coefficient (i.e., K_φ in equation (4.6)). This coefficient could be tentatively estimated according to the manufacturer datasheets by simply dividing the blocking force for the maximum rated voltage applicable to the piezo actuators. As for the actuator stiffness, though, discrepancies can be expected between the theoretical datasheet values and the actual piezo performances. An adequate estimation of the actual force generable by the piezo actuators is mandatory for the correct estimation of the needed preload forces to be applied in the final assembly.

The validated FE models were hence used to conduct an investigation of the actual value of the force generation coefficient, as anticipated. Again, the correlation between experimental data and the results of dedicated FEA was used for the purpose. The physical active fixture was excited by means of sine waves at different frequencies (100 Hz, 300 Hz and 500 Hz) and with different voltages provided to the piezo actuators (i.e., 15 V_{pp}, 30 V_{pp}, 45 V_{pp}, 60 V_{pp}, 67.5 V_{pp}, 75 V_{pp} and 90 V_{pp}). The signals were generated and fed to the piezo drivers (i.e., a pair of Noliac NDR6880) by an LMS/Siemens SCADAS Mobile VibCo system while the fixture response was measured at different positions within the fixture frame by means of monoaxial and triaxial accelerometers, as shown in Figure 4.32.

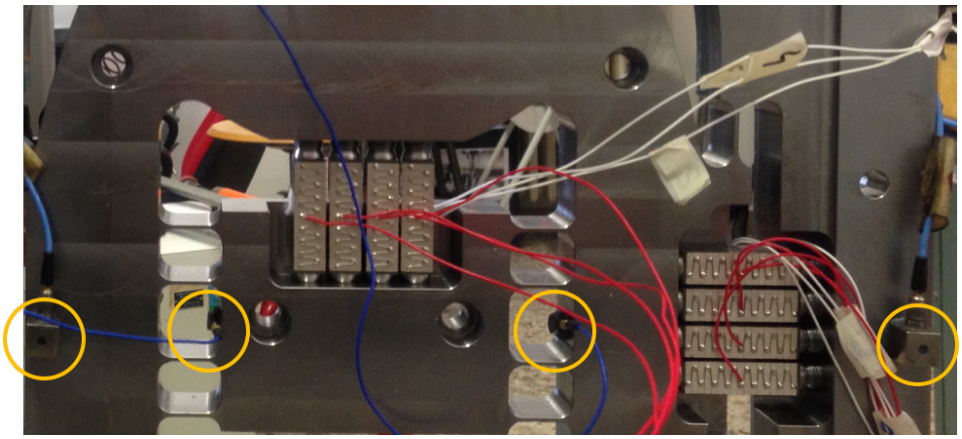

Figure 4.32: Accelerometers placed on different positions (highlighted in yellow) within the AWH prototype for the estimation of the piezo actuators force generation coefficient.

In parallel, an FRF analysis (i.e., SOL108 in MSC Nastran [80]) was numerically conducted on the validated FE fixture model, applying a 0.25 N force on each actuator of the stage under investigation (i.e., outer stage and inner stage independently) in order to provide a total force of 1 N and investigating the response of the nodes placed in close proximity of the experimental points, as shown in Figure 4.33, at the same frequencies of the experimental tests.

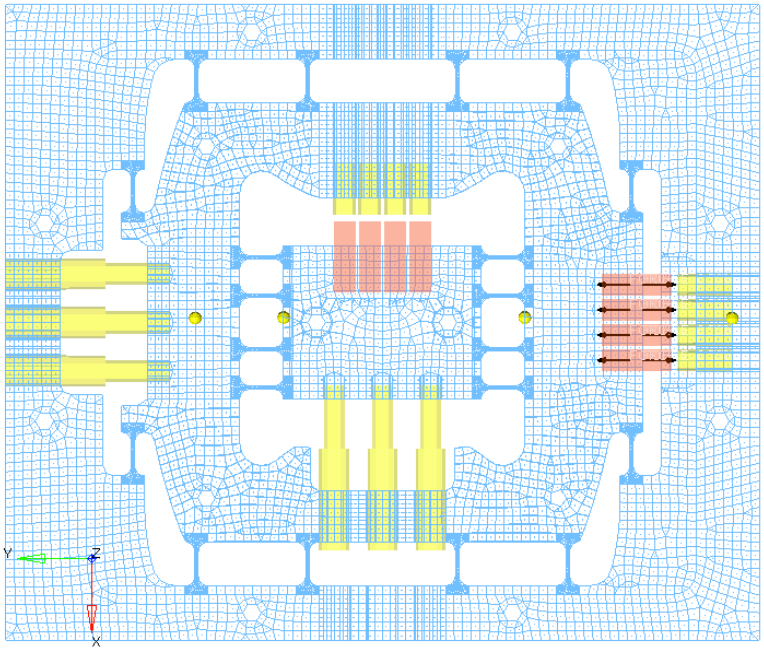

Figure 4.33: FE model used for the FRF analysis (outer frame testing). Excitation forces highlighted in black and measuring points highlighted in yellow with temporary node (FE model partially shaded and masked for sake of clarity).

Assuming the system to be linear, hence neglecting the small variations in the spring stiffness and non-linear effects on the piezo actuators (e.g., hysteresis), the force generated by the piezo actuators can be estimated by simply dividing the experimentally measured response by the FE data.

A simple linear regression analysis was then conducted on the full dataset to identify the actual value of the force generation coefficient, as shown in Figure 4.34.

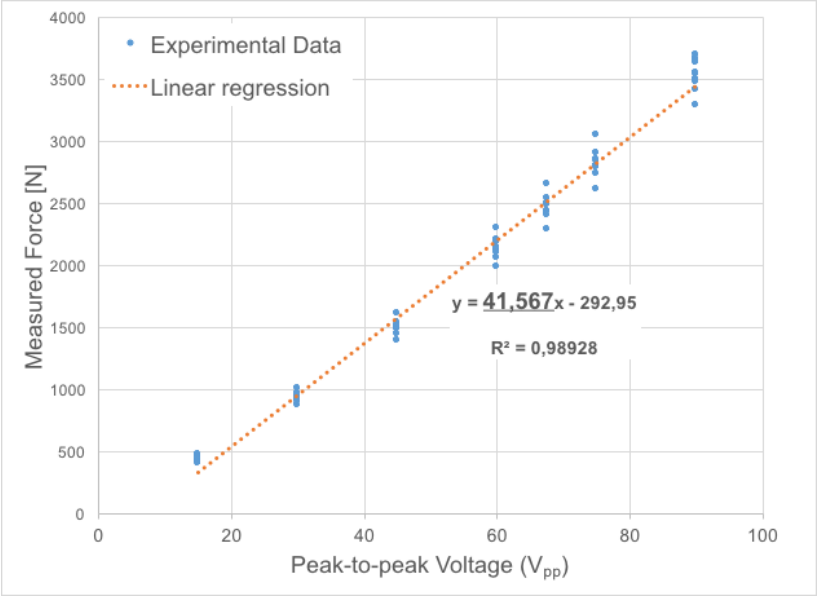

Figure 4.34: Linear regression on experimental data for K_φ estimation.

As shown in Figure 4.34, the K_φ of a single actuator can easily be identified by dividing the linear coefficient of the regression equation by the number of actuators (i.e., 4 actuators). Accordingly, $K_\varphi = 10{,}4\ N/V$ can be estimated, sensibly different from the theoretical value estimable in $K_\varphi = 16\ N/V$. It should be highlighted that the force generated by the piezo actuators shows a non-linear behavior for the lower voltages tested, which is consistent with the usual response of piezo actuators that is dependent on the entity of the electrical load applied [87].

The same identification was conducted for both the stages at several assembly steps, returning similar results with errors lower than 6%, considered consistent with the accuracy required for the preload force estimation and for the simulation of the AWH in chatter mitigation applications, as will be discussed in section 5.3.1.

4.4. Fixture assembly and testing

After having identified the actual properties of the components integrated in the fixtures, such as piezo actuators and preload springs, the ground was finally prepared for the computation of the needed preload forces and consequently for the final prototype assembly and testing, as discussed in the following sub-sections.

4.4.1. Fixture assembly/preloading

As discussed in section 4.1, adequate preload force shall be applied to prevent the piezo actuators against tensile stresses that could arise in limit operative conditions and could induce premature failures. This imply that the effects of workpiece mass, cutting forces and actuators excitations would need to be somehow estimated to derive the tensile forces the actuators would be withstanding. It should be highlighted that for the proposed design, the actuators would be intrinsically decoupled with respect to tensile stresses, given that the spherical joints at the hinge extremities would serve only as unilateral constraints. Without adequate preload, though, the actuators would get loose and could be exposed to potential shocks that could damage the PZT ceramic itself, hence adequate preload should be applied in any case.

As anticipated, in order to take into account each influencing factor, dedicated FE models have been used for the estimation of the preload force to be applied to the piezo actuators. The FE model used is shown in Figure 4.35, where the mesh is partly shaded and some components are masked for sake of clarity. An additional equivalent workpiece mass of 1 kg was included in the FE model as concentrated mass (i.e., CONM2 in MSC Nastran [80]), which is representative of a 60x60x100mm aluminum block, as employable in laboratory applications. The concentrated mass was placed in accordance with the center of gravity of the aforementioned block (i.e., in the center of the intermediate stage raised by 30 mm with respect the fixing plane), in correspondence with the node highlighted in white in Figure 4.35. On the same node an equivalent cutting force was applied (i.e., black load in Figure 4.35): the equivalent cutting force was imposed as a pure sinusoidal load with an amplitude of 1000N. The computation of the equivalent cutting force on conventional milling operations on aluminum was aided by the milling simulator that will be presented in section 5.1. The computed value is representative of a milling operation in unstable conditions (i.e., chatter). Moreover, the assumption of a mono-frequency excitation makes the investigated case more demanding and hence precautionary. As is common knowledge, indeed, being milling featured by interrupted cutting, the cutting force frequency spectra show several frequency contributions, related to the Tooth Pass Frequency (TPF), its harmonics and eventually chatter frequency, in case of unstable operations [94]. The assumption of a mono-frequency cutting force would hence represent a sort of worst case scenario, in addition this returned a consistent simplification of the FE analysis.

In the used FE model both the concentrated mass and the cutting force were distributed to the elements of the upper face of the inner stage by means of 1-D rigid elements, shown in grey in Figure 4.35.

For what concerns the actuation frequencies, the maximum force generable by the piezo actuators was modeled, as shown in black in Figure 4.35. A sinusoidal force of approximately 2000N was imposed to each actuator, according to the identified force generation coefficient previously described, for a total force of approximately 8000N acting on the stage under investigation (i.e., outer stage in Figure 4.35). The frequency of the actuation force was set equal to the cutting forces and no phase shift was considered. This is obviously representative of a limit condition, since the active fixture would be operated to counteract the cutting forces and particularly those contributions related to chatter vibrations. Such an assumption would anyway return a preload value that could prevent the fixture from damages even in case of potential controller malfunctioning.

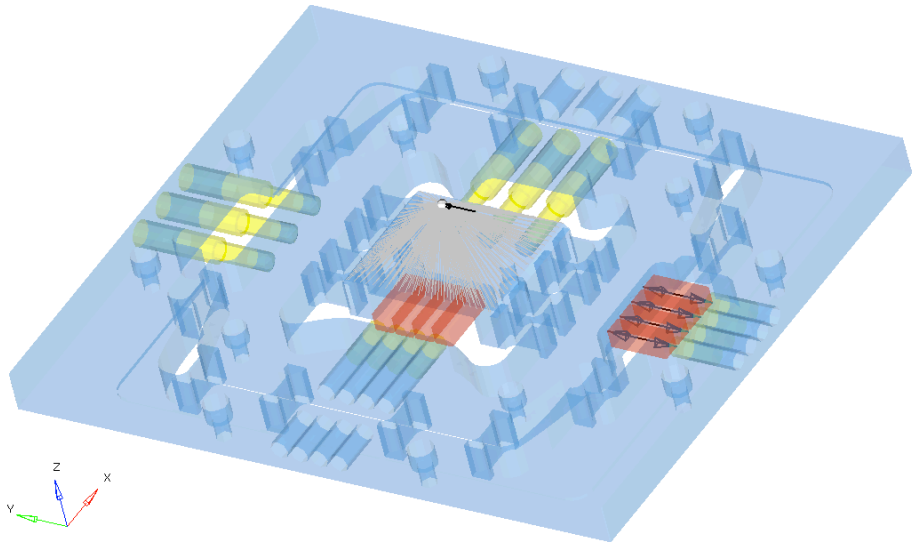

Figure 4.35: FE model for the investigation of tensile stresses on the piezo actuators in limit conditions (elements shaded and masked for sake of clarity).

Again, an FRF analysis was conducted at different frequencies (i.e., different cutting forces and actuation frequencies) and the tensile stresses on the actuators of the actuated axis were investigated. It is worth highlighting that the contact between the actuators and their support is modeled with 1-D rigid elements (i.e., RBE2), for sake of simplification of the FE model. This allows the estimation of tensile stresses on the actuators in the FRF analysis. In practice, the identified values of tensile stress generable in such limit conditions would need to be counteracted by an equal compressive stress induced in applying the preload to the piezo actuators. This would prevent any loss of contact between the actuators and their support.

The maximum value of estimated tensile stress on the actuator for the most demanding frequency investigated (i.e., stage natural frequency) was lower than 7 MPa for the actuators of the outer stage, as shown in Figure 4.36. Lower values (i.e., approximately 5.7 MPa) were achieved for the inner stage, as expectable due to the lower masses.

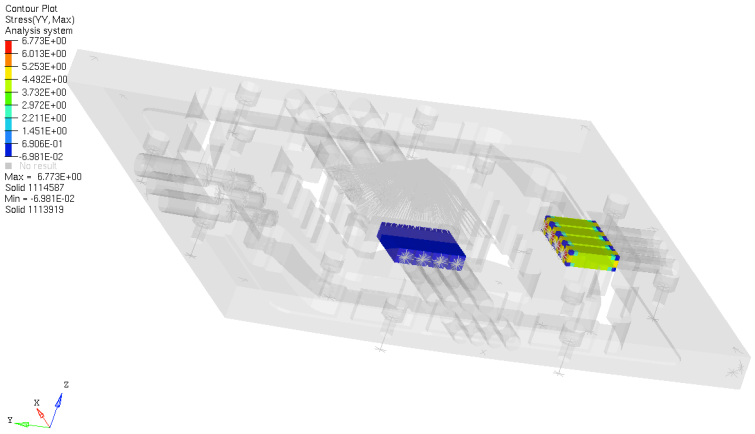

Figure 4.36: Resulting stress distributions on the actuators of the outer stage (some elements, masked for sake of clarity, such as the ones of the adapter plate).

As said, the preload forces would need to induce at least an equal compressive load to prevent loss of contacts. The derivation of the consequent preload force needed would be trivial, but the experimental measurement of the preload force during the assembly phase would present some major challenges. As partly shown in Figure 4.39, piezoelectric load cells were tentatively integrated between the central preload arrangements and the fixture frame with the purpose of cross-checking the preload force during the assembly phase. The actual measurement, though, was made practically impossible by the low stiffness of the preload springs that drastically lowered the signal to noise ratio. Moreover, drift effects on the piezoelectric load cells were found to be relevant in case of such a quasi-static application.

Taking all those factors into consideration, an approach based on displacement measurements was preferred. The application of a compressive force would indeed generate a deformation of the piezo actuators (i.e., δ in Figure 4.37) that could be more easily measurable during the preload application phase, for example by simply measuring the resulting stage displacements with a Coordinate Measurement Machine (CMM), as shown in Figure 4.39.

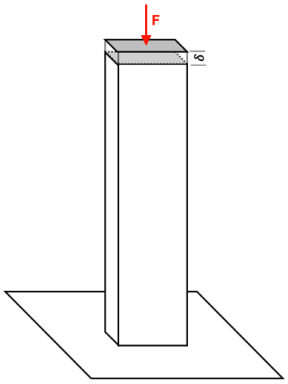

Figure 4.37: Equivalent beam deformation under the effect of a compressive load.

The actuators deflection corresponding to a given compressive stress can easily be computed according to simple beam theory relations, as:

$$\delta = \frac{\sigma_c \cdot L}{E} \tag{4.8}$$

where L is the actuator length, E is the Young modulus and σ_c is the compressive stress.

It should be noted though that equation (4.8) is only valid under the assumption of the opposite actuator extremity being rigidly fixed. In practice, also the supports of the actuators set screws would undergo deformations which could lower the actual compressive stresses on the actuators, consequently reducing the applied preload.

In order to increase the accuracy of the needed displacement estimation a dedicated FE analysis was again exploited. A simple linear static analysis was conducted, imposing a static displacement to the actuators extremities. As a tentative value a displacement equal to 0.012 mm was imposed, by maximizing by 20% the theoretical displacement derivable with equation (4.8) for the desired compressive stress. The resulting stresses for the piezo actuators integrated in the outer stage were estimated in approximately 10 MPa , as shown in Figure 4.38.

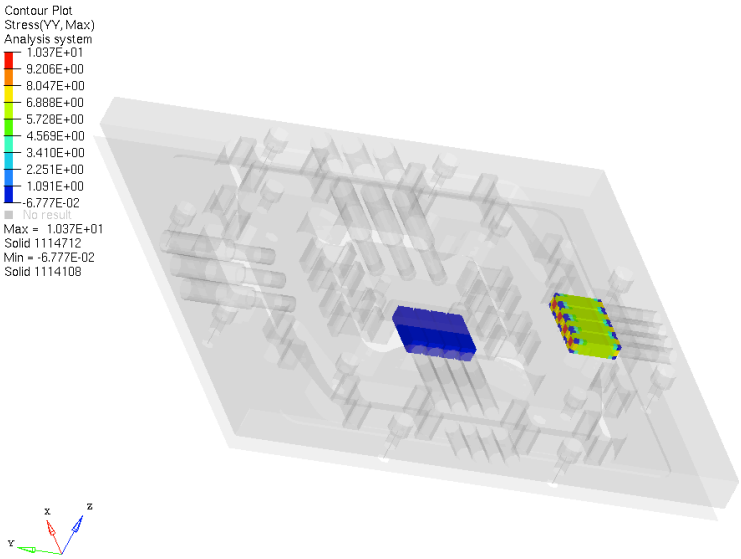

Figure 4.38: Estimation of compressive stresses on the piezo actuators as a consequence of an imposed displacement.

As shown, a 12 μm displacement would induce an adequate stress, according to the preload estimation previously described. In order to derive a more precautionary preload value, a safety factor of 2 was considered, leading to a required displacement of approximately 24 μm for the outer stage. Analogously, the displacement to be imposed to the inner stage was estimated equal to 20 μm.

As anticipated, the application of the required preload displacements was experimentally aided by a Mitutoyo Euro-C 776 Apex CMM, as shown in .Figure 4.39.

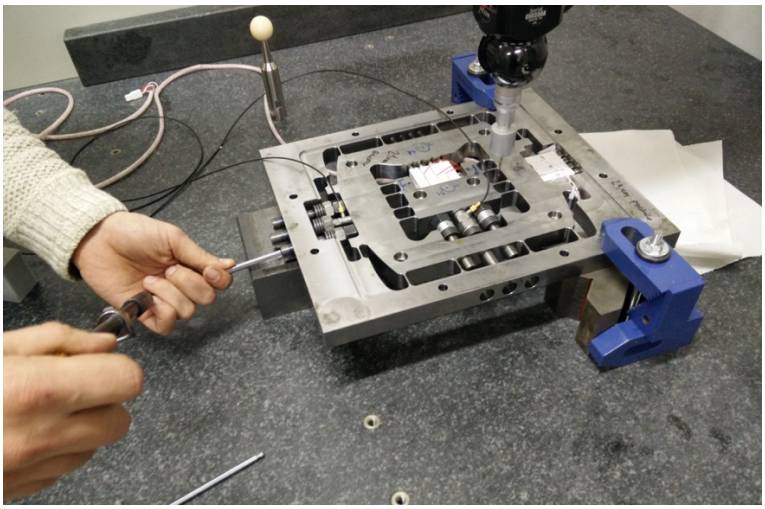

Figure 4.39: Application of the preload force to the outer stage of the AWH using the displacement measurements on the CMM.

In order to ensure an adequate distribution of the preload forces over the three preload arrangements acting in parallel, a torque wrench was used.

It should be highlighted that the application of the required preload force only ensures safe operability within the investigated frequency range, even though the safety factor used would be proficient in that sense. By increasing the actuation frequency, for example, the inertial force would grow considerably, reducing the effectiveness of the applied preload. That said, it should also be considered that relevantly increasing the actuation frequency is actually impeded also by electrical limitations in terms of current requirements on the piezo drivers, as briefly discussed in section 4.1.

4.4.2. Preliminary fixture testing

Once the active fixture prototype was assembled with the required preload, some preliminary experimental tests were conducted. In order to assess the maximum achievable displacement of the stages, some preliminary experimental tests were performed with the developed AWH prototype secured to the table of a Mori-Seiki NMV1500dcg 5-axis machining center. A Keyence LK-H085 laser displacement sensor was used to measure the displacement on a specimen workpiece, secured to the inner stage by means of two M10 screws. The experimental setup is shown in Figure 4.40.

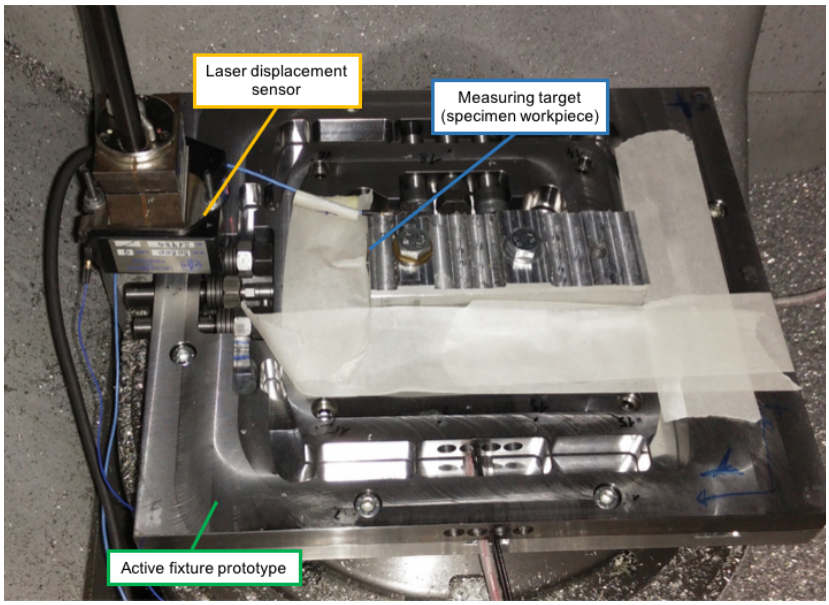

Figure 4.40: Experimental setup for the preliminary active fixture testing (outer stage displacement testing).

Several sine waves signals (i.e., different frequencies and voltages) were again fed to the piezo drivers using an LMS/Siemens SCADAS Mobile VibCo system, used also as acquisition device. As an exemplification of the achieved results, Figure 4.41 shows the displacement measured for the outer stage for different actuation voltages (V_{pp}) using 310 Hz sinusoidal signals.

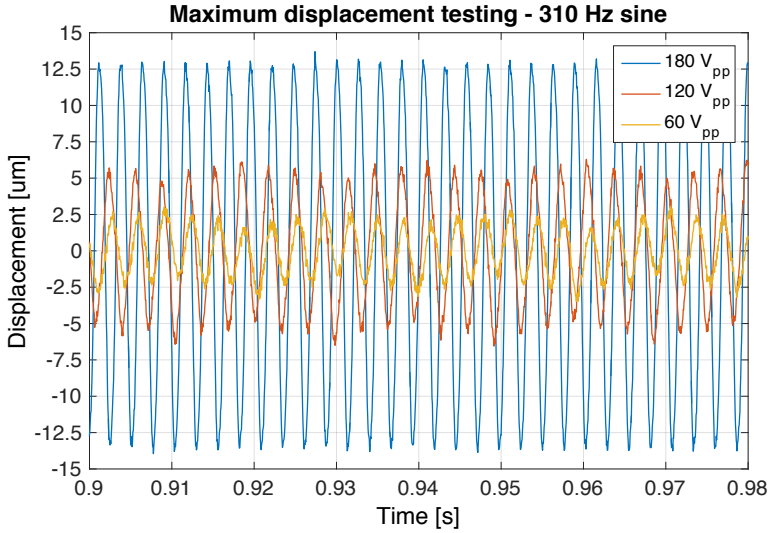

Figure 4.41: Measured outer stage displacements for different actuation voltages (Vpp).

Analogous tests were conducted for the inner stage. The experimental setup for the inner stage displacement measurements is shown in Figure 4.42, while the displacement measured for the inner stage for different actuation voltages (V_{pp}) using 150 Hz sinusoidal signals are reported in Figure 4.43.

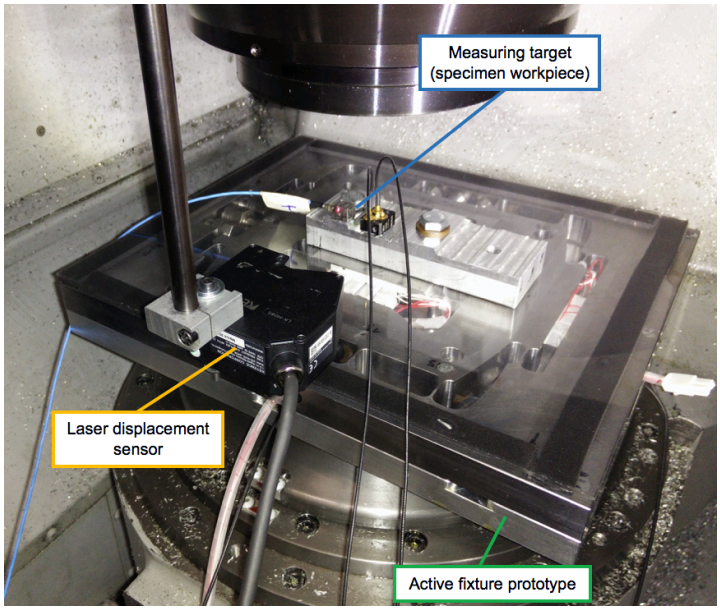

Figure 4.42: Experimental setup for the preliminary active fixture testing (inner stage displacement testing).

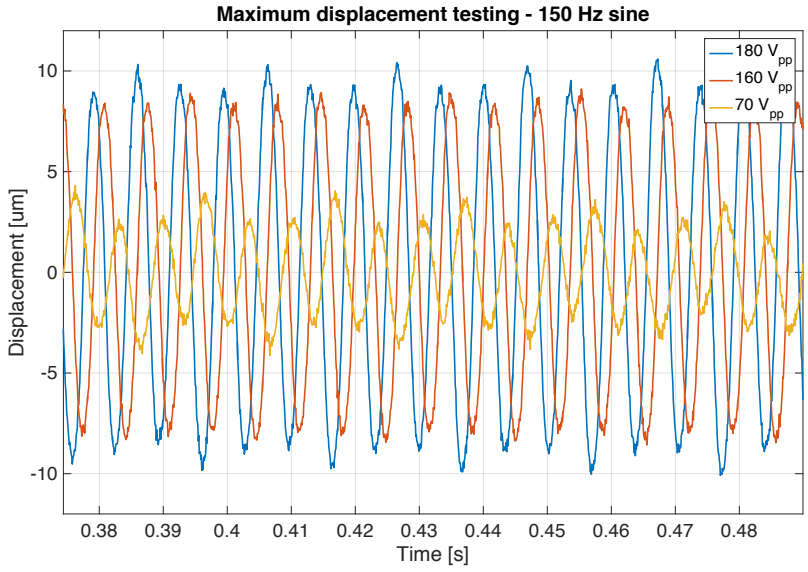

Figure 4.43: Measured outer stage displacements for different actuation voltages (Vpp).

As shown in Figure 4.41 and Figure 4.43 the device is capable of generating a maximum displacement of approximately 25 μm on both the stages, by providing $180V_{pp}$ to the piezo actuators, slightly lower to the maximum operable voltage for this specific actuators (i.e., $200V_{pp}$). This shows that the stiffness of the mechanical components integrated in the fixture (i.e., flexure hinges and preload springs) do not drastically affect the maximum displacement producible by the piezo actuators (i.e., nominally 32 μm).

It is worth highlighting that the maximum voltage should be applied to the piezo actuators to produce the maximum displacements, hence the actuation frequency could play a relevant role in defining the actual bandwidth for which the maximum displacement could be produced. Indeed, as already discussed in 4.1, the maximum current generable by the piezo driver poses an upper limit to the maximum operable frequency at full voltage. The Noliac NDR6880 piezo drivers selected feature a maximum current of 7 A, as reported in Table 4.4, which according to equation (4.3) defines a maximum operable frequency of approximately 500 Hz at full voltage (i.e., 200 V_{pp}). Within this frequency range the active fixture would be capable of exploiting the maximum producible displacements, as demonstrated also by the experimental tests conducted, that reported consistent results for all the frequencies tested, with minor differences attributed to the AWH dynamics.

Using actuation frequencies exceeding 500 Hz would be feasible only reducing the voltage applied to the piezo actuators. As an example, a 1 kHz actuation frequency would limit the maximum applicable voltage to approximately 100 V_{pp}, which would generate a maximum peak-to-peak displacement of approximately 12 μm (i.e., hysteresis, creep and non-linear phenomena neglected in this example).

4.4.3. **Preliminary testing of the AWH in chatter mitigation application**

Within the activities of the iNTEFIX European project, the developed active fixture prototype was preliminarily tested in chatter mitigation applications in real milling tests. The results of those tests are here briefly reported to show the performance achieved by the AWH prototype and to prove the robustness of the proposed design in actual applications.

The control logic used for the active fixture in that configuration was developed by the project partner Paragon SA in previous AVC activities and adapted for the specific application. The developed controller exploited a set of integrated modules to identify the chatter frequency to be mitigated and the suitable control signals needed for the purpose (i.e., the actuation parameters that would allow a condition of disruptive interference of the chatter vibrations), by providing a few preliminary cutting tests are conducted for the system "learning" phase. The mentioned modules are based on Artificial Neural Networks (ANNs) and Genetic Algorithms (GAs), following the functional scheme reported in Figure 4.44.

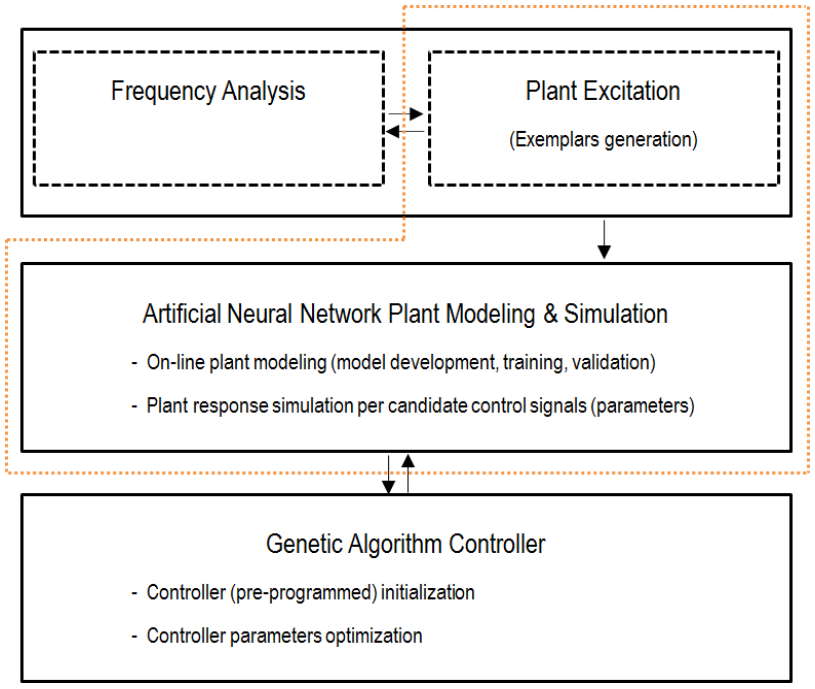

Figure 4.44: Modules of the control strategy implemented in the preliminary chatter mitigation tests [95]**.**

Some further details about the control logic are discussed by authors in a dedicated paper [95] and will not be reported here in detail given that its development did not involve the author directly and the approach used (i.e., disruptive interference) is not in line with the research goals of this thesis. Counteracting chatter vibrations using the disruptive interference phenomenon would indeed not cope with the need of a general application where chatter frequencies could exceed the operable frequencies of the AWH prototype.

In order to investigate the performance of the developed AWH in mitigating chatter vibrations, dedicated experimental tests were carried out on a DMG DMC 635V eco 3-axis milling machine, in slotting operations. A 16mm indexable mill with two cutting flutes (i.e., Widia VSM11D016Z02A16XD11L170) was used for the tests. The workpiece was a 60x132x25mm AISI P20s steel secured to the AWH by means of two M8 screws. An acrylic cover was placed below the workpiece to protect the electronics within the AWH against hot chips and cutting fluids. Three PCB356A32 triaxial accelerometers have been used as sensors for the derivation of the optimal control signals. Two of these were secured to the bottom of the fixture in order to measure the vibrations of each dynamic stage, while the third one was placed at the base of the spindle housing in order to get a better estimation of tool-tip vibrations, as necessary for the assessment of vibration reduction. An optical tachometer was used to provide constant reference of a specific point of the tool during rotation, which in turn was used to calculate the phase difference for the control signal, based on the principle of two identical waves with 180° phase difference canceling each other out (i.e., disruptive interference). The optical tachometer provided a stable point from which to make phase calculations based on the tool geometry (number of teeth). The test setup is shown in Figure 4.45.

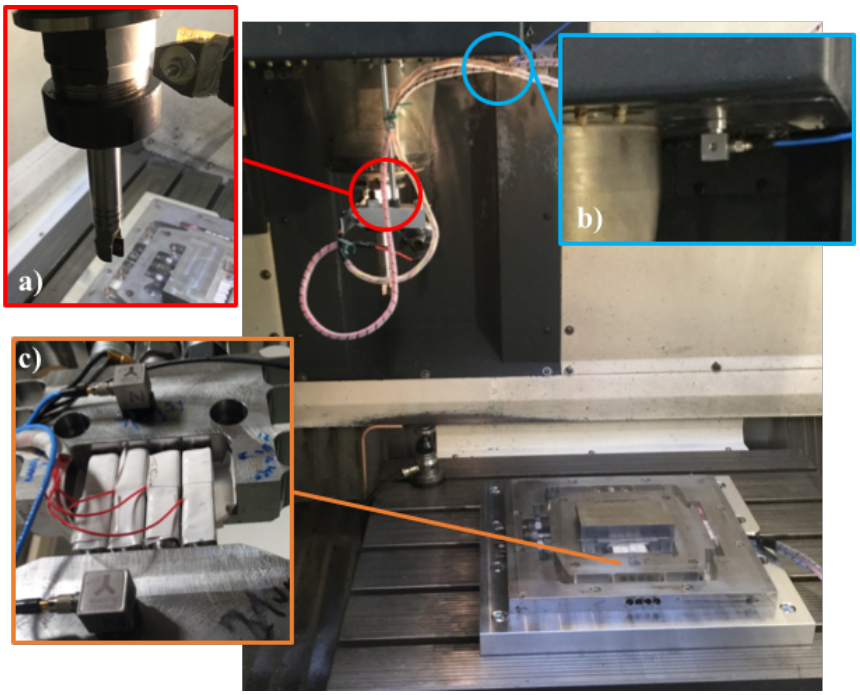

Figure 4.45: Experimental setup for the preliminary chatter tests. a) Detail of the optical tachometer, b) Detail of the triaxial accelerometer at the spindle base, c) triaxial accelerometers placed at the bottom of the AWH.

Some preliminary tests were conducted to identify both workpiece/fixture and tooltip FRFs, reported in Figure 4.46, and the consequent stability limits for the test setup. For sake of brevity the results are here only summarized. The preliminary experimental tests highlighted a natural frequency of the tool equal to 1151 Hz and an axial depth of cut limit, in slotting operation equal to 0.4 mm, for the rotational speed used in the tests (i.e., 3600 rpm).

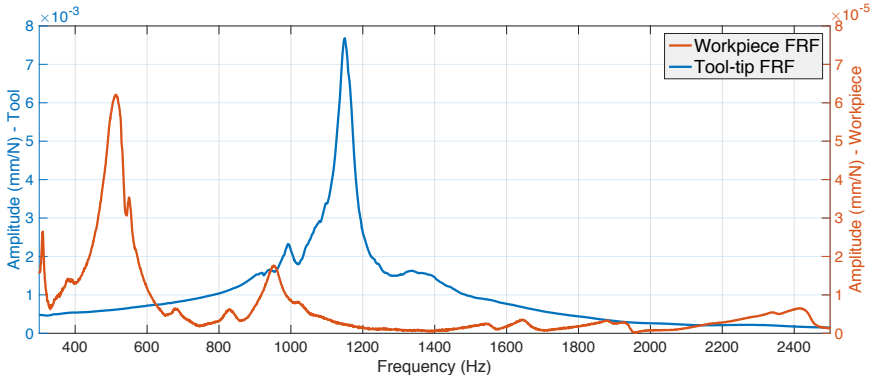

Figure 4.46: Measured FRFs of tool (blue line) and workpiece (red line).

As shown, the effect of workpiece mass pushed the dominant mode of the workpiece/fixture down at approximately 530 Hz. The amplitude at the dominant mode of the tool FRF is two order of magnitude higher respect to the workpiece/fixture FRF, suggesting that the chatter vibrations would be originated by the tool flexibility, while the fixture dynamics would play a negligible effect on the stability limits.

In order to ensure that the tests are conducted in chatter conditions, axial depth of cuts of 0.5 mm and 0.6 mm were used for the experimental tests, respectively with control turned off and on.

Figure 4.47 reports an example of the achieved results in terms of chatter mitigation during linear slot milling tests on Y direction (machine tool reference system), acquired with the accelerometer at the spindle housing.

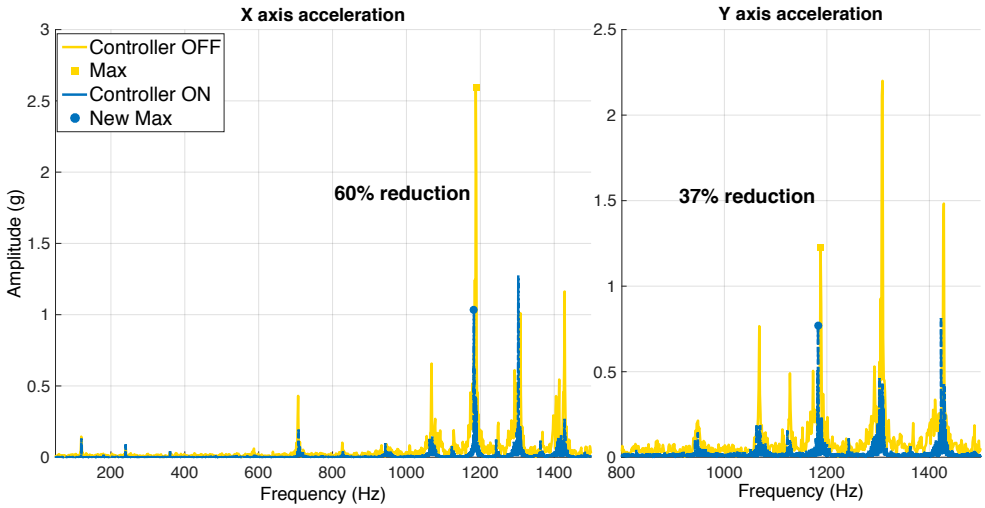

Figure 4.47: Example of chatter (X-Y axes) during linear Y cut at Ap=0.5 mm (yellow) and the resulting reduction at depth of Ap=0.6 mm (blue). Accelerations measured at the spindle housing.

For the purpose of this thesis, the main outcome of those tests was twofold: on one hand the tests proved the suitability of the developed prototype for AVC applications, even for actuation frequencies exceeding the kHz range, such as for the results shown in Figure 4.47 (i.e., chatter frequency around 1.2 kHz). On the other hand the prototype was capable of withstanding close-to industrial conditions for the whole duration of the testing campaign (i.e., four days), including relevant cutting forces (estimated approximately 1 kN) and the high temperatures generated in the cutting process, as shown in Figure 4.48. Moreover, the actuators presented negligible self-heating, confirming the better suitability of hard-doped piezo ceramics for such demanding dynamic applications.

Figure 4.48: Workpiece temperature measurement after the machining tests (max 91.2°C).

It is worth highlighting that to reach the frequency needed for the tests here briefly presented, the maximum voltage applicable to the piezo actuators needed to be decreased, due to the current limitations on the piezo drivers, as already discussed in previous sections. Even though the hard-doped piezo actuators allowed decreasing the stacks capacitance values, hence partially reducing this issue, a control logic targeted at stabilizing the process by actuating at the chatter frequency would not be suited to exploit the maximum prototype performance. More powerful piezo drivers could potentially be selected, but the limitations in terms of inertial forces would anyway impose compromises. These considerations proved once more that alternative control strategies would be advised in that sense, as will be shown in the following chapter.

5. Control logic development

The present chapter presents all the steps of the development of a suitable control logic to be implemented in the active fixture prototype developed.

As discussed in the previous sections, making the device capable of dealing with chatter frequencies sensibly exceeding the kHz range is mandatory to ensure the potential applicability to general milling applications. This consideration poses specific requirements for both the mechanical design, as described in the previous chapters, and the control logic to be implemented in the fixture. Previous literature works report the implementation of different control strategies. Brecher et al. [57] proposed a control scheme to compensate the relative displacement between workpiece and tool by using position estimators, as schematized in Figure 5.1. The application though was aimed at mitigating chatter vibrations originated by a structural weak point at 61 Hz, hence way below the target frequency range of a general application.

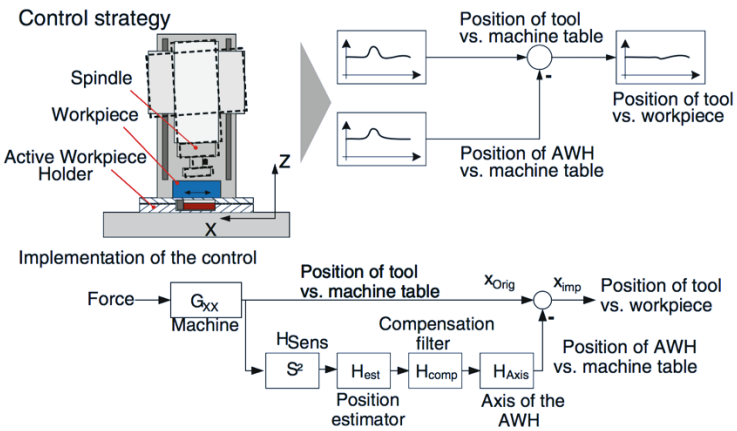

Figure 5.1: Control scheme for the compensation of relative tool-workpiece displacements [57]**.**

Similarly, both Ford et al. [56] and Rashid et al. [60] described the implementation of filtered-X Least Mean Square (fxLMS) algorithms in vibration control in milling by means of active fixtures. In particular, Ford et al. [56] investigated the effect of the proposed strategy in mitigating chatter vibrations up to 1 kHz, while Rashid et al. [60] only investigated the application to frequencies below 100 Hz. In addition, Long et al. [59] used robust mixed sensitivity method to control vibrations in peripheral milling applications within 200 Hz.

The applicability of all these techniques would directly depend on the active fixture bandwidth that, as discussed in the previous sections, is drastically limited by inertial forces and electrical and thermal issues on the actuator side. Moreover, it should be pointed out that model-based strategies, such as the ones described, would require prior system identification and modelling to derive the needed transfer functions. This would make an industrial application far more complex, also considering that the active fixture transfer function could relevantly change during the process as a consequence of the workpiece mass removal. To provide a practical exemplification of the drawbacks associated to such model-based approaches, we could refer to the control logic used in the preliminary tests discussed in Section 4.4.3. Preliminary cutting tests were needed in order to acquire the data for the system modeling modules implemented in the control logic: the number of tests depends on the number of frequencies to be controlled and the derived number of actuation parameters. Even the simplest application, such as the one shown in Section 4.4.3 (i.e., single chatter frequency to be mitigated), requires approximately 60 s of identification tests for each cutting direction, that must be repeated for each different tool and/or workpiece material.

All these considerations motivated the work reported in this chapter in investigating the feasibility of an alternative model-less control strategy capable of mitigating chatter vibrations in general applications (i.e., several kHz) by exploiting counter-excitations within the device bandwidth (i.e., below 1 kHz).

As discussed in previous works [58,96,97], modelling and simulating the cutting process, including the active fixture behavior, represents a fundamental task in developing effective control strategies to be implemented in the physical active fixtures. In order to assist the investigation and development of such a control strategy, a dedicated time-domain model was developed, as discussed in the following sections.

5.1. Time-domain simulation model

The design of a control system integrating actuators and sensors requires an accurate knowledge of the transfer functions between the inputs and the outputs of the system. A simplified model of the active fixture system, as previously described, was used to ease the development of the dedicated simulative environment. By lumping stiffness and damping of the stages (i.e., actuators, flexure hinges, preload springs, etc.), the active fixture can be schematized as in Figure 5.2, where F_{px} and F_{py} represent the force generated along the two DOFs by the piezoelectric actuators.

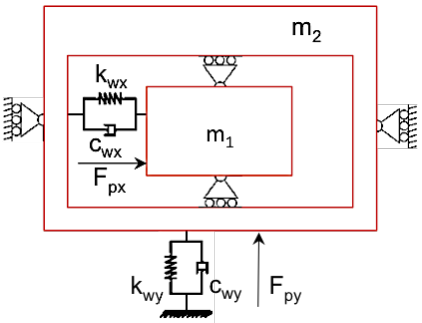

Figure 5.2: Simplified schematization of the active fixture prototype.

As discussed in the previous chapters, the piezoelectric actuators achieve the purpose of controlling the stage displacements by using the inverse piezoelectric properties of piezoelectric materials, which generate shape change if an electric field is applied. The general approach in modelling these effect is by inducing additional workpiece displacement [97] in order to simulate the actuation effect, but this simulated effect could often be not consistent with the electrical and physical operability of piezo actuators. Taking those factors into account, a dedicated model for the piezo actuators embedded in the fixture was integrated with the purpose of directly relating the effect of actuators input voltage on the fixture behavior.

The IEEE published a Standard on Piezoelectricity [98], wherein linear constitutive relations are defined, that lay a foundation upon which dynamic models of piezo actuators can be built. A more correct approach to piezoelectric materials should consider some level and type of non-linearity, in particular hysteresis, which could affect the performance of such devices, as briefly discussed in section 4.3.2. Nonetheless, even among the proponent of non-linear modeling there are some that concede the point that linear models may be sufficient for prediction, simulation and controller design [99]. For this reason, the piezo actuators can be described by means of a simple linear model, relating the input voltage and the output force, as anticipated in section 4.1, without taking into account hysteresis or creep phenomena.

The following relations can be used to define the characteristics of the piezoelectric actuators:

$$[M]\{\ddot{u}\} + [C]\{\dot{u}\} + [K_{uu}]\{\ddot{u}\} + [K_{u\vartheta}]\{\vartheta\} = \{f\} \tag{5.1}$$

$$[K_{u\vartheta}]^T\{u\} + [K_{\vartheta\vartheta}]\{\vartheta\} = \{q\} \tag{5.2}$$

where: $[K_{uu}]$, $[C]$ and $[M]$ are respectively the mechanical stiffness, damping and mass matrices, $[K_{\vartheta\vartheta}]$ is the dielectric stiffness matrix, $[K_{u\vartheta}]$ is the piezoelectric coupling matrix, $\{u\}$ is the nodal displacement vector, $\{f\}$ is the vector of the external mechanical forces, $\{q\}$ and $\{\vartheta\}$ are the nodal vectors of the electric charge and scalar electric potential respectively.

In order to simulate the actual interaction between the active workpiece holder and the cutting process, the dynamics of the milling process must be included in the model. According to literature, the dynamics of the milling process, considering the regenerative effect, can be described by an n-dimensional linear time periodic system with a single discrete time delay [1].

Without loss of generality, the simplest analytical description of the milling process involving an active workpiece holder driven by piezo actuators, requires a four DOFs lumped parameters dynamics model, as shown in Figure 5.3. Actually the milling cutter and the proposed workpiece holder architecture can be considered to have two orthogonal DOFs each. In this work the cutter is assumed to have a generic number of teeth, n, with a zero helix angle in order to reduce computational effort. With this simplification, indeed, the z-level discretization of the helix angle can be avoided.

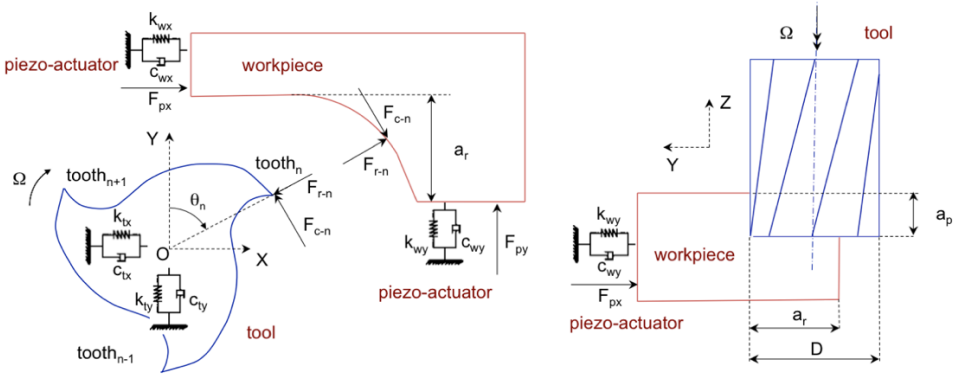

Figure 5.3: Dynamic end milling system with active workpiece holder.

The governing equation of the milling process shown in Figure 5.3 can be formulated as the following differential equations system:

$$\begin{cases} \ddot{x}_t(t) + 2\xi_{tx}\omega_{tx}\dot{x}_t(t) + \omega_{tx}^2 x_t(t) = \dfrac{\omega_{tx}^2}{k_{tx}} \cdot F_x(t) \\ \ddot{y}_t(t) + 2\xi_{ty}\omega_{ty}\dot{y}_t(t) + \omega_{ty}^2 y_t(t) = \dfrac{\omega_{ty}^2}{k_{ty}} \cdot F_y(t) \\ \ddot{x}_w(t) + 2\xi_{wx}\omega_{wx}\dot{x}_w(t) + \omega_{wx}^2 x_w(t) = -\dfrac{\omega_{wx}^2}{k_{wx}} \cdot [F_x(t) + k_{\vartheta x}\vartheta_x(t)] \\ \ddot{y}_w(t) + 2\xi_{wy}\omega_{wy}\dot{y}_w(t) + \omega_{wy}^2 y_w(t) = -\dfrac{\omega_{wy}^2}{k_{wy}} \cdot [F_y(t) + k_{\vartheta y}\vartheta_y(t)] \end{cases} \tag{5.3}$$

where the subscripts *t* and *w* identify the tool and the workpiece respectively, ζ is the damping coefficient, ω is the angular natural frequency, and k is the modal stiffness, while ϑ_x and ϑ_y are the instantaneous electric potential applied to the controlled piezo actuator along the X and Y direction respectively.

The forces $F_x(t)$ and $F_y(t)$ excite tool and workpiece in the feed (X) and normal (Y) directions, causing dynamic displacements $\Delta x\,(t)$ and $\Delta y\,(t)$ respectively, which are responsible of the regenerative instability:

$$\Delta x(t) = \Big(\big(x_t(t) - x_w(t)\big) - \big(x_t(t-\tau) - x_w(t-\tau)\big)\Big) \tag{5.4}$$

$$\Delta y(t) = \Big(\big(y_t(t) - y_w(t)\big) - \big(y_t(t-\tau) - y_w(t-\tau)\big)\Big) \tag{5.5}$$

where τ is the tooth passing interval.

According to the renowned mechanistic cutting force model [100], the tangential and normal cutting force components for the kth tooth, F_{ck} and F_{rk}, can be related to the axial depth of cut a_p and the instantaneous chip thickness $h_k(t)$ using the constant cutting coefficients K_{tc}, K_{te}, K_{rc}, and K_{re}.

$$F_{ck}(t) = K_{tc}a_p h_k(t) + K_{te}a_p \tag{5.6}$$

$$F_{rk}(t) = K_{rc}a_p h_k(t) + K_{re}a_p \tag{5.7}$$

The regenerative instantaneous chip thickness $h_k(t)$ can be assumed to be the sum of the kinematic chip thickness and the regenerative dynamic chip thickness, which is related to the dynamic displacements $\Delta x\ (t)$ and $\Delta y\ (t)$ projected in the chip thickness direction:

$$h_k(t) = \left[(f_z + \Delta x(t)) \cdot \sin\left(\phi_k(t)\right) + \Delta y(t) \cdot cos\left(\phi_k(t)\right)\right] \cdot g\left(\phi_k(t)\right) \tag{5.8}$$

where the function $g\left(\phi_k(t)\right)$, is used to indicate the engagement of the tooth:

$$g\left(\phi_k(t)\right) = \begin{cases} 1 & if\ \phi_{st} < \phi_k(t) < \phi_{ex} \\ 0 & otherwise \end{cases} \tag{5.9}$$

in which ϕ_{st} and ϕ_{st} are respectively the start and exit immersion angles of the cutter. For up-milling $\phi_{st} = 0$ and $\phi_{ex} = arcos(1 - 2a_r/D)$, while for down-milling $\phi_{st} = arcos(2a_r/D - 1)$, and $\phi_{ex} = \pi$, being a_r/D the radial immersion ratio (radial depth of cut/tool diameter).

Resolving the cutting forces in the X and Y directions leads to:

$$F_x = -\sum_{k=0}^{n-1} F_{ck}(t) \cdot cos\left(\phi_k(t)\right) + F_{rk}(t) \cdot sin\left(\phi_k(t)\right) \tag{5.10}$$

$$F_y = \sum_{k=0}^{n-1} F_{ck}(t) \cdot sin\left(\phi_k(t)\right) - F_{rk}(t) \cdot cos\left(\phi_k(t)\right) \tag{5.11}$$

By rearranging the previous equations, it is possible to reduce the dynamics of the milling process, described by equation (5.3), to an equivalent coupled delayed differential equation (DDE):

$$M \cdot \ddot{X}(t) + C \cdot \dot{X}(t) + K \cdot X(t) = K_c(t)\left(X(t) - X(t-\tau)\right) + K_\vartheta \vartheta \tag{5.12}$$

where *M, C, K* and *X(t)* represent the mass matrix, damping matrix, stiffness matrix and displacement vector of the system (4 DOFs), respectively, while $K_c(t)$ is the cutting force coefficient matrix, K_ϑ is the dielectric stiffness matrix and $\{\vartheta\}$ is the nodal vector of scalar electric potential.

The dynamic milling process considering the regenerative effect is generally modeled as a linear time periodic system with a single discrete time delay, which can be approximately solved by using the analytical or numerical methods [1,101]. On the other hand, time domain numerical simulation methods are quite powerful: they are capable of taking into account true kinematics of the milling process, mechanics of cutting, the influence of inner and outer modulation, cutter geometry, run-out and other non-linearities, but their computational cost is normally too high. In order to achieve high computational efficiency and second order accuracy, a full-discretization method based on an implicit direct integration scheme was used.

The first step to solve equation (5.12) numerically is to discretize the time period τ, hence equally divide τ into *m* small time intervals, so that $\tau = m \cdot \Delta t$, where *m* is an integer. For each time interval $t_n = t_o + n \cdot \Delta t$ the response $X_n = X\ (t_n)$ of equation (5.12) can be obtained via the direct Newmark integration scheme [102], given the initial condition $X_0 = X\ (t_0)$, $\dot{X}_0 = \dot{X}\ (t_0)$ and $\ddot{X}_0 = \ddot{X}\ (t_0)$. This method relies on the following interpolations that relate positions $X\ (t)$, velocities $\dot{X}\ (t)$, and accelerations $\ddot{X}(t)$, from step n to step $n + 1$:

$$X_{n+1} = X_n + \Delta t \cdot \dot{X}_n + \frac{\Delta t^2}{2} \cdot \left[(1 - 2\beta) \cdot \ddot{X}_n + 2\beta \cdot \ddot{X}_{n+1}\right] \tag{5.13}$$

$$\dot{X}_{n+1} = \dot{X}_n + \Delta t \cdot \left[(1 - \gamma) \cdot \ddot{X}_n + \gamma \cdot \ddot{X}_{n+1}\right] \tag{5.14}$$

where X_n, $\dot{X}_n$, $\ddot{X}_n$ are approximations to the position, velocity, and acceleration vectors at time step n, Δt is the time step size, and β and γ are the free parameters of integration.

For $\gamma = 1/2$ and $\beta = 1/4$ the method reduces to the trapezoidal rule and is energy conserving [103]. This choice of parameters leads to averaging acceleration in $[t_n, t_{n+1}]$. If $\gamma > 1/2$ and $\beta > 1/4 \cdot (1/2 + \gamma)^2$ numerical damping is induced into the solution leading to a loss of energy and momentum. In this work the average constant acceleration scheme (i.e., $\gamma = 1/2$ and $\beta = 1/4$) was considered, as it represents the unconditionally stable scheme (i.e., implicit), with asymptotically the highest accuracy [103,104].

The interpolations of equation (5.13) and equation (5.14) can be directly introduced into the equations of motions (i.e., equation (5.12)). This leads to a set of algebraic equations that can be either linear or non-linear, depending on the type of problem, with $\ddot{X}_{n+1}$ as the resulting unknown. A set of linear equations is obtained if a linear cutting force model is used, as that proposed in this work.

Application of the Newmark method to the direct time-integration of Eq. (5.12) requires a three-step procedure:

1) Evaluation of the system displacements and velocities at the time step *n+1* (predictor phase):

$$\tilde{X}_{n+1} = X_n + \Delta t \cdot \dot{X}_n + \frac{\Delta t^2}{2} \cdot (1 - 2\beta) \cdot \ddot{X}_n \tag{5.15}$$

$$\dot{\tilde{X}}_{n+1} = \dot{X}_n + \Delta t \cdot (1 - \gamma) \cdot \ddot{X}_n \tag{5.16}$$

2) Resolution of the above system of equations, resulting from the substitution of equation (5.13) and equation (5.14) into equation (5.12), for $\ddot{X}_{n+1}$:

$$\begin{aligned}[M + C \cdot \gamma \cdot \Delta t + (K - K_c) \cdot \beta \cdot \Delta t^2] \cdot \ddot{X}_{n+1} \\ = K_y \vartheta_{n+1} - K_c X_{n+1-m} - C \cdot \dot{\tilde{X}}_n - (K - K_c) \cdot \tilde{X}_n\end{aligned} \tag{5.17}$$

If the time-step Δt is uniform, the system matrix of equation (5.17) can be factored once.

3) Substitution of the result into expression to obtain X_{n+1} and $\dot{X}_{n+1}$ (corrector phase).

$$X_{n+1} = \tilde{X}_{n+1} + \beta \cdot \Delta t^2 \cdot \ddot{X}_{n+1} \tag{5.18}$$

$$\dot{X}_{n+1} = \dot{\tilde{X}}_n + \gamma \cdot \Delta t \cdot \ddot{X}_{n+1} \tag{5.19}$$

This implementation is very efficient, and may be also carried out for nonlinear problems, by customarily solving the resulting set of nonlinear algebraic equations in $\ddot{X}_{n+1}$ with either Newton-Raphson iteration, which has a quadratic convergence in the proximity of the solution, secant methods, or quasi-Newton method [104].

5.1.1. **Experimental validation**

To prove the accuracy of the proposed approach, an experimental validation was carried out using a Mori Seiki NMV1500 DCG 5-axis vertical milling machine. The selected test workpiece was a block of 6082-T4 aluminum, fixed on a Kistler 9257A piezoelectric dynamometer, as shown in Figure 5.4a.

a) 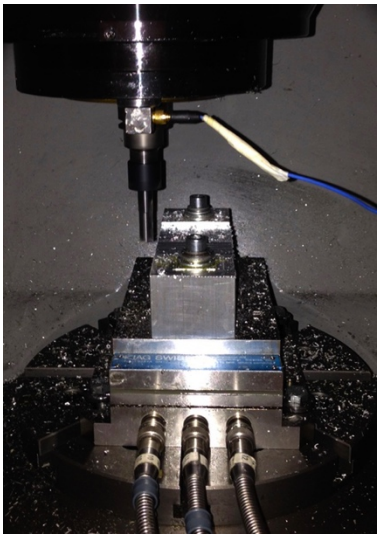 b) 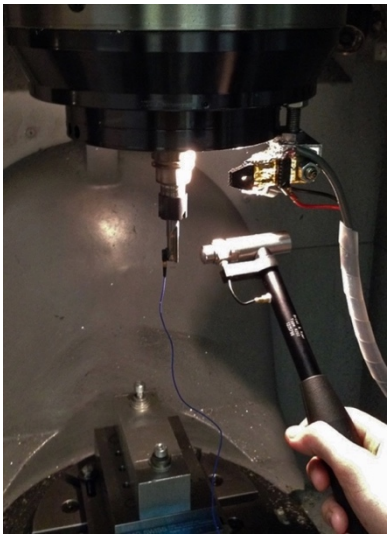

Figure 5.4: a) Cutting tests setup, b) Impact testing on the tooling.

Several cutting tests in slotting operations were performed at different depths of cut. A 10 mm Garant 201320 end mill, with regular pitch and null helix angle was used in order to avoid the influence of the helix angle on cutting forces. The cutting speed was set to 140 m/min (4458 rpm) according to the suggested tool parameters.

Tooltip FRF was measured with an LMS SCADAS III acquisition system, using a Brüel&Kjær 8202 instrumented hammer and a PCB 352C22 accelerometer (0.5g), as shown in Figure 5.4b.

Modal curve-fitting allowed identifying the modal parameters of an equivalent single degree of freedom system, for both the tooling and the fixture (i.e., piezoelectric dynamometer), as exemplified in Figure 5.5 and Figure 5.6, for the tooling and the fixture FRFs respectively.

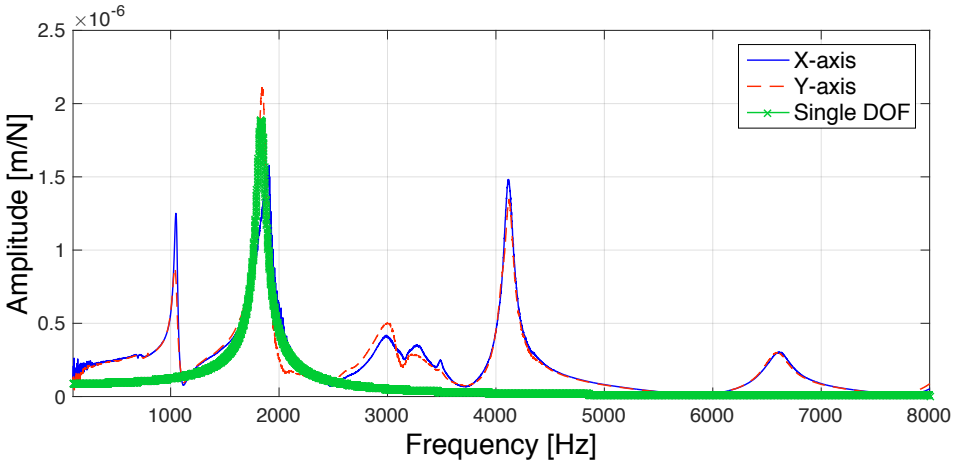

Figure 5.5: Experimental tooltip FRFs and curve fitted single degree of freedom FRF.

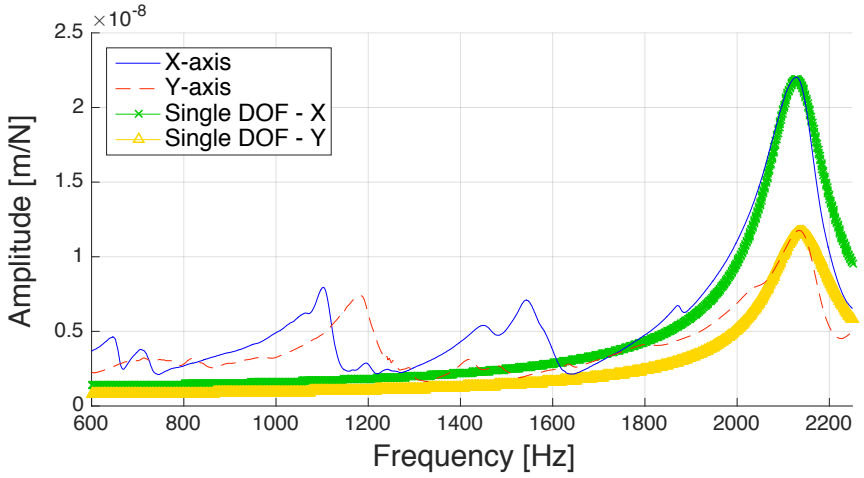

Figure 5.6: Experimentally identified FRFs of the fixture (i.e., piezo-electric table dynamometer) and curve fitted FRFs.

Table 5.1 summarizes the identified modal parameters for both tooling and fixture:

Table 5.1: Identified modal parameters.

	Direction	Natural frequency, f_n	Damping coefficient, ζ	Modal stiffness, k
Tooling	X - Y	1836 Hz	0.0231	$1.15e^7$ N/m
Fixture	X	2120 Hz	0.0286	$0.8e^9$ N/m
	Y	2140 Hz	0.0306	$1.4e^9$ N/m

Cutting force coefficients were estimated on the average measured cutting forces in stable slotting operations at different feed per tooth (f_z), close to the recommended value (i.e., f_z =0.05 mm/rev per tooth), as discussed in a previous work [22]. The identified coefficients are reported in Table 5.2. Tool run-out was experimentally measured equal to 20 μm.

Table 5.2: Identified cutting force coefficients.

K_{tc} (N/mm^2)	K_{te} (N/mm)	K_{rc} (N/ mm^2)	K_{re} (N/mm)
1086.66	764.29	139.03	33.32

Figure 5.7 shows a comparison of experimental and estimated cutting forces (a_p = 0.8mm) in which the simulation was performed considering a tool with a single tooth, and an equivalent feed per tooth (f_z = 0.09 mm), obtained by increasing the nominal value by the measured tool run-out, because the model did not take into account tool run-out at that stage. The measured cutting forces were dynamically compensated in order to ensure adequate accuracy, using a dedicated procedure developed by the author in a previous research [105].

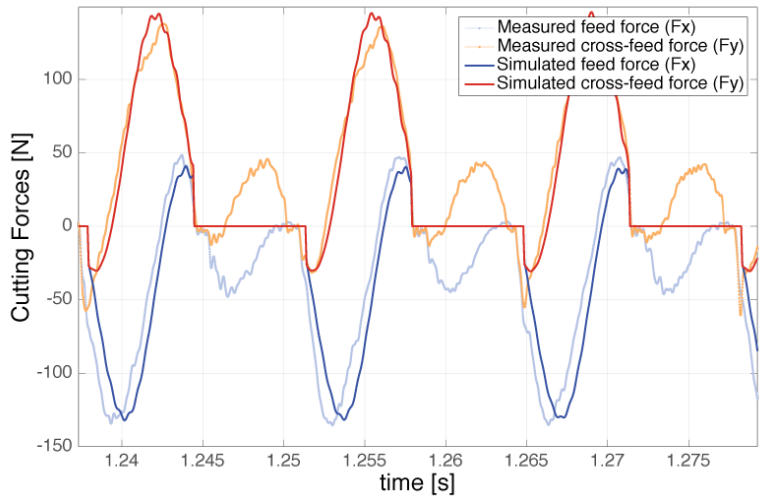

Figure 5.7: Measured and simulated cutting forces in stable condition (a_p=0.8 mm).

The predicted and measured cutting forces are in good agreement, which indicates the accuracy of the proposed time domain model.

The model is capable of correctly simulating stable and unstable cutting conditions as well as the onset of chatter phenomenon. By increasing axial depth of cut to a_p = 1mm, cutting forces clearly show the growth of chatter vibrations and the development of a new "pseudo-stable" cutting condition (i.e., the system evolves into a new equilibrium point with a relevant level of chatter vibrations). This is consistent with the periodic disengagement of the tool, as discussed in Chapter 2, which is the main cause of chatter marks on the workpiece and associated with chatter vibrations. This aspect is described by the simulated cutting force time-series reported in Figure 5.8, in which the transition phase and the "pseudo-stable" condition are highlighted.

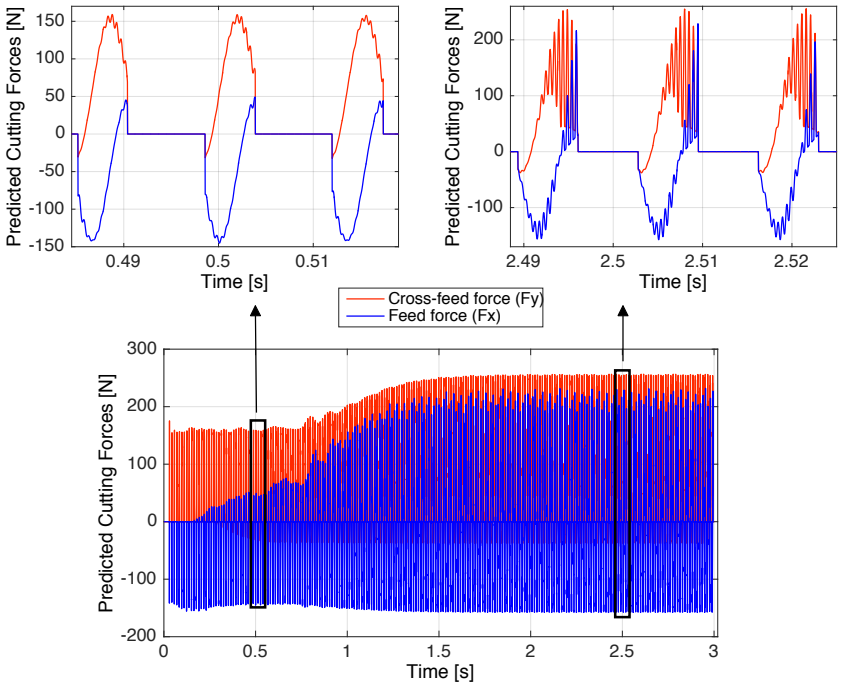

Figure 5.8: Analysis of predicted cutting forces in case of chatter.

In order to prove the model capabilities of accurately simulate the cutting process in the presence of chatter vibrations, the experimental validation tests have been extended by investigating unstable conditions in slotting operations for higher axial depths of cut. Figure 5.9 shows the comparison between simulated and measured cutting forces for a slotting test with a_p = 1mm. Again the teeth number and feed per tooth were adjusted in order to account for the evident run-out effect that is not modelled in the simulation, as for the test previously described.

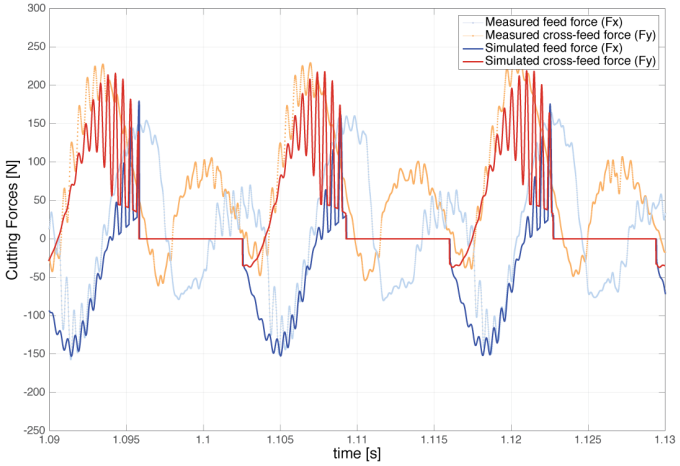

Figure 5.9: Measured and simulated cutting forces in chatter condition (a_p=1 mm).

As shown the simulated and measured cutting forces were again in good agreement. Analogous results were obtained for all the validation tests, both in stable and unstable conditions.

The proposed time domain model has been implemented in a Matlab code. The simulation of a 3 s slotting tests takes about 13 s on a 1.7 Ghz Intel dual core I7 processor with 8 Gb Ram, using a time step of 0.0168 ms (800 time intervals over the period τ).

5.2. Mathematical analysis

Hereafter a preliminary mathematical demonstration of the feasibility of a low-frequency actuation strategy to disrupt chatter vibrations is presented in order to highlight the theoretical requirements of such an alternative control approach.

By collecting all the state variables of the milling process in $\xi(t) \in \mathbb{R}^8$, the model described by equation (5.13) can be rewritten in the compact form as

$$\dot{\xi}(t) = A(t)\xi(t) + B(t)\xi(t - \tau) + C(t)\chi(t) \tag{5.20}$$

for properly defined time-varying matrices $A(t)$, $B(t)$, $C(t)$, and using as input vector $\chi(t) = \lambda(t) + \sigma(t)$, where λ depends on the feed rate f and σ on the electric potentials of the piezo actuators. Considering the intrinsic chip thickness periodicity, the time dependency of the system defined by equation (5.12) is periodic of the tooth passing period τ, hence the following conditions are satisfied

$$\begin{aligned} &A(t + \tau) = A(t) \\ &B(t + \tau) = B(t) \\ &C(t + \tau) = C(t) \\ &\lambda(t + \tau) = \lambda(t) \text{ for } f = \text{constant} \end{aligned} \tag{5.21}$$

Hereafter, the model described by equation (5.20) is approximated with a Linear Time Invariant (LTI) system by sampling the state ξ n times during the tooth-passing period, and by gathering the related temporal evolutions into a single law. By doing so, the milling process dynamics is finally described in terms of a sequence of discretized cutting profiles (i.e., the state of the workpiece during the tooth passing period), each of them related to a single tooth-pass. Such an approximation of the system represents the basis for the investigation and development of the low-frequency control strategy.

Then, let us chose n time samples inside each tooth-passing period by defining the discretization time step as $\mu = \frac{\tau}{n}$. Without any loss of generality, the initial time of the process is chosen zero, i.e. $t_0=0$, and the following samples of the state and the input are defined accordingly as:

$$\begin{aligned} &\xi_i(k) = \xi(k\tau + (i-1))\mu \\ &\chi_i(k) = \chi(k\tau + (i-1))\mu \end{aligned} \qquad i = 1, \dots, n \tag{5.22}$$

Similarly, A, B and C in equation (5.20) are sampled as well, obtaining the static matrices:

$$\begin{matrix} A(k\tau+(i-1))\mu = A_i \\ B(k\tau+(i-1))\mu = B_i \\ C(k\tau+(i-1))\mu = C_i \end{matrix} \qquad i = 1,\dots,n \tag{5.23}$$

Subsequently, the application of the Tustin discretization approach [106] to model described by equation (5.20) leads to:

$$\begin{aligned} \xi(t+\mu)-\xi(t) = \int_t^{t+\mu} \dot{\xi}(v)dv &\approx \frac{\mu}{2}\left(\dot{\xi}(t+\mu)+\dot{\xi}(t)\right) \\ &= \frac{\mu}{2}\big(A(t+\mu)\xi(t+\mu)+B(t+\mu)\xi(t-(n-1)\mu) \\ &+ C(t+\mu)\chi(t+\mu)+A(t)\xi(t)+B(t)\xi(t-n\mu)+C(t)\chi(t)\big) \end{aligned} \tag{5.24}$$

Thus, by exploiting the previous assumptions and by referring to $t = k\tau+\mu(i-1)$, the discrete time approximation of the system boils down to:

$$\begin{aligned} \left(I-\frac{\mu}{2}A_1\right)\xi_1(k) &\approx \left(I+\frac{\mu}{2}A_n\right)\xi_n(k-1)+\frac{\mu}{2}B_1\xi_1(k-1) \\ &+\frac{\mu}{2}B_n\xi_n(k-2)+\frac{\mu}{2}C_1\chi_1(k)+\frac{\mu}{2}C_n\chi_n(k-1) \\ & \qquad\qquad\qquad\qquad\qquad\qquad\qquad\qquad i = 1,\dots,n \\ \left(I-\frac{\mu}{2}A_i\right)\xi_i(k) &\approx \left(I+\frac{\mu}{2}A_i\right)\xi_i(k-1)+\frac{\mu}{2}B_{i+1}\xi_{i+1}(k-1) \\ &+\frac{\mu}{2}B_i\xi_i(k-1)+\frac{\mu}{2}C_{i+1}\chi_{i+1}(k)+\frac{\mu}{2}C_i\chi_i(k) \end{aligned} \tag{5.25}$$

The above equations can be conveniently summed up in matrix form as

$$L\xi(k)+M\xi(k-1)+N\xi(k-2)+P\chi(k)+Q\chi(k-1)=0 \tag{5.26}$$

where

$$L=\begin{bmatrix} \left(I-\frac{\mu}{2}A_1\right) & 0 & \cdots & 0 \\ -\left(I+\frac{\mu}{2}A_1\right) & \left(I-\frac{\mu}{2}A_2\right) & \cdots & 0 \\ \cdots & \cdots & \ddots & \vdots \\ 0 & 0 & \vdots & \left(I-\frac{\mu}{2}A_n\right) \end{bmatrix},$$

$$M=\begin{bmatrix} -\frac{\mu}{2}B_1 & 0 & \cdots & -\left(I+\frac{\mu}{2}A_n\right) \\ -\frac{\mu}{2}B_1 & -\frac{\mu}{2}B_2 & \cdots & 0 \\ \cdots & \cdots & \ddots & \vdots \\ 0 & 0 & \vdots & -\frac{\mu}{2}B_n \end{bmatrix}, N=\begin{bmatrix} 0 & \cdots & -\frac{\mu}{2}B_n \\ 0 & \cdots & 0 \\ \cdots & \ddots & \vdots \\ 0 & \vdots & 0 \end{bmatrix},$$

$$P=\begin{bmatrix} -\frac{\mu}{2}C_1 & 0 & \cdots & 0 \\ -\frac{\mu}{2}C_1 & -\frac{\mu}{2}C_2 & \cdots & 0 \\ \cdots & \cdots & \ddots & \vdots \\ 0 & 0 & \vdots & -\frac{\mu}{2}C_n \end{bmatrix}, Q=\begin{bmatrix} 0 & \cdots & -\frac{\mu}{2}C_n \\ 0 & \cdots & 0 \\ \cdots & \ddots & \vdots \\ 0 & \vdots & 0 \end{bmatrix}$$

It is worth stressing that the time continuous *ξ(t)* in equation (5.20) belongs to $\mathbb{R}^8$, while the discrete time *ξ(k)* in equation (5.26) is in $\mathbb{R}^{n\times 8}$. Since *L* is well conditioned and its

inverse can be accurately computed, the above second order discrete difference equation can be finally transformed into a first order discrete difference equation by defining

$$\varphi(k) = \begin{bmatrix} \xi(k) \\ \xi(k-1) \end{bmatrix}, \psi(k) = \begin{bmatrix} \chi(k) \\ \chi(k-1) \end{bmatrix}$$

and by introducing the matrices

$$\Phi = \begin{bmatrix} -L^{-1}M & -L^{-1}N \\ I & 0 \end{bmatrix}, \Psi = \begin{bmatrix} -L^{-1}P & -L^{-1}Q \\ 0 & 0 \end{bmatrix}$$

so that equation (5.26) turns into

$$\varphi(k) = \Phi\varphi(k-1) + \Psi\varphi(k) \tag{5.27}$$

Observe that if no control is applied, i.e. if $\sigma \equiv 0$, then, by the periodicity of λ already highlighted in equation (5.21), it follows that the corresponding χ is constant and so does the related ψ:

$$\psi(k) = \psi_f \quad \forall k$$

Under such conditions the system defined by equation (5.27) has a unique equilibrium in

$$\varphi_f = (I - \Phi)^{-1}\Psi\psi_f$$

that corresponds to the uncontrolled passing profile.

The crucial observation in designing the low-frequency control law is that any control input σ that satisfies the periodic condition $\sigma(t + \tau) = \sigma(t)$ also provides a constant ψ_σ. Therefore, it affects the system just by changing the passing profile according to the new equilibrium value $\varphi_\sigma = (I - \Phi)^{-1}\Psi\psi_\sigma$.

A number of observations are in order. For starters, notice that the stability of φ_f and φ_σ is the same, since it depends on the eigenvalues of Φ, which in turn depends on the feed rate *f*. Then, observe that any fixed point of equation (5.27) represents a cutting profile after a single tooth pass, independently from its shape or the presence of chatter vibrations. Stationary profiles, whether featuring chattering or not, are indeed all fixed cutting profiles, thus all correspond to the equilibria of equation (5.27). In other terms, in the discretized model the high frequency oscillations due to the chatter vibrations are already embedded into the equilibrium point itself, just because it can be regarded to as the cutting profile following a tooth pass. Therefore, if for a certain feed rate *f* the system has a stable φ_f featuring a given amount of chatter, one could try removing it by pushing the dynamics into a φ_σ that corresponds to a smoother shape just by using a proper τ–periodic control σ. Ideally, if $\sigma \equiv -\lambda$ the cutting profile turns out flat zero. In general, any other σ would shift the equilibrium by $\Delta\Psi = \varphi_\sigma - \varphi_f$.

Some important considerations have to be emphasized. The first is that λ can contain high frequency components due to the nonlinearity of the milling process. Their suppression, then, boils down to the field of the controllers acting in the same frequency range of the chatter vibrations, such as the ones used in the presented previous literature works. The second is that the smoothing of chattering is limited by the sparsity of matrix Ψ, that very likely is not able to project ψ_σ along any desired direction of the state space in order to bring the equilibrium in a fair region of smooth cutting profiles.

Nevertheless, according to the above considerations, even a fixed low-frequency feedforward control action would be able to move the equilibrium away from its current chattering condition by the vector $\Delta\Psi$, and thus it is expected to have a certain chance of

reducing its negative effects. On this very idea the proposed control strategy was developed. First, a fixed low-frequency feedforward τ–periodic control input has been pointed out so to generally shift the fixed points φ_f, for f in a range of stationary solutions, towards a region of smoother cutting profiles. Roughly speaking, such a σ is fine control in the average. Then, a fine tuning mechanism has been conceived to slowly adapt the magnitude of σ depending on the landing point φ_σ, thus providing a specialized result for the actual scenario. This has been made necessary in order to deal with situations where the impact of the chattering in terms of magnitude could be very different.

5.3. Numerical investigation of open-loop actuation strategies

In accordance with the mathematical dissertation presented above, a numerical investigation was conducted with the developed time-domain simulator in order to prove the feasibility of low-frequency actuations in actually interfering with chatter vibrations and to define the most suitable actuation parameters accordingly. The choice of exploiting the simulative environment developed was mainly due to its efficiency in testing a large variety of actuation parameters and providing more robust data about the related system response, compared to experimental data.

5.3.1. **Simulation setup**

The inputs of the time-domain model were set in accordance with what described in the previous sections: in particular, the dynamic parameters of the tooling were set as experimentally identified for the time-domain model validation tests, as shown in Figure 5.6 and summarized in Table 5.1. Analogously, the modal parameters for the active fixture were derived by curve-fitting the numerically computed FRFs over the dominant modes of the two dynamic axes, reported in Figure 5.10 and Figure 5.11 respectively. The validated FE models were used for the purpose. It should be pointed out, though, that dynamic of the fixture would play only a negligible effect, mainly in influencing the maximum displacement produced by the actuated stages.

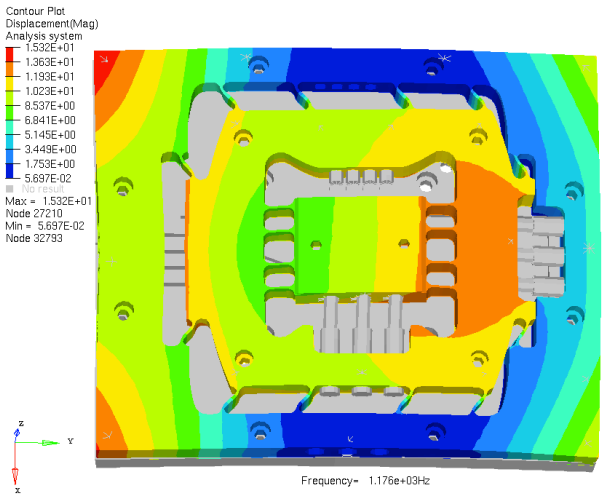

Figure 5.10: Outer stage mode shape.

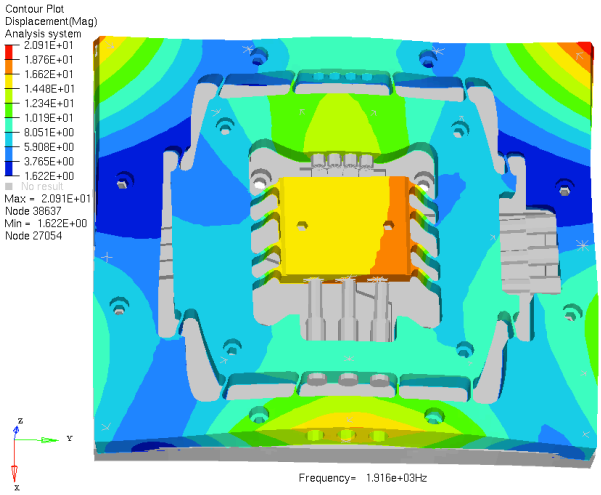

Figure 5.11: Inner stage mode shape.

The identified modal parameters used as inputs to simulate the fixture dynamics are reported in Table 5.3.

Table 5.3: Active fixture estimated modal parameters.

	Inner stage	**Outer stage**
Stiffness, k	4.28e^8 N/m	4.39e^8 N/m
Damping coeff., ζ	0.0421	0.0432
Natural freq., f_n	1916.3 Hz	1176.4 Hz

In order to include in the simulations the actual fixture performance, and particularly the maximum achievable displacements, the experimentally identified force generation coefficient was used (i.e., $K_\varphi = 10{,}4\ N/V$) to model the force of the piezo actuators.

5.3.2. **Results**

In order to assess the effectiveness of the investigated actuation strategies effectiveness the reference parameter was the maximum depth of cut (a_{p_limit}) achievable in stable condition. a_{p_limit} was identified performing process simulations, increasing the depth of cut (a_p) until triggering the onset of unstable cutting conditions. Depth of cut resolution was set to 0.02 mm and the onset of chatter conditions was assessed on the basis of tool-tip displacements frequency spectra, by using a simple detection approach based on identifying the axial depth of cut for which a dominant frequency (i.e., chatter frequency) exceeds the amplitude of nominal chatter-free spectrum (i.e., tooth pass frequency and its harmonics), as in used in a previous research activity [26].

This approach was repeated for several spindle speeds in order to numerically compute the SLD. First of all, the nominal SLD (i.e., without actuation) obtained by the proposed model was compared with the analytically predicted one [100], often used as reference, in literature and in practical applications. Figure 5.12 shows a good agreement between the two diagrams, differences are in line with the axial depth of cut resolution.

Comparison proves the reliability of the model in predicting stable and unstable conditions and the accuracy of the proposed evaluation approach in identifying the a_{p_limit}.

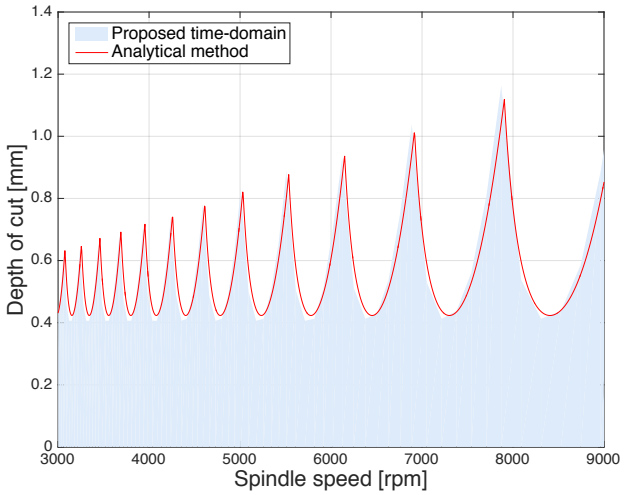

Figure 5.12: Validation of SLD obtained via proposed method.

After the assessment of the evaluation approach and the model capability of predicting chatter onset, open-loop actuation strategies were tested. The first investigation was carried out in order to analyse the influence of actuation frequency (f_A), that seems the governing parameter, as also suggested by the mathematical dissertation previously presented. For the purpose, a sine wave signal at different frequencies was provided by actuators, virtually operated at maximum voltage (i.e., 200 V) on both directions, in order to reach a fixed displacement (A ≈ 0.03 mm). As an exemplification of the producible effects, Figure 5.13 shows the result of over-imposed sine wave actuations at 187 Hz and 300 Hz within the 3000-7500 rpm spindle speed range of the SLD.

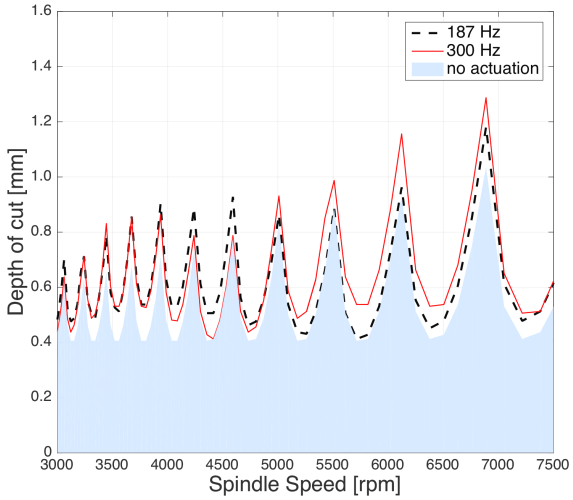

Figure 5.13: SLD with open-loop actuation at different frequencies.

As clearly shown, the maximum depth of cut in stable conditions is increased, for most of the spindle speeds. Generating workpiece vibrations at specific frequencies seems hence capable of disrupting the periodicity of the regenerative effect that generates the instability, bringing the system back to stable conditions, confirming the results of the mathematical dissertation previously described. This effect extends until a drastic chatter condition is reached (i.e., higher a_p), for which the generated actuation, in terms of displacements, is not sufficient to stabilize the system. In Figure 5.14 the effect of workpiece vibrations on suppressing chatter vibrations is exemplified for a simulated test with 7051 rpm spindle speed and 0.6 mm depth of cut. The actuation (i.e., 300 Hz sine wave) is switched on after 2 s and the instability is drastically mitigated.

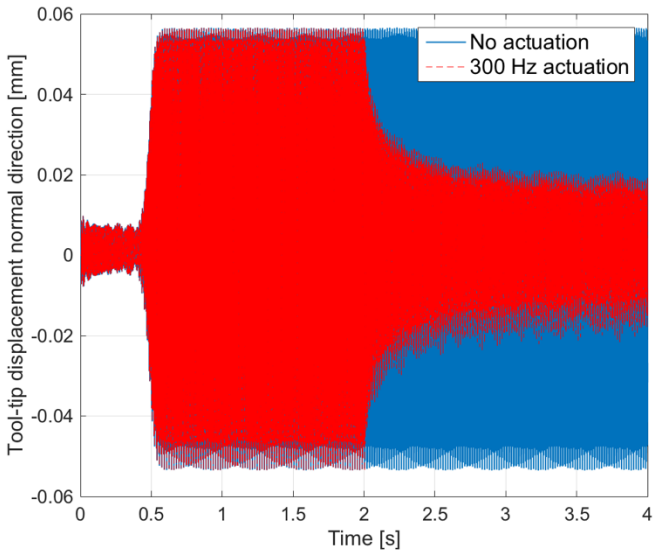

Figure 5.14: 300 Hz Actuation effect on tool-tip displacement (starting at 2 s, 7051 rpm, 0.6 mm depth of cut).

The described effect on the stability limit is not equal all over the investigated spindle speed range (Figure 5.13). The effect of workpiece excitation in extending the stability limits becomes indeed negligible as the actuation frequency gets close to the tooth pass frequency (f_{tp}) and its harmonics. Taking the 300 Hz actuation tests as an example, the a_{p_limit} value is not altered in simulated cutting with 4500 rpm (f_{tp}=150 Hz) and 3000 rpm (f_{tp}=100 Hz) spindle speeds, for which 300 Hz represents respectively the second and the third harmonic of the tooth pass frequency. This is consistent with the fact that exciting the workpiece at one of the tooth pass frequency contributions does not influence chatter regenerative effect, because it does not appreciably alter the periodic nature of the process. On the other hand, the effect of the 300 Hz actuation gets significant at different spindle speeds, until generating and increase of about 30% of a_{p_limit}.

This aspect can be further summarized by aggregating data of different tests with different actuation frequencies and plotting the limit axial depth of cut increase as a function of the actuation frequency (f_A) to rotational frequency (f_R=n/60) ratio. Figure 5.15 shows the results obtained with the aggregated data.

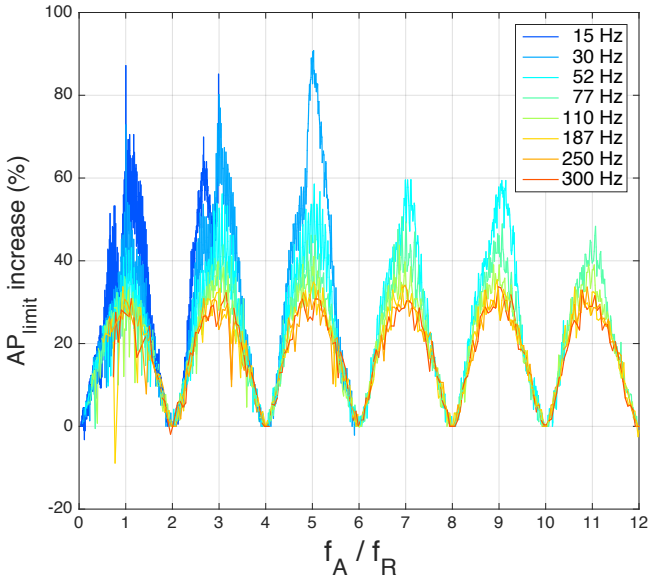

Figure 5.15: Actuation frequency effect on rotational frequency.

For each actuation frequency tested (i.e., 15÷300 Hz), the minimum a_{p_limit} increase is obtained when actuation frequency matches the tooth pass frequency and its harmonics (f_A/f_R = 2, 4, 6, … for a 2 fluted endmill). In these cases, the improvement in terms of a_{p_limit} appears absolutely negligible. Moreover, low frequency actuation seems to provide higher improvements.

In order to extend the investigation beyond the results obtained for the 2 fluted endmill, new SLDs were computed simulating tools with different numbers of flutes and maintaining the 300 Hz actuation frequency, as in most of the examples previously discussed.

The results achieved in these additional tests, in terms of increased stability limits, are summarized with the SLDs reported in Figure 5.16a and Figure 5.17a for a three and four fluted endmill respectively.

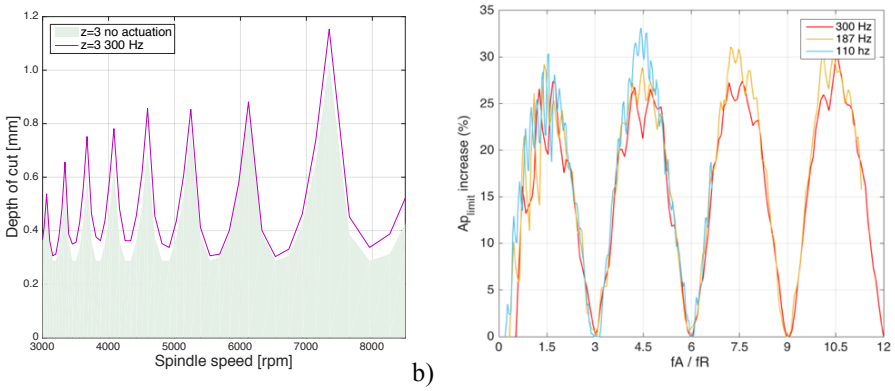

a) b)

Figure 5.16: a) SLD 300 Hz actuation b) Actuation frequency effect on rotational frequency for 3 fluted endmill.

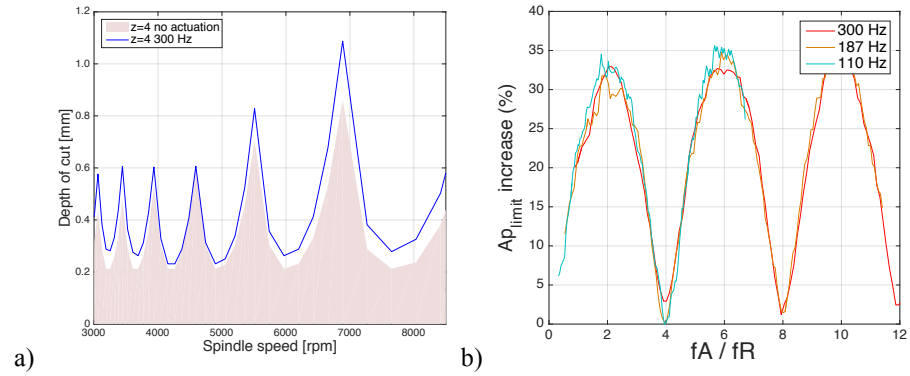

Figure 5.17: a) SLD 300 Hz actuation b) Actuation frequency effect on rotational frequency for 4 fluted endmill.

The effect generated by the 300 Hz actuation on the simulations for the three and four flutes is obviously different over the spindle speed range investigated, however the same behaviour at the tooth pass frequency can be observed again. This aspect is confirmed by aggregating results as in Figure 5.16b and Figure 5.17b where actuation frequency effect is reported one more time as a function of the actuation frequency to rotational frequency ratio.

The results for different number of flutes demonstrated that the effect on chatter stability is minimum on the tooth pass frequency and suggested the optimal actuation frequency equal to:

$$f_A = z\left(k + \frac{1}{2}\right) f_R \qquad k = 0,1,2,\ldots \tag{5.28}$$

where f_A is the actuation frequency, f_R the rotational frequency and z is the number of flutes.

This effect is due to the alteration of the periodicity of the cutting process. Indeed, low frequency actuations are exploitable for chatter suppression only if targeted on breaking chip thickness periodicity. This periodicity is due to the continuous engagement and disengagement of the teeth in the workpiece. The tooth pass frequency (f_{tp}) hence determines process periodicity; actuating at that frequency (or its harmonics) should not produce any appreciable interference with the process.

If the goal is disrupting this periodicity, the best actuation should be the one as far as possible from the periodic conditions (i.e., f_{tp} and harmonics). Indeed, results show that the best actuation frequency is in between f_{tp} and harmonics, since is the furthest from the periodicity conditions. For a two-fluted mill this condition is met actuating at 1/2 f_{tp}, 3/2 f_{tp}, etc., or for general mills as reported in the Eq. (5.28). This assessment is confirmed by the results of the numerical investigation and is in line with the mathematical dissertation previously presented, which suggested the frequency of the pure sinusoidal control signal to be τ-periodic in order to "stabilize" the process.

Once that the effect of actuation frequency was highlighted, the focus was put on the actuation direction and phase of the excitation sine waves. Simulations showed a negligible influence of actuation signals phase on the stability limit increase. This is consistent with the fact that the proposed open-loop actuation strategy is not focused on counter-acting a specific effect but altering the process periodicity, so it is not strictly dependent on the actuation offset, as long as actuation frequency itself allows for periodicity to be interrupted.

On the contrary, actuation direction clearly affects the achievable stable depth of cut, as shown in Figure 5.18.

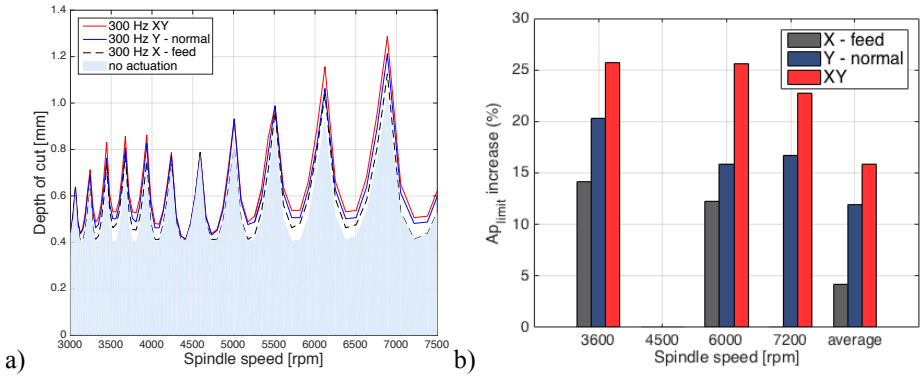

Figure 5.18: Effect of actuation directions: a) SLD for different actuation directions, b) summarization of the actuation direction effect.

Cross-feed (normal) direction seems to provide better results in increasing the stable depth of cut, compared to the actuation along feed direction. This is probably imputable to the fact that the cutting forces, and consequently tool-tip displacements, are generally higher on normal (i.e., cross-feed) direction. However, should be pointed out that the best results overall are achieved by actuating on both directions simultaneously, hence supporting the choice of a 2 DOF device, such as the designed one.

In order to show the effects of the tooling dynamics on the achievable results, different tooling systems were simulated. In particular tool natural frequency was set to 1000 Hz and 2500 Hz and the related SLDs were computed (Figure 5.19), simulating a two fluted mill.

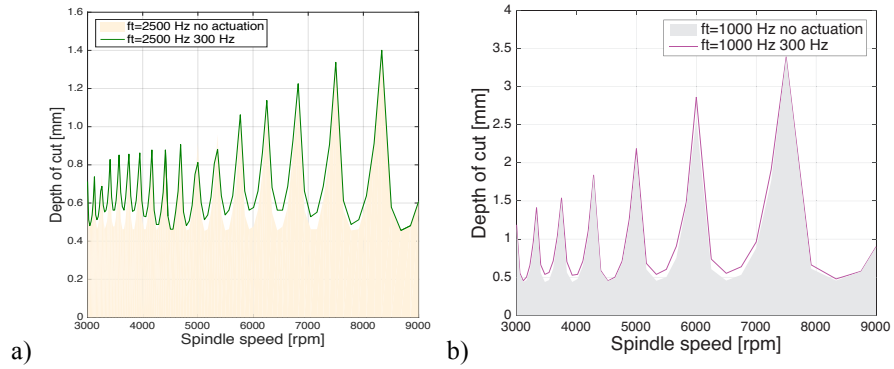

Figure 5.19: SLD for a) 2500 Hz b) 1000 Hz tool natural frequency.

As reported, the 300 Hz actuation provides appreciable results in both cases and the achievable stability limits (i.e., solid lines in Figure 5.19) show the same trend previously discussed. It shall be highlighted, indeed, that the minimum improvement is achieved for the tests with 3000 rpm and 4500 rpm tests, as obtained for the previous tests summarized in

Figure 5.15, confirming again the dependency on the rotational frequency and suggesting the negligible effect of tooling dynamics (i.e., chatter frequency value).

As a final investigation, the effect of feed per tooth (f_z) on the achievable stability limits was analysed. The results obtained using the 300 Hz actuation in three different test configurations (i.e., different feed per tooth, f_z) are presented in Figure 5.20.

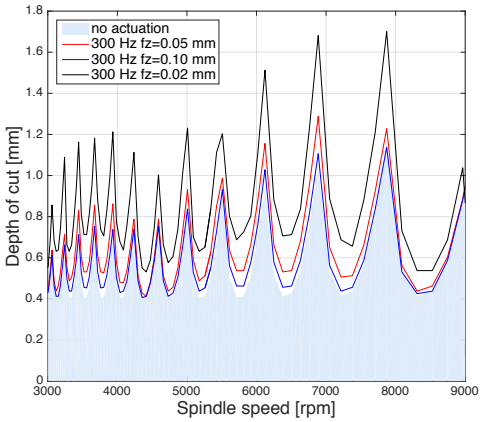

Figure 5.20: SLD for different feeds per tooth.

As shown, by increasing feed per tooth, the actuation effect clearly decreases. This is assumed to be related to an increase of chip thickness (directly proportional to f_z): the proposed actuation strategy is indeed aimed at disrupting the chatter phenomenon by altering the periodicity of the chip thickness. Thus, the impact of such a strategy is strongly dependent on the relation between the chip thickness and the actuated workpiece displacement: adequate amplitude of the actuated displacements should be generated in order to appreciably alter the chip thickness. In order to highlight this dependency, the effect of excited workpiece displacements (A in Figure 5.21 and Figure 5.22b) was investigated by keeping a constant f_z = 0.05 mm and computing SLDs using a 300 Hz actuation with three different amplitudes (i.e., three displacements magnitudes corresponding to three different input voltages to piezo actuators). The results are shown in Figure 5.21.

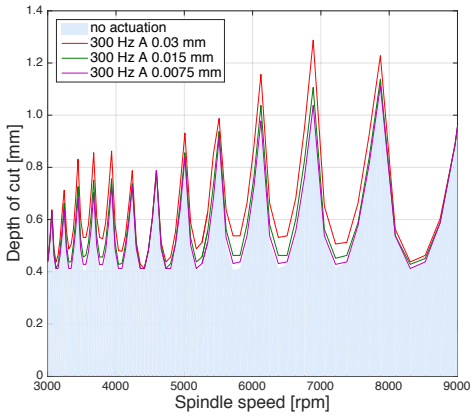

Figure 5.21: SLD for different actuated workpiece displacements.

The results showed that the higher the actuated workpiece displacement, the higher the stable depth of cut improvement, as expected. In order to further assess the influence of both f_z and A, depth of cut increase was identified by simulating tests with a fixed spindle speed (n=7051 rpm) and varying the two parameters individually. The results are shown in Figure 5.22a as a matrix in a 3d bar plot.

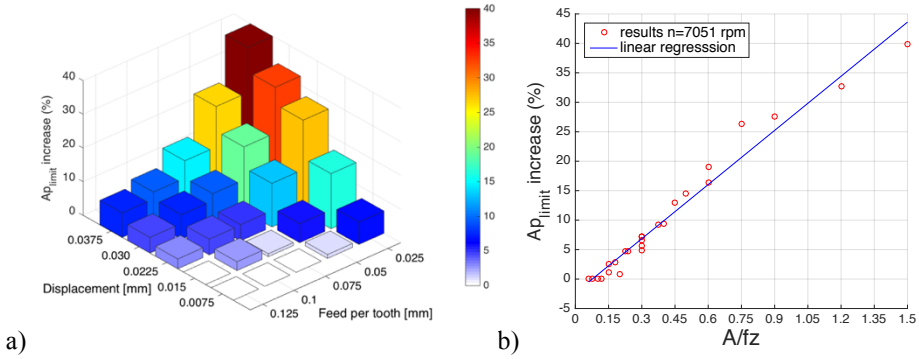

a) b)

Figure 5.22: Depth of cut increase for 7051 rpm, varying actuated displacement and feed per tooth.

Figure 5.22a shows that the actuation strategy effectiveness is directly proportional to displacement and inversely proportional to feed per tooth. Actually, the A/f_z ratio seems to be one of the key parameter in assessing the effectiveness of the proposed actuation strategy, as should be expected since a lower A/f_z ratio is representative of cases in which chip thickness is sensibly higher than the actuated displacement and hence the effect could only be limited. This aspect is confirmed by the fact that the main matrix diagonal reporting tests with the same A/f_z (equal to 0.3) shows very similar and reduced depth of cut improvement (blue bars).

In order to formalize this aspect, the generated results are reported in Figure 5.22b, where the dependency between a_{p_limit} increase and A/f_z shows a linear behaviour. In addition, the results showed that in order to provide a significant effect on the stable axial depth of cut (i.e., at least a 5% improvement), A/f_z ratio should exceed 0.25. Moreover, the maximum effect is achieved for $A/f_z > 1$ (i.e., actuated displacement exceeds the feed-per-tooth value). It should indeed be expected, since this actually translates in the capability of the proposed actuation strategy to generate a disengagement of the tool from the workpiece. This aspect stresses once more the need of maximizing the displacement generated by the dynamic axes in order to increase the effectiveness of the proposed actuation strategy. The achievable peak-to-peak displacements produced by the developed active fixture prototype is approximately 25 µm, as reported in section 4.4.2. This would suggest that the device, coped with this proposed actuation strategy, could be suitable for most general applications, given that, at least for solid end-mills, the usual feed per tooth values are not so different from the achievable peak-to-peak displacements produced. The proficient application of the proposed approach to operations with indexable mills, usually associated to higher feeds per tooth, would possibly require some modifications to the proposed active fixture design in order to increase the achievable peak-to-peak voltage. Particularly, different actuators would need to be selected for the purpose and consequently the fixture frame design (e.g., flexure hinges) would need to be adapted.

5.4. Closed-loop adaptation

As highlighted in the concluding remarks of Section 5.2, an adequate amplitude modulation of specific low frequency counter-excitation could produce a better mitigation of the chattering phenomenon. In order to ease the development of such a control strategy in a numerical environment, the dedicated time domain simulation model presented in section 5.1 was coded in a Simulink model, reported in Figure 5.23 for the case of a two teeth tool.

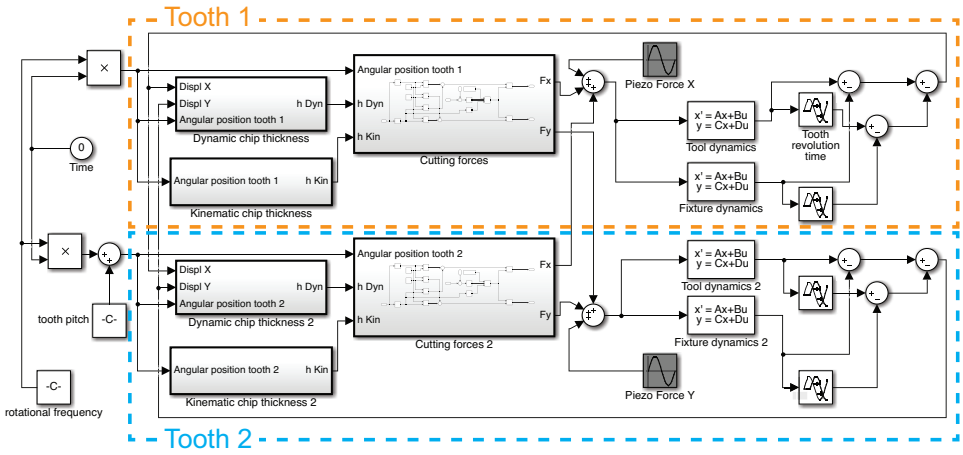

Figure 5.23: Simulink model of the milling process with over-imposed piezo forces (2 cutting flutes tool).

Considering the simplest approach, the main idea was hence to develop a closed-loop controller capable of generating an amplitude modulation of a given sinusoidal signal, based on a control signal that could be estimated over sensor data. Figure 5.24 shows the details of the developed proportional controller. The control signal is computed in time-domain over the raw acceleration signals (i.e., tooltip accelerations in the Simulink model) acquired at the given time step, *a(i)*, by subtracting the signal acquired at the previous rotational period, a(i-τ), by using a dedicated delay block, highlighted in green in Figure 5.24. As common practice in pre-processing signals for chatter detection approaches [107], this should allow cleansing the signal from the periodic contributions, hence theoretically filtering out all those contributions that are not related to chatter vibrations. Once the absolute value of the derived signal is computed, a low-pass filter is used to smooth the control response. Finally, a PID block, used as a simple proportional controller, scales the amplitude of a pre-defined actuation signal, highlighted in red in Figure 5.24, based on a reference threshold (blue constant block in Figure 5.24). The PID block was preferred to a simple gain block because it allows the definition of saturation limits, used as trigger in this case: more in detail, a stable cutting condition will return a negative control signal once subtracted by the reference threshold. A lower saturation limit of 0 on the PID block allows to avoid triggering the controller in that case. Analogously an upper saturation limit of 1 avoids exceeding the maximum allowed amplitude of the actuation signal.

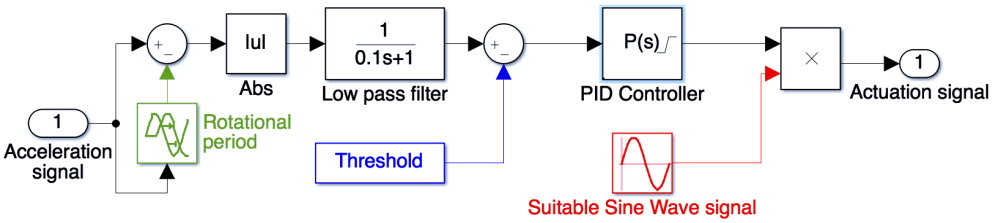

Figure 5.24: Proportional controller for the amplitude modulation of a suitable sinusoidal input.

In practice, by having pre-defined a suitable open-loop actuation strategy, for example in accordance with the parameters defined in the previous section, the closed-loop controller is capable of adapting the actuation amplitude on the basis of the identified chatter level, in real time. In stable cutting, for example, the controller would not be triggered, hence the proportional gain would be automatically set to zero (i.e., consequent null voltage provided to the piezo actuators). As chatter grows, the controller automatically adapts the required voltage level in accordance to the identified entity of chatter vibrations.

It is worth highlighting that such a control strategy is configured to be both model-less and suitable for a potential industrial context, since it only relies on the definition of the given spindle speed and number of cutting flutes for the selected tool. Those two parameters can be easily settable by the operator itself or automatically extracted by interfacing with the machine tool NC.

It should be noted that, keeping the actuation signals within the low-frequency range, alternative control signals and more complex controller architectures could be used, for example by using a combination of multiple sine-waves and/or an additional phase modulation. Nevertheless, having the practical aspects of the control implementation in mind, the proposed approach seems more suitable. Indeed, the simple amplitude modulation approach avoids the need of additional sensor for phase tracking, such as the tachometer integration described in section 4.4.3, while pure sine-waves are more easily manageable by the piezo driver from a current generation point of view. Nonetheless, fine-tuning of the proposed control strategy would be objective of future developments, as will be formalized in the concluding remarks of this thesis.

6. Experimental testing of the active fixture prototype

Once the prototype was fully assembled and validated, and the proposed control strategy was adequately outlined, dedicated experimental tests were set up in order to investigate the actual performance of the developed AWH prototype as a whole in mitigating chatter vibrations in real milling operations.

The controller presented in the previous section was compiled on a National Instrument PXI-8110 real-time controller that served also as acquisition system and I/O interface by means of a PXI-6259 DAQ module. The controller was set to run at 20kHz and data were sampled at the same rate.

The active fixture set-up on the Mori-Seiki NMV1500dcg milling machine is reported in Figure 6.1.

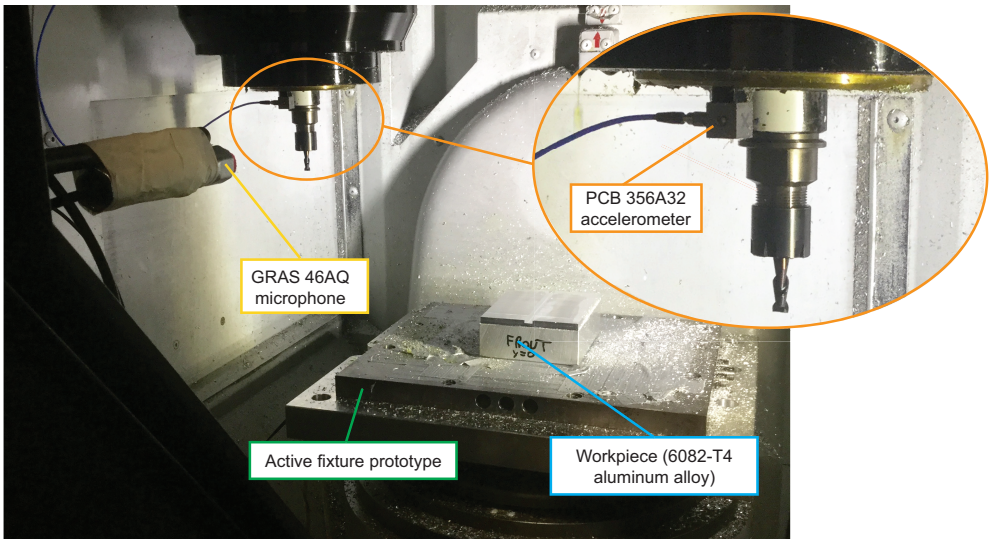

Figure 6.1: Experimental setup.

A PCB 356A32 triaxial accelerometer was positioned on the spindle housing in close proximity to the rotating tool and the acceleration signals measured along X and Y directions (i.e, machine tool reference system) were fed to the proportional controller to modulate the

actuation along X and Y axis respectively. An additional Gras 46AQ microphone was employed only as a cross-reference sensor to ease the analysis of the results.

The tests were conducted with an 8mm Garant 201270 endmill with two cutting flutes on a 6082-T4 alloy workpiece in slot milling operations. Two different spindle speeds, 11800 rpm and 17500 rpm, were tested in order to investigate different cutting conditions. The feed per tooth was set in accordance to the producer suggested parameters equal to 0.03 mm/tooth. According to the numerical investigation described in section 5.3, the proposed control strategy is expected to interfere with the unstable process, being the maximum displacement generated by the fixture (25 μm) comparable to the feed per tooth value.

The tooltip frequency response functions were experimentally identified, by means of impact testing, in order to highlight the dominant mode responsible for triggering the chatter vibrations. The measured FRFs, shown in Figure 6.2, show a dominant mode around 4.5 kHz suggesting that the chatter vibrations will be originated in proximity to that frequency. This further underlines the actual need of a low-frequency control approach: actuating at 4.5 kHz would indeed be made practically impossible by both inertial forces and current limitations on the piezo drivers, as extensively discussed.

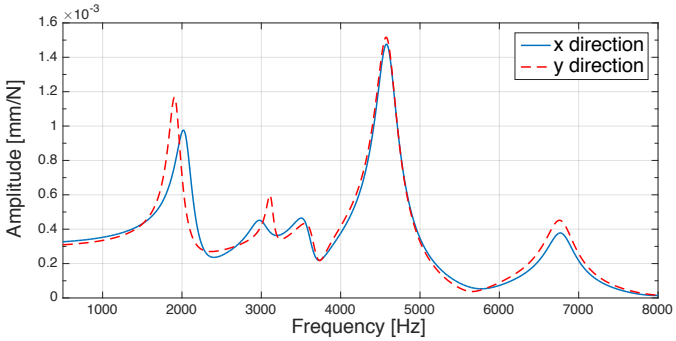

Figure 6.2: Measured tooltip FRFs.

As mentioned in the previous section, the developed proportional controller modulates the amplitude of the sinusoidal control actuation on the basis of a dedicated control signal. As exemplified in Figure 6.3, moving from stable to unstable conditions the control signals clearly tracks the onset of chatter vibrations. Once the threshold value is experimentally defined, the onset of chatter vibration triggers the proportional controller that modulates the amplitude of the counteracting control excitations proportionally to the threshold value.

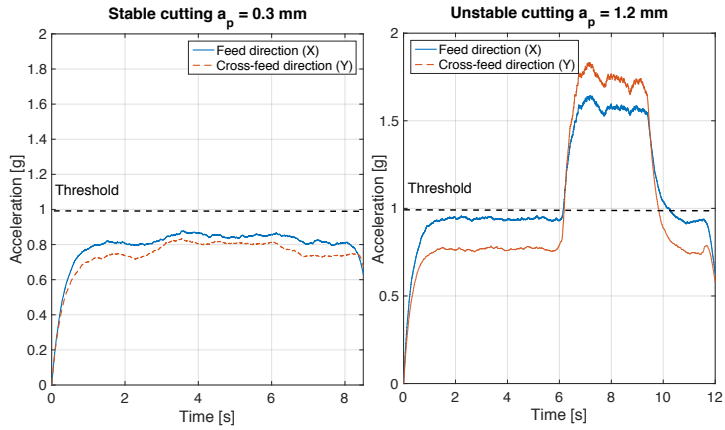

Figure 6.3: Control signals for stable and unstable cutting conditions (11800rpm).

Some preliminary linear cutting tests at fixed axial depth of cuts (a_p) were conducted in order to investigate the control capabilities in interacting with the process and mitigating the amplitude of chatter vibrations. First, both the open-loop and closed-loop controls were tested in order to highlight the different performance achievable.

Figure 6.4 and Figure 6.5 report the results in clear unstable conditions (i.e., $a_p = 1.2$ mm at 11800 rpm, the stability boundary being identified in approximately $a_p = 0.5$ mm).

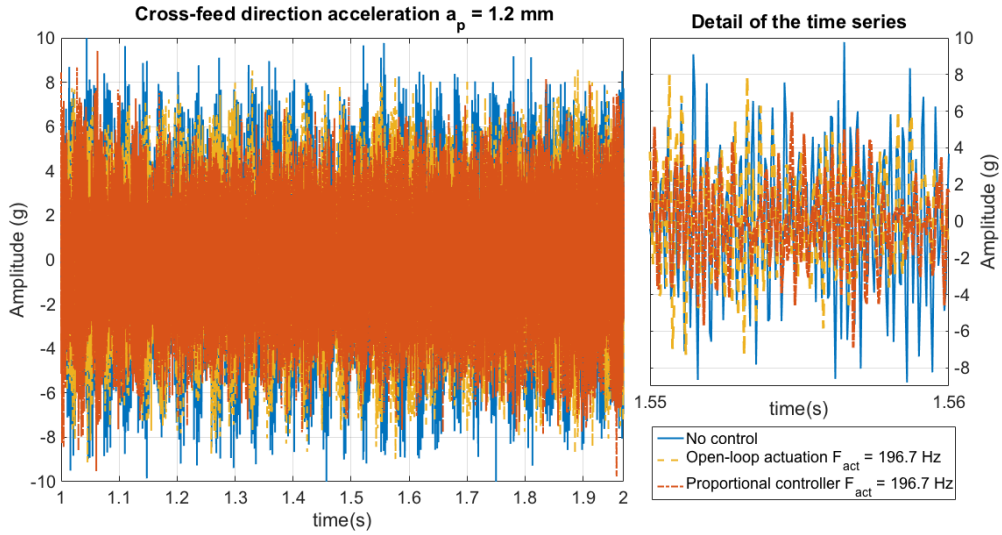

Figure 6.4: Effect of open-loop and closed-loop control on chatter mitigation (cross-feed measured accelerations windowed time series, using a 2 s Hamming window centered at 1.5 s).

As shown in both the time series (Figure 6.4) and more clearly in the frequency spectra reported in Figure 6.5b, both the open-loop and closed-loop controllers are capable of generating an evident average amplitude reduction of the chatter frequency spectral

contribution. The estimated reduction, with respect to the signal measured without control, is equal to 32% and 43% with the open-loop and closed-loop respectively.

On the other hand, as highlighted in Figure 6.5a, the comparison of the control signals show that the effect provided by the open-loop control is unregular, suggesting that the absence of an amplitude modulation of the sinusoidal excitation pushes the system back into highly unstable conditions after having disrupted the chatter vibrations. The proportional controller avoids this issue by automatically reducing the gain, once the chatter vibration is mitigated.

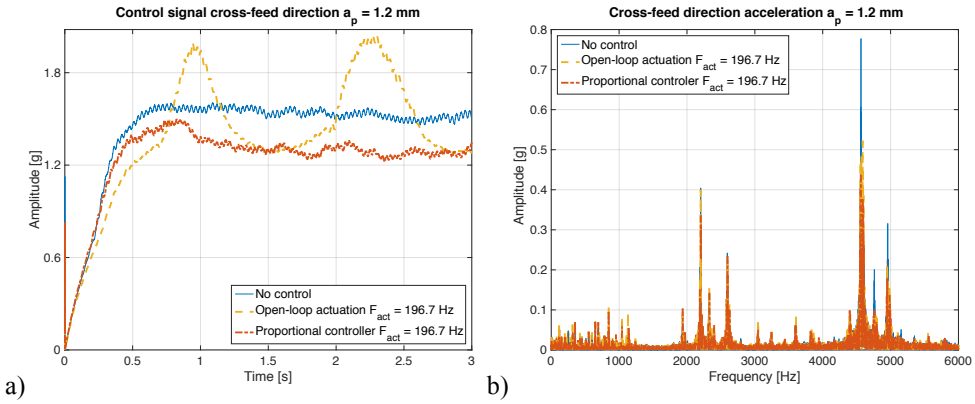

a) b)

Figure 6.5: Effect of open-loop and closed-loop control on chatter mitigation. a) control signals, b) frequency spectra of measured acceleration signals. (11800 rpm).

In order to investigate how the proposed technique could impact on the stability boundaries, dedicated tests have been conducted by linearly increasing the axial depth of cut, following the slope test procedures suggested by Quintana et al. [27].

As common practice [26], a threshold on the amplitude of the spectral contribution associated to chatter vibrations was used to define the crossing of the stability boundary. By doing so, the corresponding axial depth of cut can easily be identified on spectrograms of acceleration signals. As shown in Figure 6.6 for the 11800 rpm, the spectrograms of accelerations measured in cross-feed direction during the cutting tests, reported in , show that the threshold on the chatter frequency amplitude is exceeded for higher depth of cut when the active fixture is activated (i.e., a_{p_limit} = 0.49 mm without control and a_{p_limit} = 0.61 mm with control).

The spectrograms were computed with a frame size of 0.1 s without overlapping. Zero padding was used to increase the number of lines and reduce the effect of frequency smearing, easing the result presentation. 10000 lines were hence used within the bandwidth investigated (0-10 kHz). The spectrogram plots are reported limited to the chatter frequency range to ease the analisys of the effect produced by the proposed technique in mitigating chatter vibrations.

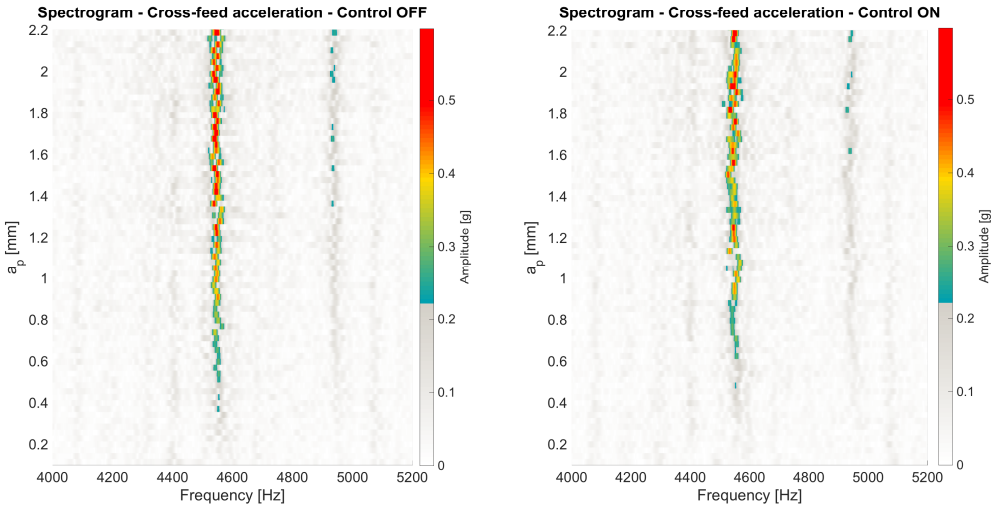

Figure 6.6: Spectrogram of measured accelerations in cross-feed directions as a function of the increasing axial depth of cut without and with control of the active fixture activated. 11800 rpm test.

Furthermore, the amplitude of chatter vibrations appears slightly mitigated for the tests with the control turned on. This effect lasts until severe chatter condition arise, when the proposed approach results practically ineffective. This effect is shown in Figure 6.7, where one could see that below 0.6 mm axial depth of cut the vibration levels are reduced by the control activation. Nonetheless, as the axial depth of cut increases, the effectiveness is sensibly reduced and the process evolves similarly to the test without control.

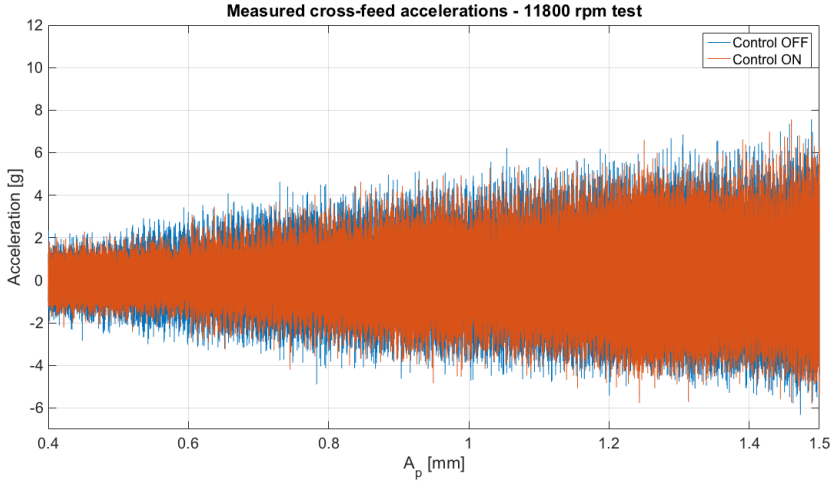

Figure 6.7: Measured cross-feed accelerations with and without control turned on for the 11800 rpm test with linearly increasing axial depth of cut.

An analogous trend is noticeable for the 17500 rpm cutting test, reported in Figure 6.8, where the improvement achieved by activating the active fixture was approximately 43% (i.e., a_{p_limit} = 0.69 mm without control and a_{p_limit} = 0.99 mm with control).

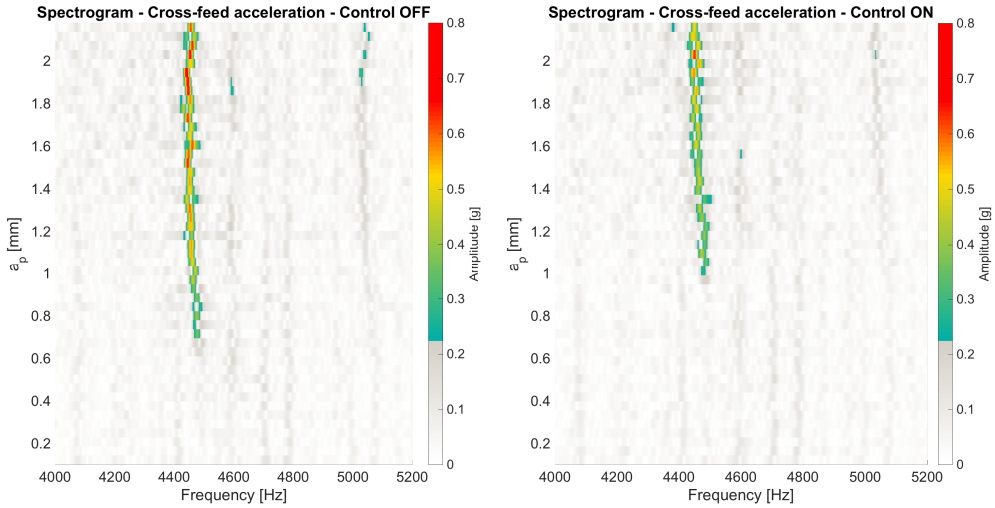

Figure 6.8: Spectrogram of measured accelerations in cross-feed directions as a function of the increasing axial depth of cut without and with control of the active fixture activated. 17500 rpm test.

This time the effect is self-evident even in the time series of the measured accelerations signals, shown in Figure 6.9.

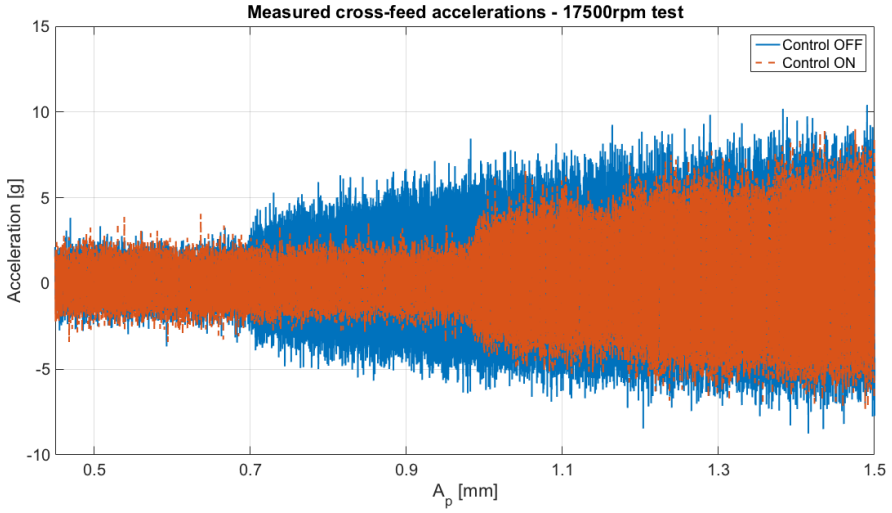

Figure 6.9: Measured cross-feed accelerations with and without control turned on for the 17500 rpm test with linearly increasing axial depth of cut.

As shown, the active fixture is effective in delaying the onset of chatter vibrations to a higher axial depth of cut. It is worth noting that even beyond the identified limit axial depth of cut (i.e., approximately 1 mm for the test reported in Figure 6.9), the controller is capable of reducing the vibration level by increasing the amplitude of the counteracting excitations. This effect last until a severe chatter condition is reached, where the controller have reached the maximum allowed gain and the proposed actuation strategy start to loose effectiveness, which is consistent with the results of the numerical investigation discussed in section 5.3.2.

7. Conclusions and final remarks

The activity presented in this Ph.D. thesis deals with the development of an active fixture for the mitigation of chatter vibrations in milling, that represent one of the most limiting factors in modern machining operations due to their detrimental effects. The main aim of this work was to address some of the major limitations experienced in the development of such devices, especially in terms of applicability to general milling applications where chatter frequencies could easily exceed the kHz range. From this point of view, the main open issues are twofold: on the one hand, referring to literature solutions, the device bandwidth itself appears too narrow to deal with such requirements. On the other hand, the adoption of renowned control strategies, derived by general active vibration control applications, would be made complex by several limitations that would actually impede the use of high-frequency workpiece excitations.

According to these topics, the research work was focused on both the active fixture design aspects and the development of an alternative control logic. By carefully addressing the design of such a mechatronic device, indeed, the bandwidth of the actuated axis was sensibly increased with respect to previous literature works and the use of dedicated actuation technologies allowed for improved reliability. Extensive use of finite element (FE) models allowed to consider these aspects form the early design stage, providing a guidance for the whole prototype development.

During the whole design flow, many lessons were learnt regarding the development of such active workpiece holders (AWHs): those lessons have been formalized into this thesis to provide a sort of design guidelines and dedicated design tools that could assist the development of this kind of devices, such as the empirical stiffness and the reduced models of the flexure hinges. Moreover, the FE models combined with experimental data provided a better understanding of the actual capabilities and requirements of the developed AWH prototype, such as the actual force producible by the integrated piezo actuators or the estimation of the preload force to be applied to the actuators themselves.

On the control side, the development of a dedicated milling time-domain simulator represented a key step, given that it allowed the effective investigation and development of a suitable control logic aimed at exploiting low-frequency actuations with the purpose of interfering with the chatter vibrations. The development of such a control strategy was also aided by a mathematical stability analysis of the process, which in turn provided a definition of the crucial features of a suitable actuation signal and some hints for further improvements. Accordingly, a specific low-frequency actuation strategy was pointed out at first, highlighting the main influencing factors in assessing its effectiveness. In that sense the actuation frequency resulted to be the key parameter, as expectable, and should be related to the rotational frequency and the number of tool cutting flutes. In addition, the effectiveness

of the proposed control strategy directly depends on the entity of the displacements producible with the active fixture prototype, highlighting the need of carefully addressing the design of the device itself.

Subsequently, a closed-loop adaptation of the proposed actuation strategy was developed by implementing a simple amplitude modulation on the basis of a dedicated control signal. This made the controller to be capable of more easily adapting to different chatter conditions and automatically switch the actuation off in case of stable cutting.

Finally, dedicated experimental tests proved the feasibility of the proposed chatter mitigation strategy, showing that the developed AWH was actually capable of reducing the amplitude of chatter vibrations and increasing the limit axial depth of cut.

The following sections highlight the aforementioned conclusions, emphasizing the principal achievements, even in an industrial perspective, and presenting the foreseen future developments.

7.1. Summary of the principal achievements

In summary the main contributions of this research activity are:

- The formalization of the main design aspects, such as the definition of proper kinematic architectures, that could ease the development of such mechatronic devices, especially in the earlier stages.
- The effects of the geometry of flexure hinges, integrated in the AWH to decouple the axes motion, was investigated and described by dedicated empirical equations in order to provide a better understanding of the achievable stiffness along all the 6 DOFs and to assist the design of these mechanical components, that represent a crucial feature of the active fixture.
- Dedicated reduced models of the flexure hinges were proposed to reduce the computational efforts and time in the numerous design iterations involved in the definition of a suitable active fixture geometrical design, for example with the purpose of maximizing the device bandwidth along the actuation directions, or to generally improve its dynamic response. The proposed reduced model, combined with the derived empirical stiffness equations, would allow an easy implementation in optimization algorithms to further simplify this kind of analysis.
- The main aspects that should drive the selection of suitable actuation devices were formalized and the better suitability of piezo actuators based on hard-doped piezo ceramics was shown. This would sensibly contribute to the increase of the design bandwidth and to an extended reliability in demanding dynamic applications. Moreover, dedicated procedures based on finite element analysis were presented to aid the computation of the required preload forces needed to prevent potential failures and to investigate the actual performance of the integrated piezo actuators.
- A dedicated milling time-domain simulator was developed to investigate the interaction between the active fixture and the cutting process, by integrating specific piezo models and by including the effect of fixture dynamics. In practice, this simulative tool would allow to efficiently test the effect of alternative control strategies, as shown in this thesis.

- The stability of the system (i.e., cutting process with over-imposed active fixture excitations) was mathematically analyzed in order to show that suitable actuation signals could be capable of moving the process into a new equilibrium state, reducing chatter vibrations. More in detail, the results proved that low frequency excitations could be used for the purpose, either in open or closed loop, providing that a given periodicity condition is satisfied (i.e., the actuation frequency should be related to the tool rotational period).
- By means of a dedicated numerical investigation of different actuation signals, the most suitable actuation parameters were defined and an expression of the optimal actuation frequency was derived. Subsequently a closed-loop adaptation of such a low-frequency control strategy was proposed and experimentally tested. According to the result, the proposed model-less control strategy would be capable of mitigating the amplitude of chatter vibration occurring at frequencies higher than 4 kHz. Moreover, in dedicated chatter tests, the AWH prototype with the proposed controller was shown to be capable of significantly increasing the limit axial depth of cut, hence potentially returning an appreciable improvement in terms of material removal rate. It should be pointed out that the novel model-less control strategy here proposed simply require the definition of the employed spindle speed and the number of tool cutting edges. The required expertise and setup times are consequently drastically reduced.

7.2. Progress with respect to the state of the art

This thesis addresses some open issues in the state of the art related to active fixtures for chatter suppression in milling. Relevant contributions are provided on the device design, formalizing the major requirements and proposing specific design guidelines that could aid the development of alternative prototypes. Moreover, the extensive modeling activities conducted for the investigation of the active fixture performance could represent the basis for potential future investigation of alternative designs and control strategies in a numerical environment.

Furthermore, this research activity contributed to the state of the art mainly with the investigation of alternative control strategies and particularly with the definition of a suitable control strategy, capable of exploiting low frequency actuation to interfere with the cutting process, mitigating the chatter vibrations and potentially leading to an increase of the limit axial depth of cut. Such a kind of control strategy appears to complement the state of the art of active vibration control in milling, currently reporting the application of conventional active vibration control solutions, mainly targeted in the chatter frequency range. While the effectiveness of such approaches has been proved by several studies, the actual applicability is limited to structural chatter vibrations, that are generally triggered in heavy duty milling operations only.

The developed control strategy, on the other hand, would allow to extend the application to a wider range of milling operations, generally featuring high-frequency chatter vibrations impossible to be counteracted by conventional approaches.

Moreover the proposed control strategy prepares the ground for manifold future developments and potential industrial oriented solutions, as discussed in the following sections.

7.3. Industrial applicability of the developed solution

As clearly stated at the beginning of this thesis, the selection of the research topic was motivated also by a clear industrial perspective. Indeed, active fixtures could be easily configured to be retrofittable into a variety of different machine tools, without requiring relevant intervention or specific expertise. To the author, this appeared to be a key feature for a potential industrial application of chatter suppression/mitigation techniques. It is worth stressing that the variety of chatter suppression techniques presented in literature often show poor applicability to an industrial context given the intrinsic requirements in terms of expertise and intervention costs, as highlighted in Chapter 2.

From the perspective of an industrial application, the main contribution provided by the present work is related to the development of the model-less control strategy. Even though the prototype is still into a development stage, hence not mature enough for an actual industrial application, the features of the proposed control strategy make it already suitable for the purpose. In practice, the sole inputs required to operate the device would be easily settable by the machine tool operator, as previously underlined, without requiring any particular expertise or procedure.

Moreover, the implementation of the developed AWH would be facilitated by the fact that the device, as is, could be easily installed on different machine tools, as also shown in this work. In more mature development phases this aspect could be improved further with minor efforts, also taking into account specific standards and regulations that would need to be consider for an effective industrially oriented development.

7.4. Potential future developments

Some future developments are already under consideration with the purpose of improving the achieved results and extending the investigation to different applications. The foreseen future developments of the proposed research can be summarized as follows:

- A deeper experimental investigation is advised and will be the first objective of future developments. In particular, the effectiveness of the developed AWH needs to be investigated in applications involving tools with higher numbers of flutes and different cutting conditions, such as side and flank milling operations, not investigated yet. It is worth noticing that the results are expected to be similar to the ones presented in this work, at least for what concerns tools with different flutes numbers, according to the results of the numerical investigation presented in section 5.3.2. Nonetheless, an adequate experimental validation will be needed to prove it.
- Fine-tuning of the proposed control strategy could be investigated with the purpose of improving the achievable reduction of chatter vibrations. Particularly, the integration of additional phase controller is advised to improve the achievable performance, especially in different cutting conditions with respect to the ones here investigated (e.g., side and flank milling). In that sense it is author belief that the development of eventual phase controllers should follow simple configurations, such as phase follower configurations or simple PID schemes that would avoid the need of

integrating additional or complex sensors. This would not compromise the industrial suitability of the proposed solution.

- Alternative chatter detection algorithms could be implemented in the closed-loop controller to improve its effectiveness and more in particular to avoid the need of pre-define the intervention thresholds, as needed now. This would foster the applicability of the proposed AWH.
- The effects in terms of tool wear and surface finishing would need to be investigated. The focus of the research was in improving the material removal rate by reducing the extent of unstable vibrations. This requirement is usually associated to roughing operations, where productivity needs to be maximized and surface finishing is neglected. It is expected though that the proposed control strategy could sensibly affect the surface in finishing operations, hence a dedicated investigation is advised on either numerical or experimental tests. For what concerns tool wear, instead, it would be interesting to assess the effect induced by the over-imposed vibrations in increasing or reducing the tool wear. Particularly a comparison with chatter related tool wear would provide a better understanding of the practical outcomes related to the use of such active fixtures.
- Once that adequately robust results would be produced with the aforementioned steps on the AWH prototype used as a test platform, a different perspective could be investigated. It is author belief that it would be worth investigating the feasibility of integrating the proposed low-frequency actuation strategy into the machine tool NCs, somehow following the approach of Munoa et al. [42], that proved the feasibility of a similar application for active structural control. In that sense the main uncertainty would be related to the actual exploitable bandwidth of the machine tool feed drives, but the use of low-frequency actuations would more easily cope with that. It should be noted that by using the machine tool drives to over-impose the proposed “actuation” strategy, drastically higher displacements could be produced, potentially extending the applicability even to high-feed roughing operations.

Acknowledgements

The present thesis work was carried out in the Department of Industrial Engineering of the University of Florence. Foremost, I would like to express my sincere gratitude to all the people working in this Department, starting from my supervisors, Dr. Eng. Antonio Scippa and Dr. Eng. Gianni Campatelli. I owe to them a big part of my professional and personal growth and I am very grateful for how they encouraged me, supporting my motivation for the research topic and allowing me plenty of autonomy in conducting my research, although keeping a constant and valuable supervision on it. I'm also thankful to my supervisors for having created and managed an excellent research team at the Manufacturing Technology Research Lab (MTRL) here in Firenze. I feel privileged to work with this team of friends, part of my accomplishments is definitely due to them and to the enjoyable and cheerful working environment every one of them contributed to. I should definitely express my gratitude in particular to my colleagues and friends Mr. Filippo Montevecchi and Dr. Niccolò Grossi for their valuable help and support in some of the activities reported in this thesis.

I am grateful also to the researchers from the Information Department at University of Firenze, particularly to Prof. Michele Basso and Dr. Giacomo Innocenti that made available their expertise in supporting the development of the control logic. I also want to acknowledge the work of all the partners of the iNTEFIX European project for the stimulating and motivating experience this project has brought to my background and for providing valued inputs for my research. Among them I want to particularly thank Irene Villoresi and Claudio Corsi from TECMA Srl for manufacturing the fixture prototype and for having provided valuable hints for the general fixture layout and manufacturability requirements.

An acknowledgement is due also to EC for funding part of my activities within the iNTEFIX project and to the Machine Tool Technology Research Foundation (MTTRF) for supporting our research with the loaned machine tool.

In addition to the ones I have already cited, I have had the chance to meet and establish professional collaborations with several people in the years of my PhD, thanks to the several activities I was involved in at MTRL. I want to sincerely thank each and every one of them for the contribution they brought to my professional growth. A particular mention goes to Mauro and Claudio Rossi from Meccanica Ceccarelli & Rossi, that through these years of collaboration indirectly encouraged my work and provided me a technical perception and background on machining that I consider undeniably valuable for me, both personally and professionally. This surely contributed to the achievements reported in this thesis.

Last but definitely not least, I owe a huge thank to my whole family that never stopped encouraging me and believing in me, way more than I would have done myself. Among them I want to include my girlfriend, Fabiana, and thank her for her patience and understanding, for the way she believed and believes in me and in my capabilities and for having accompanied and supported my life throughout these demanding years.

Bibliography

[1] Altintas Y. Manufacturing Automation: Metal Cutting Mechanics, Machine Tool Vibrations, and CNC Design 2012.

[2] Quintana G, Ciurana J. Chatter in machining processes: A review. Int J Mach Tools Manuf 2011;51:363–76.

[3] Le Lan J-V, Marty A, Debongnie J-F. A stability diagram computation method for milling adapted to automotive industry. CIRP - High Perform Cut 2006.

[4] Altintas Y, Budak E. Analytical Prediction of Stability Lobes in Milling. CIRP Ann - Manuf Technol 1995;44:357–62.

[5] Budak E, Tekeli A. Maximizing chatter free material removal rate in milling through optimal selection of axial and radial depth of cut pairs. CIRP Ann - Manuf Technol 2005;54:353–6.

[6] Smith S, Tlusty J. Stabilizing Chatter by Automatic Spindle Speed Regulation. CIRP Ann - Manuf Technol 1992;41:433–6.

[7] Monnin J. Active Structural Methods for Chatter Mitigation in Milling Process. ETH Zurich, 2013.

[8] Seguy S, Dessein G, Arnaud L, Insperger T. Control of Chatter by Spindle Speed Variation in High-Speed Milling. Adv Mater Res 2010;112:179–86.

[9] Kimman MH, Langen HH, Munnig Schmidt RH. A miniature milling spindle with Active Magnetic Bearings. Mechatronics 2010;20:224–35.

[10] Abele E, Hanselka H, Haase F, Schlote D, Schiffler A. Development and design of an active work piece holder driven by piezo actuators. Prod Eng 2008;2:437–42.

[11] Tobias SA. Machine tools vibration (Vibraciones en Maquinas-Herramientas). Spain: URMO; 1961.

[12] Taylor F. On the Art of Cutting Metals. TransASME 1907;28:31–350.

[13] Schmitz TL, Smith SK. Machining Dynamics: Frequency Response to Improved Productivity. 1st ed. Springer-Verlag US; 2009.

[14] Tobias SA. Vibration of Machine Tools. Cranf. Conf. Pap., Cranfield: 1964, p. 599–608.

[15] Kiss AK, Bachrathy D, Stepan G. Cumulative Surface Location Error for Milling Processes Based on Tool-tip Frequency Response Function. Procedia CIRP 2016;46:323–6.

[16] Merritt HE. Theory of Self-Excited Machine-Tool Chatter: Contribution to Machine-Tool Chatter Research. J Eng Ind 1965;87:447–54.

[17] Tlusty J, Ismail F. Basic Non-Linearity in Machining Chatter. CIRP Ann - Manuf Technol 1981;30:299–304.

[18] Munoa J, Beudaert X, Dombovari Z, Altintas Y, Budak E, Brecher C, Stepan G.

Chatter suppression techniques in metal cutting. CIRP Ann - Manuf Technol 2016;65:785–808.
[19] Tobias SA, Fishwick W. Theory of regenerative machine tool chatter. Eng 1958;205:199–203.
[20] Tlusty J. Manufacturing Processes and Equipment. Prentice Hall; 2000.
[21] MAL - Manufacturing Automation Laboratiories. Cutpro software n.d.
[22] Grossi N, Sallese L, Scippa A, Campatelli G. Speed-varying cutting force coefficient identification in milling. Precis Eng 2015;42:321–34.
[23] Grossi N, Sallese L, Scippa A, Campatelli G. Chatter Stability Prediction in Milling Using Speed-varying Cutting Force Coefficients. Procedia CIRP 2014;14:170–5.
[24] Özşahin O, Budak E, Özgüven HN. In-process tool point FRF identification under operational conditions using inverse stability solution. Int J Mach Tools Manuf 2015;89:64–73.
[25] Hajdu D, Insperger T, Stepan G. Robust Stability of Machining Operations in Case of Uncertain Frequency Response Functions. Procedia CIRP 2016;46:151–4.
[26] Grossi N, Scippa A, Sallese L, Sato R, Campatelli G. Spindle speed ramp-up test: A novel experimental approach for chatter stability detection. Int J Mach Tools Manuf 2015;89:221–30.
[27] Quintana G, Ciurana J, Teixidor D. A new experimental methodology for identification of stability lobes diagram in milling operations. Int J Mach Tools Manuf 2008;48:1637–45.
[28] Bediaga I, Muñoa J, Hernández J, López de Lacalle LN. An automatic spindle speed selection strategy to obtain stability in high-speed milling. Int J Mach Tools Manuf 2009;49:384–94.
[29] Okuma. Machining Navi n.d.
[30] Altıntas Y, Engin S, Budak E. Analytical Stability Prediction and Design of Variable Pitch Cutters. J Manuf Sci Eng 1999;121:173–8.
[31] Kono D, Matsubara A. Investigation on Direction Dependency of Tool-Workpiece Compliance of Machine Tool. Procedia CIRP 2016;46:529–32.
[32] Law M, Altintas Y, Srikantha Phani A. Rapid evaluation and optimization of machine tools with position-dependent stability. Int J Mach Tools Manuf 2013;68:81–90.
[33] Moradi H, Bakhtiari-Nejad F, Movahhedy MR, Vossoughi G. Stability improvement and regenerative chatter suppression in nonlinear milling process via tunable vibration absorber. J Sound Vib 2012;331:4688–90.
[34] Aguirre G, Gorostiaga M, Porchez T, Munoa J. Self-tuning semi-active tuned-mass damper for machine tool chatter suppression. Proc Int Conf Noise Vib Eng ISMA 2012 2012:109–23.
[35] Yusoff AR, Turner S, Taylor CM, Sims ND. The role of tool geometry in process damped milling. Int J Adv Manuf Technol 2010;50:883–95.
[36] Park G, Bement MT, Hartman D a., Smith RE, Farrar CR. The use of active materials for machining processes: A review. Int J Mach Tools Manuf 2007;47:2189–206.
[37] Brecher C, Baumler S, Brockmann B. Avoiding chatter by means of active damping systems for machine tools. J Mach Eng 2013;13:117–28.
[38] Huyanan S, Sims ND. Vibration control strategies for proof-mass actuators. J Vib Control 2007;13:1785–806.
[39] Bilbao-Guillerna A, Barrios A, Mancisidor I, Loix N, Muñoa J. Control laws for

chatter suppression in milling using an inertial actuator. Isma 2010 2010:265–78.
[40] Kleinwort R, Schweizer M, Zaeh MF. Comparison of Different Control Strategies for Active Damping of Heavy Duty Milling Operations. Procedia CIRP 2016;46:396–9.
[41] Munoa J, Mancisidor I, Loix N, Uriarte LG, Barcena R, Zatarain M. Chatter suppression in ram type travelling column milling machines using a biaxial inertial actuator. CIRP Ann - Manuf Technol 2013;62:407–10.
[42] Munoa J, Beudaert X, Erkorkmaz K, Iglesias A, Barrios A, Zatarain M. Active suppression of structural chatter vibrations using machine drives and accelerometers. CIRP Ann - Manuf Technol 2015;64:385–8.
[43] Micromega Woelfel group. Micromega - Active damping devices n.d.
[44] CSA Engineering. CSA Engineering - Inertial actuators n.d.
[45] van Dijk N. Active chatter control in high-speed milling processes. Eindhoven University of Technology, 2011.
[46] Denkena B, Gümmer O. Process stabilization with an adaptronic spindle system. Prod Eng 2012;6:485–92.
[47] Denkena B, Will JC, Möhring B. Tool deflection compensation with an adaptronic milling spindle. Int Conf Smart Mach Syst ICSMS 2007.
[48] Monnin J, Kuster F, Wegener K. Optimal control for chatter mitigation in milling-Part 1: Modeling and control design. Control Eng Pract 2014;24:156–66.
[49] Aggogeri F, Al-Bender F, Brunner B, Elsaid M, Mazzola M, Merlo a., Ricciardi D, De La O Rodriguez M, Salvi E. Design of piezo-based AVC system for machine tool applications. Mech Syst Signal Process 2013;36:53–65.
[50] Zatarain M, Bediaga I, Muñoa J, Lizarralde R. Stability of milling processes with continuous spindle speed variation: Analysis in the frequency and time domains, and experimental correlation. CIRP Ann - Manuf Technol 2008;57:379–84.
[51] Al-Regib E, Ni J, Lee SH. Programming spindle speed variation for machine tool chatter suppression. Int J Mach Tools Manuf 2003;43:1229–40.
[52] Bakker OJ, Papastathis TN, Popov a. a., Ratchev SM. Active fixturing: literature review and future research directions. Int J Prod Res 2013;51:3171–90.
[53] Tansel I, Nedbouyan A, Student G. Design of a Smart Workpiece Holder (SWH) To Extend the Useful Life of Micro-Tools. Mech Eng 1995:116–20.
[54] Lockwood S, Haase F, Ford DG. Active vibration control of machine tool structures –Part 1: DSP algorithms. Trans Eng Sci 2003;44:441–50.
[55] Haase F, Lockwood S, Ford DG. Active vibration control of machine tool structures –Part 2: An experimental active vibration system. Trans. Eng. Sci., vol. 44, 2003, p. 451–60.
[56] Ford DG, Myers A, Haase F, Lockwood S, Longstaff A. Active Vibration Control for a CNC Milling Machine. Proc Inst Mech Eng Part C J Mech Eng Sci 2013.
[57] Brecher C, Manoharan D, Ladra U, Köpken HG. Chatter suppression with an active workpiece holder. Prod Eng 2010;4:239–45.
[58] Yutaka N, Hiroki T, Yu A. Improvement of Workpiece Chatter Stability in Endmilling Process By Workpiece Excitation. 22nd Int. Congr. Sound Vib., Florence: 2015, p. 12–6.
[59] Long X, Jiang H, Meng G. Active vibration control for peripheral milling processes. J Mater Process Technol 2013;213:660–70.
[60] Rashid A, Mihai Nicolescu C. Active vibration control in palletised workholding system for milling. Int J Mach Tools Manuf 2006;46:1626–36.

[61] Parus A, Powalka B, Marchelek K, Domek S, Hoffmann M. Active vibration control in milling flexible workpieces. J Vib Control 2012.
[62] Haase F. The Investigation and Design of a Piezoelectric Active Vibration Control System for Vertical Machining Centres. Huddersfield University, 2005.
[63] Yong YK, Moheimani SOR, Kenton BJ, Leang KK. Invited review article: high-speed flexure-guided nanopositioning: mechanical design and control issues. Rev Sci Instrum 2012;83:121101.
[64] Yong YK, Liu K, Moheimani SOR. Reducing cross-coupling in a compliant XY nanopositioner for fast and accurate raster scanning. IEEE Trans Control Syst Technol 2010;18:1172–9.
[65] Li Y, Huang J, Tang H. A compliant parallel XY micromotion stage with complete kinematic decoupling. IEEE Trans Autom Sci Eng 2012;9:538–53.
[66] Acer M, Sabanovic A. Micro position control of a designed 3-PRR compliant mechanism using experimental models. 2013 9th Asian Control Conf ASCC 2013 2013.
[67] Kenton BJ, Leang KK. Design and Control of a Three-Axis Serial-Kinematic High-bandwidth Nanopositioner. IEEE/ASME Trans Mechatronics 2012;17:356–69.
[68] Lobontiu N. Compliant Mechanisms: Design of Flexure Hinges. CRC Press; 2002.
[69] Xu W, King T. Flexure hinges for piezoactuator displacement amplifiers: flexibility, accuracy, and stress considerations. Precis Eng 1996;19:4–10.
[70] Chen GM, Jia JY, Li ZW. Right-Circular Corner-Filleted flexure hinges. Proc 2005 IEEE Conf Autom Sci Eng IEEE-CASE 2005 2005;2005:249–53.
[71] Meng Q. A Design Method for Flexure-Based Compliant Mechanisms on the Basis of Stiffness and Stress Characteristics. Univeristy of Bologna, 2012.
[72] Schotborgh WO, Kokkeler FGM, Tragter H, van Houten FJAM. Dimensionless design graphs for flexure elements and a comparison between three flexure elements. Precis Eng 2005;29:41–7.
[73] Tian Y, Shirinzadeh B, Zhang D, Zhong Y. Three flexure hinges for compliant mechanism designs based on dimensionless graph analysis. Precis Eng 2010;34:92–100.
[74] Lobontiu N, Paine JSN, Garcia E, Goldfarb M. Corner-Filleted Flexure Hinges. J Mech Des 2001;123:346.
[75] Meng Q, Li Y, Xu J. New Empirical Stiffness Equations for Corner-filleted Flexure Hinges. Mech Sci 2013;4:345–56.
[76] Lobontiu N, Garcia E, Hardau M, Bal N. Stiffness characterization of corner-filleted flexure hinges. Rev Sci Instrum 2004;75:4896–905.
[77] Tseytlin YM. Notch flexure hinges: An effective theory. Rev Sci Instrum 2002;73:3363.
[78] Yong YK, Lu T-F, Handley DC. Review of circular flexure hinge design equations and derivation of empirical formulations. Precis Eng 2008;32:63–70.
[79] Timoshenko S. History of Strength of Materials: With a Brief Account of the History of Theory of Elasticity and Theory of Structures. Dover Publications; 1953.
[80] MSC. MSC Nastran 2016 Quick Reference Guide. 2016.
[81] Gandhi M V, Thompson BS. Smart Materials and Structures. Springer Netherlands; 1992.
[82] Culshaw B. Smart Structures and Materials. Artech House; 1996.
[83] Yao Q, Dong J, Ferreira PM. Design, analysis, fabrication and testing of a parallel-kinematic micropositioning XY stage. Int J Mach Tools Manuf 2007;47:946–61.

[84] Keoschkerjan R, Harutyunyan M, Wurmus H. Analysis of self-heating phenomenon of piezoelectric microcomponents actuated harmonically. Microsyst Technol 2002;9:75–80.
[85] APC International. Piezo-Mechanics: An Introduction. PA: Pleasant Gap; 2003.
[86] Andersen B, Ringgaard E, Bove T, Albareda A, Pérez R. Performance of piezoelectric ceramic multilayer components based on hard and soft PZT. Actuators 2000 Seventh Int. Conf. New Actuators, 2000, p. 423–6.
[87] Pickelmann L. First Steps towards Piezoaction. Mackeyville, PA: APC International; 2012.
[88] Leang KK, Fleming AJ. High-speed serial-kinematic SPM scanner: design and drive considerations. Asian J Control 2009;11:144–53.
[89] Oberg E, Press I. Section 02. Mechanics & Strength of Materials -- Machinery's Handbook 29: Industrial Press; n.d.
[90] Mubea GmbH. Mubea Disc Springs Manual n.d.
[91] Ewins DJ. Modal testing: theory, practice, and application. Research Studies Press; 2000.
[92] Peeters B, Auweraer H Van Der, Guillaume P, Leuridan J. The PolyMAX frequency-domain method : a new standard for modal parameter estimation? Shock Vib 2004;11:395–409.
[93] Allemang RJ. The modal assurance criterion - Twenty years of use and abuse. Sound Vib 2003;37:14–21.
[94] Insperger T, Stépán G, Bayly P., Mann B. Multiple chatter frequencies in milling processes. J Sound Vib 2003;262:333–45.
[95] Sallese L, Grossi N, Tsahalis J, Scippa A, Campatelli G. Intelligent fixtures for active chatter control in milling. Procedia CIRP 2016;55:176–81.
[96] Ganguli A, Deraemaeker A, Romanescu I, Horodinca M, Preumont A. Simulation and Active Control of Chatter in Milling via a Mechatronic Simulator. J Vib Control 2006;12:817–48.
[97] Weremczuk A, Rusinek R, Warminski J. The Concept of Active Elimination of Vibrations in Milling Process. Procedia CIRP 2015;31:82–7.
[98] Meitzler AH, Berlincourt D, Coquin GA, Wlesh FS, Tiersten HF, Warner AW. IEEE Standard on Piezoelectricity. IEEE; 1988.
[99] Adriaens HJMT a, de Koning WL, Banning R. Modeling piezoelectric actuators. IEEE/ASME Trans Mechatronics 2000;5:331–41.
[100] Altintas Y, Weck M. Chatter Stability of Metal Cutting and Grinding. CIRP Ann - Manuf Technol 2004;53:619–42.
[101] Kyrychko YN, Hogan SJ. On the Use of Delay Equations in Engineering Applications. J Vib Control 2010;16:943–60.
[102] Newmark NM. A Method of Computation for Structural Dynamics. J Eng Mech Div 1959;85:67–94.
[103] Bathe KJ, Saunders H. Finite Element Procedures in Engineering Analysis. vol. 106. 1984.
[104] Hughes TJR. The finite element method: linear static and dynamic finite elment analysis. Dover Publications; 2000.
[105] Scippa A, Sallese L, Grossi N, Campatelli G. Improved dynamic compensation for accurate cutting force measurements in milling applications. Mech Syst Signal Process 2015;54:314–24.
[106] Rabbath CA, Léchevin N. Discrete-Time Control System Design with Applications.

Springer New York; 2014.
[107] Kuljanic E, Totis G, Sortino M. Development of an intelligent multisensor chatter detection system in milling. Mech Syst Signal Process 2009;23:1704–18.